Electrochemical Energy Reviews (2023) 6:34
https://doi.org/10.1007/s41918-023-00200-x

REVIEW ARTICLE

Printed Solid-State Batteries

Shiqiang Zhou[1,2] · Mengrui Li[1,2] · Peike Wang[1,2] · Lukuan Cheng[1,2] · Lina Chen[1,2] · Yan Huang[1,2,3] · Suzhu Yu[1,2] · Funian Mo[1,2] · Jun Wei[1,2,3]

Received: 10 July 2022 / Revised: 9 March 2023 / Accepted: 14 August 2023 / Published online: 20 October 2023

Abstract
Solid-state batteries (SSBs) possess the advantages of high safety, high energy density and long cycle life, which hold great promise for future energy storage systems. The advent of printed electronics has transformed the paradigm of battery manufacturing as it offers a range of accessible, versatile, cost-effective, time-saving and ecoefficiency manufacturing techniques for batteries with outstanding microscopic size and aesthetic diversity. In this review, the state-of-the-art technologies and structural characteristics of printed SSBs have been comprehensively summarized and discussed, with a focus on the cutting-edge printing processes. Representative materials for fabricating printed electrodes and solid-state electrolytes (SSEs) have been systematically outlined, and performance optimization methods of printed SSBs through material modification have been discussed. Furthermore, this article highlights the design principles and adjustment strategies of printing processes of advanced SSB devices to realize high performance. Finally, the persistent challenges and potential opportunities are also highlighted and discussed, aiming to enlighten the future research for mass production of printed SSBs.

Keywords Additive manufacturing · Solid-state batteries · Energy storage devices · Printed batteries

1 Introduction

Lithium-ion batteries have emerged as an ideal choice of power source for electronic products due to their high energy density, low self-discharge rate, long cycle life, and light weight [1–3]. In previous years, most of the research on lithium-ion batteries has been focused on liquid electrolyte batteries. Although liquid electrolyte has high ionic conductivity and good wettability, its electrochemical stability and thermal stability are poor, lithium ion migration number is low, and safety is poor [4]. Meanwhile, since entering the twenty-first century, electronic products, electric vehicles, aerospace, large-scale power storage and other fields are booming, and there is a large demand for high-energy density lithium-ion batteries. However, after more than two decades of development, the energy density of lithium-ion batteries is basically close to its development bottleneck. The theoretical specific capacity of the widely used graphite anode is only 372 mAh g^{-1}, and it is difficult to achieve the energy density required by the next generation battery [5]. Lithium metal has the lowest electrochemical potential (− 3.04 V vs. the standard hydrogen electrode) and the highest mass specific capacity (3 861 Wh kg^{-1}), and the energy density of the battery can be significantly improved when matched with a high potential cathode material, which jumps to become the most promising battery structure type [6, 7].

However, the main bottleneck of lithium metal battery research involves fundamental safety issues, the application of which has been limited to a large extent in the past [8].

Shiqiang Zhou and Mengrui Li have contributed equally to this work.

✉ Suzhu Yu
szyu@hit.edu.cn

✉ Funian Mo
mofunian@hit.edu.cn

✉ Jun Wei
junwei@hit.edu.cn

[1] Shenzhen Key Laboratory of Flexible Printed Electronics Technology, Harbin Institute of Technology, Shenzhen 518055, Guangdong, China

[2] School of Materials Science and Engineering, Harbin Institute of Technology, Shenzhen 518055, Guangdong, China

[3] State Key Laboratory of Advanced Welding and Joining, Harbin Institute of Technology, Harbin 150001, Heilongjiang, China

During the battery cycle, not only the lithium metal anode undergoes redox reaction, but also the shape of lithium deposited on the anode cannot be effectively controlled [5]. Lithium metal will undergo a large volume change in the deposition direction, which causes changes in internal pressure and surface height [9]. On the one hand, lithium dendrites grow when the negative electrode is constantly exposed to fresh surface and electrolyte reaction, irreversibly generating a new solid electrolyte interface film. The growing lithium dendrites may also "break" and become "dead lithium" which loses electrochemical activity, and the accumulation of "dead lithium" will lead to a decrease in the Coulombic efficiency of the battery, an increase in the conduction path, and an increase in the polarization [10]. Meanwhile, the lithium dendrites generated by the uneven deposition of lithium metal may pierce the diaphragm and connect the positive and negative electrodes of the battery, causing an internal short circuit and releasing a lot of heat [11]. Traditional lithium-ion batteries use a flammable organic electrolyte, so the battery is prone to thermal runaway, leading to electrolyte expansion, decomposition, spontaneous combustion and even explosion, posing serious safety risks. Overall, lithium dendrites generated in liquid electrolyte lithium metal batteries not only lead to low Coulombic efficiency and short cycle life of the battery, but also may inherently cause safety accidents [12]. To truly realize the industrialization of lithium metal electrodes, the above-mentioned bottlenecks must be broken. Solid-state lithium batteries are promising candidates for revolutionizing battery systems for portable devices and electric vehicles [13, 14].

The solid-state battery (SSB) is regarded as the safest battery system since it employs a solid electrolyte that does not include any combustible or volatile components, fully avoiding the risk of battery smoke and fire brought on by battery leakage [15]. The SSB consists of the cathode, anode and solid-state electrolyte (SSE), and leads the wire through the collector. The structure is simpler than traditional lithium-ion batteries, and the solid electrolyte has the dual purpose of conducting lithium ions and a separator, which greatly simplifies the steps, quality and costs of battery construction [16, 17]. At the same time, lithium metal is used directly for the anode, further reducing the amount of anode material and enabling SSBs to have higher energy density [18, 19]. Compared with conventional liquid electrolyte batteries, SSBs have many advantages, such as no electrolyte leakage, nonflammability, excellent mechanical properties, and effective inhibition of lithium dendrite growth [10, 20, 21]. On the basis of the ions transported, solid electrolytes can be classified as lithium ions, sodium ions, oxygen ion solid electrolytes, etc. Among all cations, the lithium ion has the smallest in-core proton number, the lowest redox potential and can provide the largest mass energy density, which makes lithium-ion solid electrolytes the main object of research and application [16]. The solid electrolyte is light in weight and has an electrochemical window of up to 5 V, which can be matched with high-voltage cathode materials and lithium metal anodes, greatly improving the energy density of the battery [12, 22]. In addition, SSEs are applied in emerging lithium metal battery systems (such as lithium/sulfur, lithium/oxygen, and lithium/carbon dioxide batteries), which have more attractive potential to solve the current environmental pollution and energy crisis. Therefore, solid-state lithium metal batteries are expected to become energy storage systems for next-generation emerging electric vehicles and smart grids [11]. Despite the rapidly growing interest in SSBs, there are still lack of concern in manufacturing and in the fundamental understanding of the technology.

For SSBs, the production process requires breakthroughs in electrodes, electrolytes, interface engineering, and packaging technology. The optimization of production processes is an important part of realizing the engineering and commercial application of SSBs. Most current SSB devices are fabricated by stacking electrode sheets and SSEs. In the entire production process of SSBs, the electrolyte film-forming process is a key process. As the core process of SSBs, the electrolyte film-forming process can be divided into two categories: the dry process and wet process [23]. Different processes will affect the thickness and ionic conductivity of the solid electrolyte membrane. If the solid electrolyte film is too thick, the mass energy density and volume energy density of the SSB will be reduced, and the internal resistance of the battery will also be increased. Long-standing issues in SSBs, such as the form factor, interfacial contact resistance, balance between ionic conductivity and mechanical strength, and fabrication processability, limit their applications [24]. Conventional manufacturing processes are too complex and limited in controlling the structure and geometry of battery components to achieve complex shapes or configuration designs with high-aspect-ratio 3D architectures [25, 26]. One of the major challenges is the high interfacial resistance due to poor solid–solid contact. To reduce the impact of interfacial resistance on performance, increasing the contact area by introducing printing techniques has become a promising strategy [27]. Due to the large surface area of the printed electrolyte, the total electric field can be uniformly distributed, resulting in uniform Li deposition and lower battery resistance. The emergence of new approaches such as printing techniques has filled this gap, making it possible to control the architecture of SSB systems from the micro to the macro with high precision [28, 29].

Printing is a technology that allows specific patterns to be formed on a specified surface by integrating a functional material into an ink system [30, 31]. Printed electronics

involves the use of standard or specific printing processes and equipment to print electronic circuits and components, such as sensors, light-emitting devices, and supercapacitors, on different substrates such as paper, plastic, and textiles [32, 33]. Several main types of printing technologies have been invented and widely used: inkjet printing, 3D printing, direct ink writing, roll-to-roll printing, spray and screen printing, etc. Advances in printed electronics over the past few years and the need for low cost and simple processing have led to the potential replacement of traditional processing techniques in some areas. The most important advantages of printed electronics are low cost, flexibility, and simplicity of production and integration, promising new applications and opening new markets. Advances in the battery sector related to printing technology are expected to have a huge impact on the growth segment of small portable and wearable electronics for applications such as smart cards, remote sensors, and medical devices [34].

Typically, printed SSBs work by combining specific ink materials and various printing and deposition methods to create customizable, thin, low-cost, mechanically flexible, and large-area battery systems [35]. In addition to anode and cathode materials, solid electrolytes with ionic conductivity close to high-performance liquid electrolytes are also the basis of printing manufacturing [36, 37]. Printing methods vary widely in ink rheology, achievable resolution, and material selection. For example, low-, medium-, and high-viscosity inks can be used for inkjet printing, screen printing, and 3D printing, respectively, and inks with a wide viscosity range can be patterned by using pen-based direct ink writing. Printed SSB technology paves the way for new production models for specific applications, which can reduce production steps and costs. A schematic summary of the main printing methods for fabricating printed SSBs, as well as some printed electrode materials and electrolyte materials, is shown in Fig. 1.

Despite the continued interest in printed SSB technology and its proven benefits, many key challenges remain in the fundamental understanding and fabrication of printed batteries as follows.

1. The application of printed SSBs confronts a handful of practical difficulties due to the specific requirements of different printing technologies for printing inks. For example, inks for inkjet printing (IJP) typically have nanometer-sized solid particles, which portend a risk of nozzle clogging during long-term operation. Direct ink writing (DIW) printing inks require good shear thinning properties, which are influenced by the concentration, composition, solid particle size and ratio of the different components. The raw materials for fused deposition modeling (FDM) and stereolithography (SLA) are usually limited to thermoplastic and light-curable materials, respectively.
2. The temperature and time of sintering for printing SSBs become very critical. Although high temperature sintering can yield the crystal structure required for high ionic conductivity, prolonged high temperature sintering can lead to severe loss of lithium and sodium and correspondingly low ionic conductivity due to the volatility of light elements at high temperatures.
3. The process parameters for printing SSBs have a significant impact on battery performance. For instance, the printing process can lead to potentially porous structures and poor composition control, further distorting the shape and complex structure of the electrolyte layer, leading to its shrinkage and eventual deformation.
4. Interfacial stability during the printing process needs to be improved, which has a limited effect on the performance of the battery. For example, the interface within the solid electrolyte and poor physical contact at the solid electrolyte/electrode interface lead to high interfacial impedance. In addition, 3D structures printed in layers have relatively weak binding interfaces.
5. The cycle lifetime of some of these printed SSBs has been reported to be poor. Printing optimization is essential for producing high-quality SSB devices.

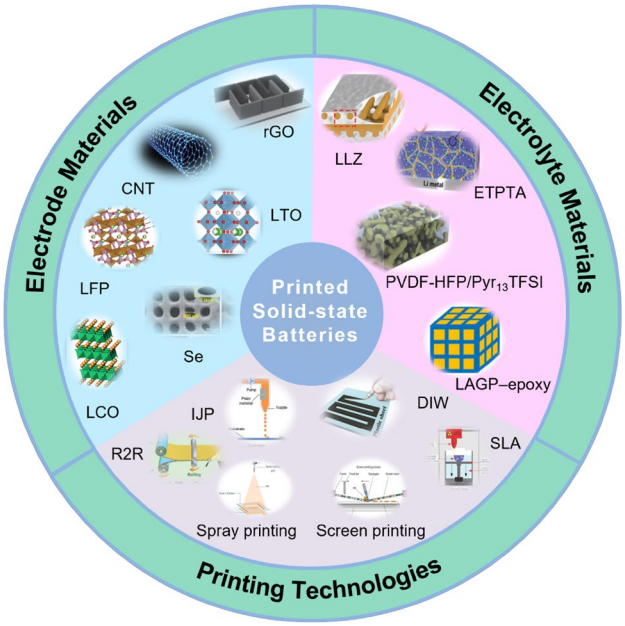

Fig. 1 Schematic outline of the review for printed SSBs: printed electrode materials, electrolyte materials and main printing technologies

Although SSBs are an important class of energy storage devices with great promise, a comprehensive review of printed SSBs is still required. In this review, the state-of-the-art of SSB technologies and the structural characteristics of

SSBs have been comprehensively summarized and discussed, with a focus on the cutting-edge printing processes. Representative materials for fabricating printed electrodes and SSEs have been systematically outlined, and performance optimization methods of printed SSBs through material modification have been discussed. Furthermore, this article highlights the design principles and adjustment strategies of printing processes of advanced SSB devices to realize high performance. Finally, the persistent challenges and potential opportunities are also highlighted and discussed, aiming to enlighten the future research for mass production of printed SSBs. We believe that this review will attract scientific research, academics, and industry worldwide, and also strongly believe that printing technologies can be broadly used for energy storage and conversion with further research and development in the future.

2 Device Configurations of Printed SSBs

Lithium-ion batteries have been widely used as power sources for electronic devices over the past few decades. Next-generation batteries are expected to be flexible, lightweight, low-cost, customizable, and available in a variety of sizes. However, traditional manufacturing processes limit the complexity and variety of batteries in terms of size and shape. Among the existing technologies, printed electronics manufacturing can be considered the most advanced technology to meet the requirements of next-generation batteries [29, 34, 35]. Several reviews on SSBs have given a good summary of the basic structure and physics as well as performance evaluation methods [9, 21, 38]. In basic research, the weight performance is traditionally used as an index to evaluate the quality of electrode materials, while the area performance and volume performance are the key parameters to evaluate the practical application potential, especially for the pursuit of printed SSBs with aesthetics and high performance. Since size and weight are the primary considerations for portable devices, it is also critical that the energy density is not significantly reduced due to the adoption of these new materials and designs. Unfortunately, high flexibility and high energy density are often trade-offs, and the high flexibility of batteries conferred by printing techniques often require the introduction of redundancy in capacity to relieve stress in the battery. Indeed, further research is needed to improve the mechanical properties of printed batteries while maintaining high electrochemical performance.

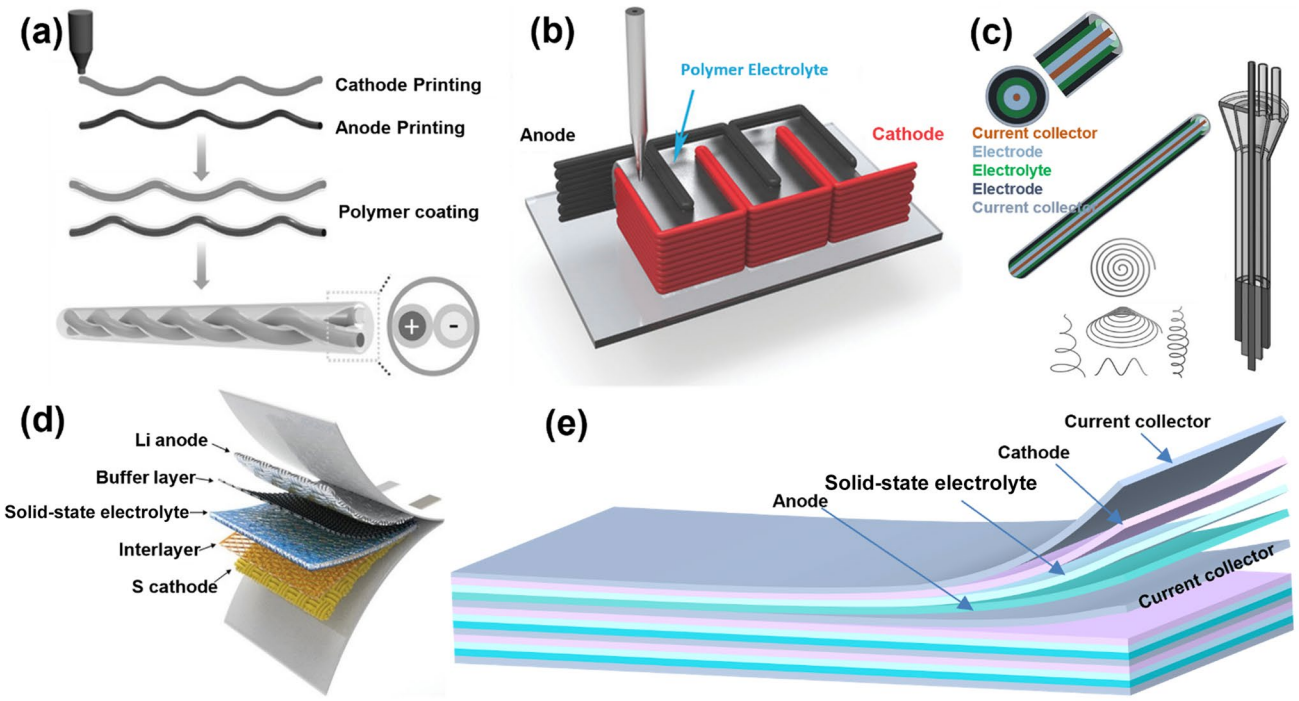

Fig. 2 Configurations of printed batteries. **a** Fiber type. Reprinted with permission from Ref. [39]. Copyright © 2017, John Wiley and Sons. **b** Planar type. Reprinted with permission from Ref. [40]. Copyright © 2016, John Wiley and Sons. **c** Concentric tube type. Reprinted with permission from Ref. [41]. Copyright © 2019, ECS. **d** Sandwich type. Reprinted with permission from Ref. [42]. Copyright © 2020, John Wiley and Sons. **e** Bipolar type

The configuration of printed batteries has a significant impact on their device performance and applications. In general, these printed batteries can be designed in four configurations based on geometric features, including the fiber type [43], planar type [44], concentric tube type [45], and sandwich type [46] (Fig. 2). The fiber-based configuration is a unique battery configuration in which researchers are working to develop fiber-based energy storage devices with a coaxial or twisted structure [35]. Coaxial structures enable the coating of various active materials into the core–shell structure. However, achieving a thin and uniform coating on a bent fiber remains challenging. Twisted structures involve the twisting of two fiber electrodes (the anode and cathode) at an angle into an integrated fiber-like device. With the fiber configuration being widely studied as a flexible and wearable energy storage device, there is a great desire to develop one-dimensional fiber-shaped energy storage devices that can be twisted and woven into flexible, wearable and breathable textiles [47]. For instance, Hu and coauthors used 3D printing to fabricate flexible all-fiber lithium-ion batteries. As shown in Fig. 2a, lithium iron phosphate (LFP) fiber cathodes and lithium titanium oxide (LTO) fiber anodes were printed with polymer inks containing carbon nanotubes and LFP or LTO, respectively. By twisting the printed LFP and LTO fibers together with the gel polymer as a quasi-solid electrolyte and maintaining the good flexibility of the fiber electrodes, they can potentially be integrated into textile fabrics for future wearable electronics applications [39].

Planar configuration, is a classic 3D printed battery design, in which the microelectrodes are arranged in parallel and printed on the same plane of the substrate (Fig. 2b). It allows the integration of microelectrodes in a very limited area, and the size of the microelectrodes and the distance between the microelectrodes can be precisely controlled by a printing procedure. For example, Hu et al. [40] printed a pair of miniature interdigital electrodes on a glass substrate and filled the channels between the two interdigitated annealed electrodes with a polymer composite ink containing a mixture of Al_2O_3 nanoparticles to assemble an interdigitated battery. This proof-of-concept device demonstrates that any shape, size and design of interdigitated battery arrays can be printed on glass substrates to meet specific voltage and current requirements. This small printable battery could act as a power source to integrate various electronic components and facilitate an all-print approach to electronic system fabrication.

A concentric tube type is a unique battery configuration in which uniformly aligned and vertical electrode columns are uniformly covered with a solid electrolyte, and the area between the columns is filled with counter electrode material (Fig. 2c). This structure is common in 3D micro-batteries and usually consists of etched 3D electrodes, especially the common 3D silicon anode [35]. Using stereolithography printing techniques, concentric tubular micro-batteries are manufactured with printed porous polymer substrates coated layer by layer with thin film electrodes and polymer ceramic electrolytes deposited by electrophoresis [45].

Sandwich configurations are a common design for cost-effective mass production, where each module is placed on a different plane and assembled by stacking them layer by layer (Fig. 2d) [42]. Sandwich configurations can be printed with batteries designed to customize any shape. Among the configurations of sandwich batteries, there is a special configuration called a bipolar battery [48, 49]. This type of battery is different from a normal lithium battery. As shown in Fig. 2e, it uses a series stacking of electrodes. The positive and negative materials of the battery act on a common carrier (collector), eliminating the aluminum case of previous lithium batteries. A large portion of internal space is saved and more power materials can be filled in the same volume. In the past, nearly half of the space of lithium batteries assembled in parallel was occupied by separate compartments, and the effective space was too small, which is the reason for the lack of range of current new energy vehicles. This printing technology can print large area flat batteries. The flat shape allows the battery to be perfectly embedded in the car chassis, saving a lot of space inside the car and leaving plenty of room for upgrades and modifications. This battery has only a very thin shell, making the production cost of lithium batteries much lower, and battery life can also achieve a substantial increase. Based on the flat design, a car can carry twice the volume of the old "bipolar battery" [50].

In fact, it is quite challenging to meet the mechanical strength of sandwich-type printed electrodes and cells compared to compact electrodes and cells. In addition, in solid-state cells, large volume expansion and contraction occurs during the interfacial reaction, resulting in poor mechanical stability. The addition of fillers such as carbon filler [51], silica [52] and cellulose [53] to the ink or filament is currently a common strategy to improve the mechanical properties of electrodes. The other strategy is to construct soft polymeric scaffolds, which are wrapped by mechanically strong polymeric scaffolds to enable them to withstand mechanical forces [54]. However, such nonactive fillers or polymeric scaffolds can reduce the specific gravity of the active material, which in turn reduces the energy density of the cell. Notably, further studies are required to enhance the mechanical properties of the printed electrodes with high electrochemical performance.

3 Printing Technology

Printing technology is the process of preparing different functional nanomaterials into printing inks to be molded on a substrate in the form of printing. Post-treatment of the target product is required after ink deposition, namely, the solvent required for the printing process itself needs to evaporate. Printing technology serves as an additive manufacturing process for the manufacture of electronic devices. As printing technology evolves, an increasing number of printing technologies are being used for highly innovative energy storage systems, offering the possibility of better integration into devices and new applications. Each printing technology provides unique characteristics in terms of accuracy, feature size, printing speed and layer thickness, and handles inks with a range of grain sizes [55]. In this section, the most common printing technologies are presented to set the stage for the subsequent description of the various functional parts of printed SSBs, and some representative research work on printed SSBs is briefly described according to the different printing technologies, and more research progress on printed SSBs will be described in the next section.

3.1 Inkjet Printing

Among all printing technologies, inkjet printing is the most flexible, which is classified as a digital manufacturing technology with many advantages over traditional printing technology, the ability to print variable data on commercial items, barcodes, serial numbers, identification graphics and anti-counterfeiting elements on packaging. All inkjet technologies are based on digitally controlled precise generation and ejection of liquid ink droplets in diameter ranging from 10 to 150 mm (typically 50–80 mm) from the printhead nozzles onto the substrate [56, 57]. Inkjet printing technology offers several droplet volumes ranging from picoliter (pL) to microliter (μL), print resolutions ranging from 100 to 5 000 dpi, depending on the ink used and implementation substrate. In addition, because inkjet printing technology is very flexible in implementation and affordable, it is also widely used for research and development purposes in the most advanced application areas such as "printing functions" and "printing electronics or microelectronics". Many researchers around the world focus on developing printed electronics, e.g., active and passive devices such as capacitors, thin film transistors, resistors, inductors, and antennas, based on sensors and detectors of humidity, pressure, stress, strain, light, gas concentration, and heat for energy harvesting/utilization and power devices such as batteries, organic photovoltaics and piezoelectric actuators [32].

As shown in Fig. 3a, b, inkjet printing is usually achieved by two different modes of printhead operation: continuous inkjet (CIJ) and drop on demand (DOD). A continuous stream of ink droplets is ejected under pressure through a tiny nozzle in the CIJ process (Fig. 3a). The droplet is charged by electrode located at the droplet breakpoint and then directed by a high voltage deflection plate to a position on the substrate proportional to the applied charging voltage, or to a recovery tank. Typically, only a small fraction of droplets are used for imaging, and most are directed to drains and recirculated through pumps

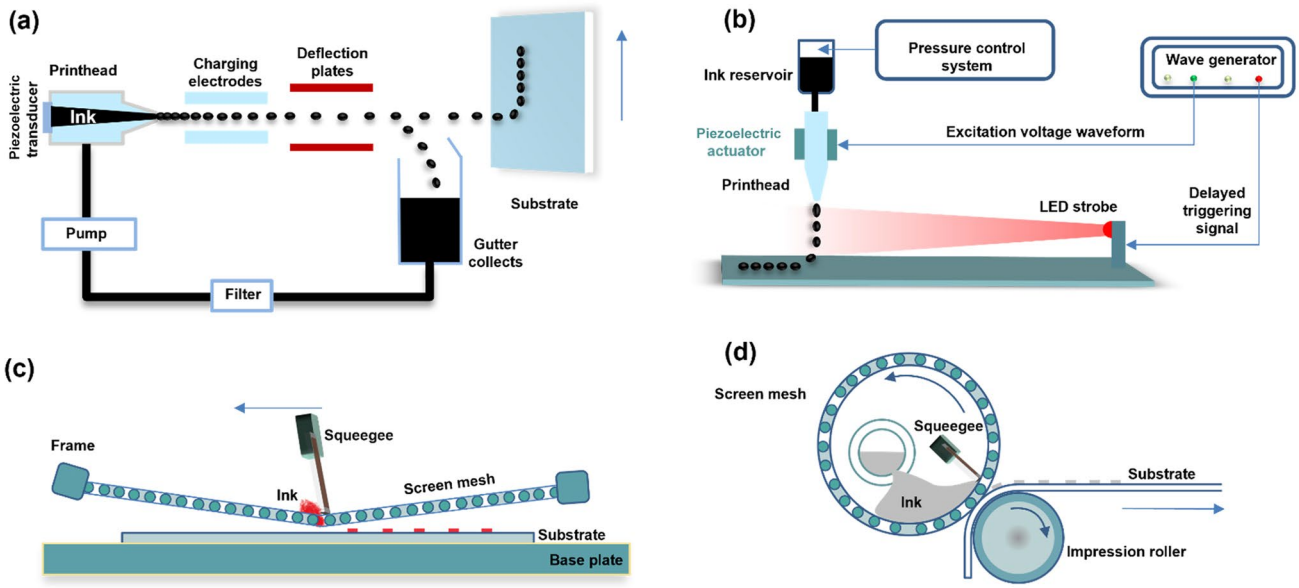

Fig. 3 Schematic representation of printing techniques. **a** Inkjet printing, continuous and **b** drop on demand; **c** flatbed screen printing and **d** rotary screen printing

and filters. The drop generation frequency range for CIJ printers is 50–175 kHz, and the drop velocity at the nozzle is typically > 10 ms^{-1} [58]. High-speed droplets are maintained over long distances between the printhead and substrate, and very high droplet ejection frequencies enable very high print speeds. One of the advantages of CIJ is that volatile solvent-based inks can be used, which can dry quickly and aid adhesion on many substrates. The disadvantages of CIJ are the relatively low resolution of printed patterns, the need to charge the ink droplets, the limitations of microfabrication, and the use of environmentally unfriendly volatile solvents. In drop-on-demand printing, ink droplets are formed by pressure pulses and are ejected from the print head only when commanded by a digital signal.

DOD printers (Fig. 3b) operate at typical audio frequencies in the 1–20 kHz range [58]. The generation of pressure pulses is performed by thermal heating, piezoelectric elements or electrostatic fields. In thermal inkjet printers, droplets are formed by rapid heating (350–400 °C) of resistive elements in small ink cartridges, which causes the ink to evaporate rapidly and leads to the formation of air bubbles. This bubble creates a pressure pulse that forces the ink to drip out of the nozzle. The advantages of thermal DOD printing are: small droplet size, compact equipment, and low cost of printheads. The main disadvantage is related to the limitations of the fluids: they should have higher vapor pressures and should be stable at higher local temperatures to prevent them from damaging and forming a hard coat on the inner surface of the printhead. In piezoelectric DODs, pressure pulses are generated by direct mechanical actuation using a piezoelectric transducer: a piezoelectric crystal (usually lead zirconium titanate) deforms when an electric field is applied. This creates a pressure pulse that causes a drop of ink to be ejected from the nozzle. An important advantage of piezoelectric DOD technology is that it is suitable for a variety of water-based and solvent-based ink formulations. In electrostatic ink jetting, ink droplets are ejected from a nozzle under the influence of an electrostatic field between an electrode and an orifice. If the electrostatic force exceeds the surface tension of the ink, ink droplets are produced. The advantage of this technology is the potential high resolution, even higher than that of piezoelectric inkjet printing (which can produce very small droplets), while the disadvantage is the ink limitation: only conductive liquids can be used as inks. Overall, the common advantages of DOD printing compared to CIJ printing are a wider choice of ink formulations and higher spatial resolution of droplets on the substrate. Today, most industrial printers use piezoelectric DOD technology, and most functional material printing is done by this method.

For orderly and reliable patterning during inkjet printing, single droplets should be generated stably without long tails and satellites. Representative characteristic dimensionless numbers that affect ink behavior are the Reynolds number (*Re*) [59], the Weber number (*We*) [60], and the Ohnesorge number (*Oh*) [61]:

$$Re = \frac{v\rho\alpha}{\eta} \tag{1}$$

$$We = \frac{v^2\rho\alpha}{\gamma} \tag{2}$$

$$Oh = \frac{\sqrt{We}}{Re} = \frac{\eta}{\gamma\rho\alpha} \tag{3}$$

where v, α, ρ, η and γ represent the velocity, characteristic length (typically drop diameter), density, viscosity and surface tension of the ink, respectively. *Re* and *We* refer to the ratio of the inertial force to the viscous force, and the balance between the inertial force and the surface tension, respectively, while *Oh* relates the viscous force to the inertial force and surface tension. Generally, the *Z* parameter ($Z = 1/Oh$) is commonly used to indicate printability [62], where a *Z* value between 1 and 10 is expected to generate a stable drop formation. At a low value of *Z*, viscous dissipation prevents drop ejection, whereas at a high value the primary drop is accompanied by a large number of satellite drops. Thus, by modulating the ink composition, inks with the desired viscosity and surface tension can be achieved to inkjet print stable droplets [63].

In functional material-based inks, avoiding solute congestion during printing is as important as generating stable droplets. Excess solute, solvent evaporation in the orifices, and/or poor ink dispersion are all common causes of clogging. To ensure smooth printing, the size of the solute should be less than one-tenth the diameter of the nozzle of the printer's print head. Methods such as membrane filtration and ultrasonic-driven cracking processes can be used to obtain solutes of suitable size for inks with too large functional materials. High boiling point inks should keep solvent volatility low enough to avoid evaporation in the nozzle. Van der Waals forces are primarily responsible for caking and precipitation in poorly dispersed inks. This problem is usually solved by functionalizing the material with appropriate chemical groups/polymer coatings, adding surfactants, and introducing good solvents. Delannoy et al. [64] used an inkjet printing process to fabricate porous composite electrodes and SSEs [silica-based ionic gels: *N*-methyl-*N*-propylpyrrolidinium bis(trifluoromethan) suflonylimide (PYR13-TFSI), with an added Li salt lithium bis(trifluoromethan)sulfonylimide (Li-TFSI)]. Over the course of 100 cycles, whole cells combining LFP and LTO porous composite electrodes have a surface capacity of 0.3 mAh cm^{-2}.

3.2 Screen Printing

Screen printing is a printing process that involves depositing ink onto a substrate using a stencil screen, with the exception of locations where the ink is rendered impenetrable by blocking the stencil. The blade or scraper moves across the screen to fill the open mesh with ink, and the reverse stroke causes the screen to momentarily contact the substrate along the line of contact. This causes the ink to wet the substrate and pull out of the mesh as the screen bounces back after the blade has passed. Due to their simplicity and versatility, a variety of functional inks and substrates are available for screen printing. There are two main types of screen printing, flatbed screen printing and rotary screen printing techniques (Fig. 3c, d). Flatbed technology is a step-by-step process in which the ink is pressed onto a substrate through a flat patterned screen. After printing, the patterned screen is lifted, the substrate is replaced or removed by hand, and the deposition process is repeated. Therefore, flat screen technology enables precise multi-layer printing. It also shows great potential for lab-scale printing due to the low cost and malleability of the patterned screen. Rotary screen printing, on the other hand, is the process of pressing ink through a polyester screen cylinder and perforated metal to deposit onto a substrate. As the screen rotates at the same speed as the substrate, a stationary doctor blade is used to continuously press the ink onto the substrate, each rotation creating a complete print cycle. Therefore, rotary technology can achieve much higher printing speeds than flatbed technology. During screen printing, the wet thickness of the printed pattern is determined by many parameters, such as the concentration of functional ink, mesh per inch, emulsion thickness, and ink fraction transferred to the substrate. The quality of a screen printed pattern depends on the screen mesh, printing parameters, substrate and ink viscosity [32]. Park et al. [65] fabricated thick-film $LiCoO_2$ cathodes by screen-printing technology to improve the discharge capacity of lithium-ion microbatteries. An all-solid-state microbattery was assembled by using LiPON solid electrolytes and Li was evaporated onto a printed $LiCoO_2$ cathode thick film without delamination or electrical problems and with stable open-circuit voltage. Ohta et al. [66] constructed an all-solid-state lithium-ion battery with Li_3BO_3 as the cathode and Nb doped $Li_7La_3Zr_2O_{12}$ as the solid electrolyte by a screen printing process, which exhibited good electrochemical performance and low interface resistance, comparable to lithium-ion batteries with liquid organic electrolytes. Screen printing is suitable for patterns with high aspect ratios, and the movement of the paste can be easily controlled during the printing process, making it easier to obtain thick functional films compared to other techniques. However, due to the high viscosity of the ink, the high roughness and low resolution of screen printed films limit its application.

3.3 3D Printing

3D printing, also known as additive manufacturing, is a design and manufacturing technology that integrates materials, structures, and functions. This is the opposite of subtractive manufacturing processes, where a final design is cut from a larger block of material. As a result, 3D printing creates less material wastage. In the past few years, 3D printing technology has been successfully used to fabricate a variety of batteries and microbatteries with outstanding features of no forming and high shape consistency [26, 35, 67]. In the 3D printing manufacturing process, the printable ink (or filament) of the electrode material is first prepared and then directly printed according to predetermined specifications. Compared to traditional tape casting and deposition techniques, the 3D printing process is more convenient, customizable and intelligent. According to the International Organization for Standardization and the American Society for Testing and Materials (ISO/ASTM 52900:2015), 3D printing processes are classified into seven categories: (1) binder jetting; (2) material extrusion [e.g., direct ink writing (DIW), fused deposition modeling (FDM)]; (3) directed energy deposition; (4) material jetting [e.g., ink jet printing (IJP), aerosol jet printing (AJP)]; (5) powder bed fusion (e.g., selective laser sintering, direct metal laser sintering); (6) reduction photopolymerization [stereolithography (SLA), digital light processing, two-photon lithography]; (7) laminate lamination (e.g., laminated object manufacturing) [68]. In order to meet the precise performance and architectural requirements of SSBs, the right printing technology is chosen depending on the processability and feature size of the final product. Other energy storage devices can also be printed by utilizing binder jetting processes, but they are more expensive. Understanding the printing process as well as the features of various technologies is therefore critical for future material design and technology development. Among the many 3D printing technologies, we summarize the most commonly used representative technologies that can print currently available battery modules, including AJP, FDM, DIW, and SLA.

3.3.1 Aerosol Jet Printing

Aerosol jet printing (AJP) is to form an aerosol of nanoconductive ink by ultrasonic atomization or airflow, and then transmit the aerosol to the inkjet port by using a carrier gas to print the conductive ink on the required substrate [69]. At the same time, aerosol printing uses a bundle of sheath gas to cover the outside of the ink to control the direction of the printing airflow and ensure the accuracy of printing (Fig. 4a). Since the aerosol is formed by ultrasonically oscillating or air-flowing the ink containing an organic solution, it can be adapted to the range required by most conductive

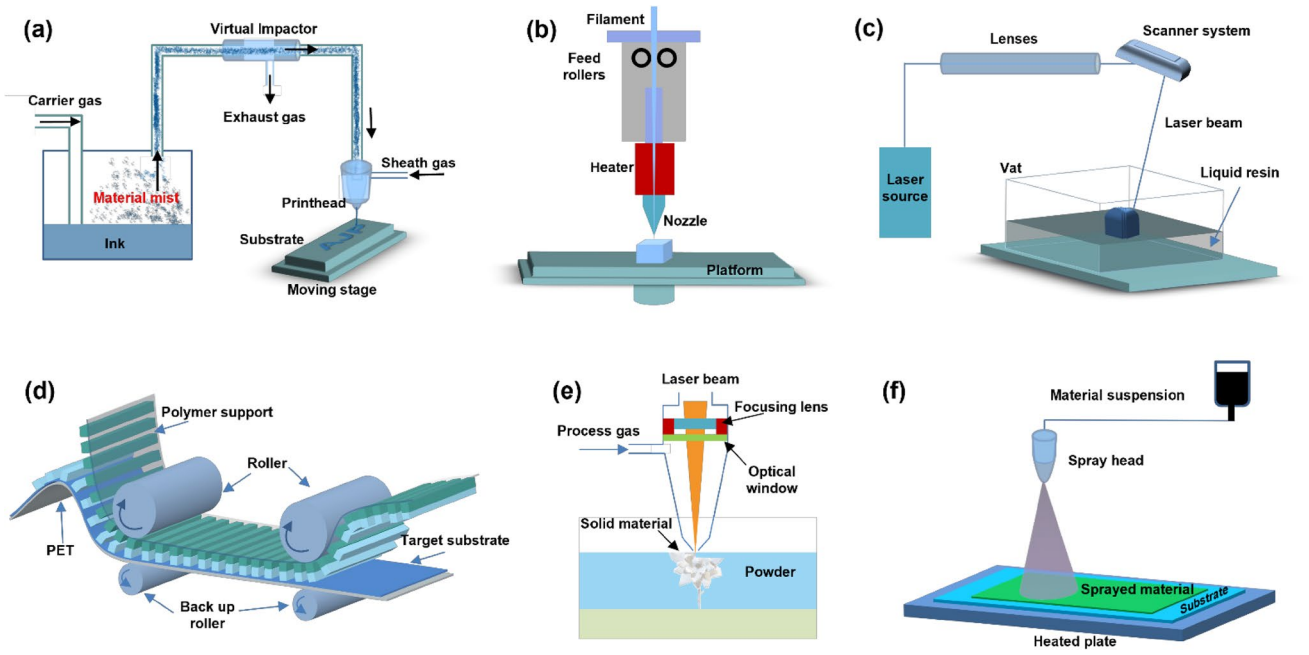

Fig. 4 Schematic representation of printing techniques: **a** aerosol jet printing, **b** fused deposition modeling, **c** stereolithography, **d** roll-to-roll printing, **e** laser printing and **f** spray printing

inks. Moreover, aerosol printing mainly transmits the carrier gas through airflow. Under the combined action of the sheath gas and the atomizing airflow, the aerosol will not have any contact with the inner wall of the nozzle, and will only be sprayed out under the cover of the sheath gas, so it is extremely difficult to cause common problems such as nozzle blockage. The aerosol printing height can be adjusted more easily, and the encapsulated aerosol can be printed on a substrate with a specified structure dependent on the direction control of the sheath gas. The printed graphics will first be completed by numerical control commands, and then the flow rate will be concentrated by setting the nozzle to align the coaxial position of the substrate. The distance between the nozzle and the substrate will remain constant to adapt to the flow rate and flow of the sheath gas to ensure printing accuracy. The printing process can be described by system geometry and key process parameters (aerosol and sheath gas flow rates, deposition nozzle size, and aerosol droplet size). Other parameters such as ink, print speed, atomizer power and substrate temperature are controllable on the fly but have peripheral effects on the core process. Ink temperature (which affects viscosity) and atomizer power affect the inputs to the process, namely droplet size distribution and aerosol density. Additionally, print speed affects print thickness, and substrate temperature affects post-deposition drying, which in some cases affects resolution, film uniformity, and topography [70, 71]. Deiner et al. [72] used AJP technology to print lithium-ion conducting solid-state polymer composite electrolytes on LFP cathode substrates. Aerosol jet printed electrolytes composed of polyethylene oxide, alumina nanoparticles, and lithium difluoro(oxalato)borate are conformal, smooth, and nonporous. Conductivity of the printed solid polymer electrolytes tracks salt anion identity and concentration. The most conductive printed electrolyte, PEO/LiDFOB/alumina, achieves conductivity $> 1 \times 10^{-5}$ S cm^{-1} at 45 °C.

3.3.2 Direct Ink Writing

Direct ink writing (DIW) is a typical extrusion-based 3D printing technique that dispenses ink through movable nozzles controlled by pneumatic or mechanical pumping devices to create free-form structures. This direct extrusion mechanism enables a higher diversity of printable materials, including volatile solvents, liquid metal alloys, and various types of composites [73–76]. The nozzle can be moved horizontally on a flat surface, and the platform can be moved vertically downward after each new layer is deposited with the help of computer-aided manufacturing or computer-aided design software. Print resolution is usually determined by a combination of nozzle diameter, applied pressure, and the characteristics of the ink being squeezed. To print battery module architectures at high resolution, the rheological properties of the ink are critical. Low-viscosity inks are prone to droplet formation and will not have enough yield stress to support the entire 3D architecture after the ink is extruded, while those with extremely high-viscosity inks tend to clog the nozzles and require higher printing pressures. Therefore, inks with appropriate rheological

properties are beneficial for the DIW process. After extrusion, the printed structures can be cured by liquid evaporation, UV light and heat treatment depending on the ink properties.

Typically, shear thinning behavior is required for printable inks in DIW processes [77]. Shear thinning behavior refers to the decrease in the apparent viscosity of a fluid as the shear rate increases [78]. Through this behavior, the viscosity of the ink is reduced under the shear force during extrusion, allowing the ink to flow easily through the nozzle without the need for super high pumping pressure. To achieve such rheological properties of inks, one of the most promising approaches is to add nanomaterials as fillers. For example, the addition of ceramic nanoparticles including TiO_2 and Al_2O_3 has been reported as a promising strategy to obtain desired rheological properties and improved ionic conductivity for electrolyte inks [79, 80]. DIW is applicable to an almost infinite number of printable materials, ranging from plastics, novel functional nanomaterials (e.g., perovskites, graphene, covalent organic frameworks, metal–organic frameworks, 2D MXenes), metals, ceramics, hydrogels, to food and living cells, etc., which provides a variety of possibilities for printing SSB active materials. In fact, DIW printing has been extensively explored for high-quality 3D active materials in battery modules [81, 82]. However, one of the main challenges of DIW lies in the preparation of printable inks with the desired battery materials. It presents a set of technical specifications for printable inks, including high viscosity yield stress behavior, well-controlled viscoelasticity, and requirements for smooth extrusion under printing pressure. Liu et al. [81] printed a solid electrolyte of $Li_{1.3}Al_{0.3}Ti_{1.7}(PO_4)_3$ with arbitrary shape and high electrical conductivity by DIW, which exhibited high ionic conductivity up to 4.24×10^{-4} S cm^{-1}. Moreover, using this printing method, $Li_{1.3}Al_{0.3}Ti_{1.7}(PO_4)_3$-based hybrid SSEs can be directly printed on LFP cathodes for solid-state lithium batteries, where a high discharge capacity of 150 mAh g^{-1} at 0.5 C is obtained. The DIW strategy of SSEs demonstrates a new avenue for advanced solid-state energy storage with high ion transport and custom fabrication.

3.3.3 Fused Deposition Modeling

Fused deposition modeling (FDM) is based on the principle of material extrusion, in which thermoplastic filaments are drawn through a nozzle, heated to their melting (or glass transition) point, and then deposited layer by layer (Fig. 4b). Once the deposited thermoplastic layer fuses with the underlying layers, it cools and hardens. Repeat this process until the 3D structure is complete. The most commonly used polymer for FDM is acrylonitrile butadiene styrene, but polycarbonate and polyetherimide are also used. With the increase in 3D printing and FDM applications, it is necessary to develop new printable polymers with unique properties for use in SSBs. Polymer properties and processing conditions play an important role in determining the final mechanical properties of a finished part, and processing conditions often depend on polymer properties. Therefore, the temperature-dependent rheological behavior of polymer melts is important for describing and controlling the behavior of polymers in the liquefier (where the polymer melts), during extrusion, and after the polymer has been extruded. Despite its popularity, FDM has shown great difficulty in 3D printing of electrochemical energy storage devices due to the relatively low ionic conductivity of plastic filaments, which greatly affects the performance of the electrolyte [83]. Recently, by changing the chemical composition of plastic filaments, researchers developed solid polymer electrolyte filaments for FDM. For example, Maurel et al. [84] designed a PEO/LiTFSI filament with a conductivity of 2.18×10^{-3} S cm^{-1} at 90 °C for FDM of solid-state polymer electrolytes. Although PEO:LiTFSI (20:1) filament is printable, it still suffers from poor mechanical strength due to its flexibility and sticky behavior, as clearly demonstrated by nanoindentation experiments. Future research may focus on introducing comb-like block polymers to impart some rigidity. Furthermore, another way to promote printability might be to use a modified FDM technique that directly uses particles or powders as material sources instead of filaments.

3.3.4 Stereolithography

Light and ink-based 3D printing is an important fundamental technique for creating batteries among the different additive manufacturing processes [85]. Light-based 3D printing methods mainly include stereolithography (SLA), selective laser sintering (SLS) and two-photon polymerization [86]. SLA is a technique for polymerizing curable liquid photosensitive resins into solid objects and creating tiny plates using a grating laser [85]. The UV laser draws the cross-section layer by layer as the liquid polymer is gradually subjected to light (Fig. 4c). Repeat the process until the model is created. Solid items are 3D printed by drawing the object out of the resin, leaving space at the bottom of the container for the uncured liquid resin to produce the next layer of the object. SLS is a technique for creating three-dimensional objects by heating and fusing polymer particles in a powder bed using a grating laser. The resolution of light-based 3D printing technologies is typically excellent; nevertheless, there are inherent trade-offs between resolution, object volume, and speed, as well as limited material alternatives, which are primarily limited to stiff thermosetting polymers and thermoplastic polymer powders. Two-photon polymerization is the most precise 3D printing process with a lateral resolution of 100 nm and an axial resolution of 300 nm, and has been used to create many complex structures for

advanced photonic and nanoscale applications, such as photonic crystals or microfluidic devices [87]. Zekoll et al. used SLA-based 3D printing to construct 3D ordered polymer templates with precisely controlled microstructures and obtained a $Li_{1.4}Al_{0.4}Ge_{1.6}(PO_4)_3$ hybrid solid electrolyte composed of 3D ordered bicontinuous conducting ceramics and insulating polymer microchannels by a derivative fabrication method [88]. Liu et al. fabricated a solid polymer electrolyte by SLA-based 3D printing. The three-dimensional Archimedes spiral structure solid-phase extraction is rationally designed, which shortens the transport path of lithium ions from the electrolyte to the electrode, enhances the interfacial adhesion, and increases the mass loading of active materials. The battery exhibits an ionic conductivity of 3.7×10^{-4} S cm^{-1} at 25 °C, decreased interfacial impedance after 250 cycles and a high specific capacity of 128 mAh g^{-1} [89]. This work opens up promising prospects for the preparation of high-performance solid electrolytes in next-generation energy storage materials.

3.3.5 Roll-to-Roll (R2R) Printing

Roll-to-roll processing is a fabrication method used in manufacturing that embeds, coats, prints or laminates varying applications onto a flexible rolled substrate material as that material is fed continuously from one roller onto another [90]. As shown in Fig. 4d, the roll-to-roll technique typically consists of several rollers, known as the web path, which winds the substrate material over and through these rollers as it carries out a number of operations. The technique applies additive or subtractive materials onto the substrate as it moves along the web to generate or produce a product or part. A substrate is derived from a web made of thin, flexible, and long material. The web materials are then stored or transported as rolls for and between roll-to-roll processing stages. The materials consist of paper, foil, plastic films, textiles, metals, and even nanomaterials. R2R processing is used in numerous manufacturing and industrial sectors such as IT, electronics and computing, energy, textiles, medical, metal fabrication and biosciences [91]. Many applications require flexible materials to complete the finished product. From electronic devices, solar panels, thin-film batteries to fuel cell membranes, coating textiles with reagents and more are produced by roll-to-roll processing. For example, in the production of large-area electronic devices, flexible displays or circuit boards are realized by R2R processing of rolls of plastic film or metal foil [92].

These high throughput and low cost are factors that differentiate roll-to-roll manufacturing from slower and more expensive traditional manufacturing due to the multiple steps involved. Roll-to-roll printing technology simply consists of manufacturing techniques that involve the continuous processing of material on a flexible substrate as it is transferred between moving rolls of material. It involves the application of various solution processable materials and composition printing techniques. The advantages of roll-to-roll solution-processed polymer solar cells have been well demonstrated in terms of bulk, robustness, and reproducibility [92]. Roll-to-roll printing is a competitive cost and scale method for manufacturing SSBs. Baade et al. [93] demonstrated curtain coating as a method to fabricate composite solid electrolytes in a roll-to-roll process at roll speeds in excess of 80 m min^{-1}. The method is compatible with existing lithium-ion battery electrode production lines and is capable of producing uniform SSE membranes with thicknesses below 15 µm [93]. Roll-to-roll printing is also used in other energy storage devices, such as supercapacitors [94].

3.3.6 Laser Printing

Laser printing is an electrostatic digital printing process (Fig. 4e). A main attraction of laser printing is that objects with complex geometries can be flexibly fabricated without specialized fabrication tools. Such printing processes have been developed for a range of materials, including metals, ceramics and polymers. The laser printing method generally works as follows: a laser beam is moved onto the top surface of a basin of smooth-surfaced liquid or powder, irradiating some parts of it, causing solidification without hitting other parts. In general, the laser beam can move along a line in any direction. In other cases, the system systematically scans the entire area and turns on the laser beam only for those parts to be machined. It is also possible to combine these methods, such as a vector scan of the contour followed by a raster scan of the interior. The resulting planar structure is then lowered slightly in the bath, again covering its surface with a thin layer of liquid or powder. The laser can then be used to build another layer of solid material. Repeat this technique until the desired solid workpiece has reached its full height. Following that, the formed workpiece is removed from the bath, the residual liquid or powder is removed, and further processes (such as polishing) may be used to improve the surface quality.

When constructing an SSE for microbatteries, it is also crucial to think about how it is made. The power consumption and available footprint of microbatteries cannot be understood until the microdevice is constructed while producing microdevices. Ollinger et al. [95] used laser printing to deposit a nanocomposite SSE membrane from a suspension solution consisting of an ionic liquid-polymer matrix and dispersed nanoparticles. The printed nanocomposite SSEs are shown to exhibit the proper electrochemical behavior for ionic liquids while maintaining the strength and flexibility of the polymer matrix. This combination of physical properties and deposition technique makes these deposited nanocomposite membranes ideally suited for use as an

electrolyte/separator in Li micro-batteries. Kim et al. [96] used laser-printed thick-film electrodes ($LiCoO_2$ cathode and carbon anode) deposited on metal current collectors for the fabrication of lithium-ion microbatteries. These microbatteries exhibit significantly higher discharge capacity, power, and energy density compared to microbatteries fabricated by sputter-deposited thin-film techniques. These laser-printed electrodes are separated by laser-cut porous membranes impregnated with gel polymer electrolyte to construct millimeter-sized solid-state rechargeable lithium-ion microbatteries. The resulting encapsulated microbatteries exhibited a power density of about 38 mW cm^{-2} and a discharge capacity of about 102 μAh cm^{-2} at a high discharge rate of 10 mA cm^{-2}. This enhanced performance is attributed to the porous structure of the laser-printed electrodes, which can improve the transport of ions and electrons through thick electrodes without a significant increase in internal resistance.

3.3.7 Spray Printing

Spray printing is a technique in which ink is sprayed onto the surface of a substrate through air or an electric field [34]. In electrostatic spraying technology, droplets are sprayed in the direction of the substrate by a high voltage applied to a nozzle (Fig. 4f) [97]. The most common type uses compressed gas to atomize and guide the ink particles. There are also hybrid spray technologies based on electrostatic and air pressure spray technologies. Finally, spray printing allows printing a relatively wide range of ink viscosities and ink thicknesses, which primarily determine the size of the ink droplets. Typically, the printed layers are dried after each printing unit. For mass production of printed electronics, several parameters must be considered, such as the physical properties of the ink, flow rates, distance between nozzle and substrate, substrate temperature. Solvents with different vapor pressures determine the evaporation rate of the sprayed ink, which in turn affects the quality of the sprayed film. Low nozzle pressure or small diameter can result in slow flow rates, resulting in dispersed droplets and an uneven coating. The distance between the nozzle and the substrate is another key parameter that determines the quality of the coating film [32]. Spray printing technology has been widely used in the preparation of energy storage devices such as supercapacitors and lithium-ion batteries [98, 99]. To obtain micro- or nano-scale thin-film SSEs, Hu and coworkers printed precursor thin films on aluminum or copper foils and ceramic substrates (MgO and Al_2O_3) at 60 °C using a spray printing technique [100]. Leung et al. used a spray technique to fabricate porous organic electrodes. After spray-printing the interconnected porous honeycomb electrodes, a polymer ionic liquid-based solid electrolyte (ionic conductivity: 10^{-4} S cm^{-1}) was sprayed and infiltrated into the porous electrodes as a second layer. A symmetrical all-organic battery is then formed by adding another set of identical electrode and electrolyte layers [101].

4 Printable Materials for SSBs

The processability, performance, and long-term dependability of the materials used for printing are essential for the successful printing of SSBs, exactly as in other printing fields. The key components of SSBs, namely electrodes, electrolytes, and current collectors, have specific requirements in the printed SSBs. Inks for different battery components need to be developed with specific formulations and properties according to specific printing methods, and usually active materials are dispersed in solvents together with binders and additives to obtain stable colloidal suspensions, viscous pastes or mixture [32]. By adjusting the ratio of each component, inks with specific properties, such as viscosity and surface tension, can be obtained to meet the requirements of different printing technologies. Inks for different battery components should be designed considering compatibility with printing processes and electrochemical performance [102, 103]. Depending on the printing technique, the ink should have specific properties to allow design processability and prevent irregular patterns, uneven film morphology or low resolution. These properties include rheology (viscoelasticity, thixotropy, shear thinning and thickening behavior) and physical/chemical (the boiling point, surface tension, solubility, contact angle, density and specific gravity) properties and affect the colloidal stability of the ink composition and volumetric uniformity [104, 105]. Once different binder/solvent interactions can be observed, such as electrostatic repulsion and van der Waals forces, the stability of the ink is affected by the choice of solvent. Binders in colloidal solutions also exhibit two distinct force mechanisms: steric interactions and depletion interactions. Additionally, the use of surfactants affects these forces and can provide a certain degree of agglomeration or particle dispersion. Excellent electrochemical performance is actually achieved by dispersing agglomerates of different components. All these properties affecting electrochemical performance, once they affect ion/electron transport, are related to the dispersion of battery components (interconnected particle networks) and the development of new transport channels [102]. In this chapter, we will mainly discuss printable electrodes and electrolytes for printed SSBs. Unlike common liquid batteries, there are often non-printed in SSBs, such as current collectors, which normally serve as supports for the printed structure.

4.1 Electrode Materials

The anode materials of SSBs generally use ultra-high-capacity lithium metal or lithium-silicon-based materials. The cathode material is the most critical component in SSBs. The discovery and development of cathode materials that match the anode are expected to achieve excellent energy or power density. Therefore, the development of low-cost, high-performance cathode materials is the focus of future SSB research. So far, the cathodes of SSBs generally use composite electrodes. In addition to electrode active materials, composite electrodes also include solid electrolytes and conductive agents, which play the role of transporting ions and electrons in the electrodes. Oxide cathodes such as $LiCoO_2$, LFP, and $LiMn_2O_4$ are widely used in SSBs. In order to further improve the energy density and electrochemical performance of SSBs, researchers are also actively developing new high-energy cathode materials, mainly including high-capacity ternary cathode materials and high-voltage materials, such as $LiNi_{1-x-y}Co_xMn_yO_2$ (NCM) and $LiNi_{1-x-y}Co_xAl_yO_2$ (NCA), both having layered structure and high theoretical specific capacity. In addition to the above-mentioned electrode active materials, metals, alloys, sulfides, silicon-based materials, carbon-based materials, organic compounds, etc. are used as electrodes for SSBs. But they often suffer from poor cycle life, and in order to fully realize the potential of these electrode materials, new electrode structures are required to achieve more efficient charge transport beyond the limitations of conventional electrodes. Using printing technology, the design and synthesis of cathode materials to address the charge transport limitations in highly loaded electrodes enables composite electrodes with an unprecedented combination of energy and power density.

Typically, electrodes are printed directly on current collectors or electrolytes, the latter approach providing lower interfacial resistance between the solid electrolyte and electrodes. The capacity enhancement of SSBs is mainly pursued through a series of interface engineering strategies. The choice of solvent and binder system can tune the electrostatic and steric interactions within the ink, which can prevent the agglomeration of the active material and help improve the active material-electrolyte interface within the electrode [102]. The surface chemistry of the active material, the concentration and type of conductive additives, polymer loading, and solvent play an important role in forming the electrode microstructure [106]. This section highlights recent strategies aimed at increasing metal nucleation active sites and maintaining a sustainable Li-ion supply by carefully designing electrode materials in SSBs, which can be classified into carbon-based [40], elemental-based [107], oxide [108], and organic ones [101].

4.1.1 Carbon-Based Electrode Materials

Carbon-based materials have the advantages of high surface area, tunable properties, high conductivity, low density, cheap and ubiquitous precursors, and well-known and simple chemistry, which can be used to produce state-of-the-art printed solid-state lithium batteries. The 3D structure and surface chemistry of carbon allotropes formed by sp^2 hybridization of carbon atoms, namely carbon nanotubes (CNTs) and graphene, play a key role in determining their electrochemical performance for reversible Li metal storage [109]. Graphite can be chemically oxidized and exfoliated to obtain graphene oxide (GO). Printable inks require better viscosity and higher yield stress under compression and shear, which requires well-controlled rheology. GO, which exhibits excellent ink-forming ability, unique viscoelasticity, and functional properties suitable for printing due to its abundant amphiphilicity, stable dispersion, and tunable rheology, is often chosen to prepare various water-based composite inks [110, 111]. Developing printable GO inks is highly challenging because most GO-based aerogels come from dilute precursors (<5 mg mL^{-1}) of GO suspensions with low and unprintable viscosity [112, 113]. For different printing purposes, the rheological properties of the required printing ink, such as good formability, high porosity, good electrical conductivity and mechanical stability, are manipulated by varying the concentration and ratio of Go-based inks and additives such as calcium ions, CNTs and cellulose nanofibers [114–116]. Through a thermal annealing process, GO can be easily reduced to conductive graphene (rGO), which exhibits good electrical conductivity and can be used as a promising battery electrode material. Most research to date has focused on customizing the ink properties of graphene oxide [117], fabrication strategies [118], and building design objects, such as periodic scaffolds [119], nanowires [120], and microlattices [114]. At the same time, these 3D printed rGO structures exhibit good electrical conductivity, ultra-light weight, and high compressibility, which are promising energy storage applications [112].

In electrode materials, the rheological properties required for printing inks, such as good formability, high porosity, excellent electrical conductivity, and mechanical stability, were controlled by varying the concentration and ratio of GO-based inks. Kong et al. [121] fabricated a compressible quasi-SSB by a layer-by-layer stacking 3D printing method. As shown in Fig. 5a, b, the printing of self-supporting periodic rGO aerogel microlattice electrodes with tunable thickness was achieved by using highly conductive 2D rGO nanosheet inks. During the process of printing electrodes, the self-assembly of complex multidimensional superstructures of various carbon materials promotes the formation of hierarchical pore structures that provide multiple channels for ion diffusion. The addition of ultrathin $Ni(OH)_2$

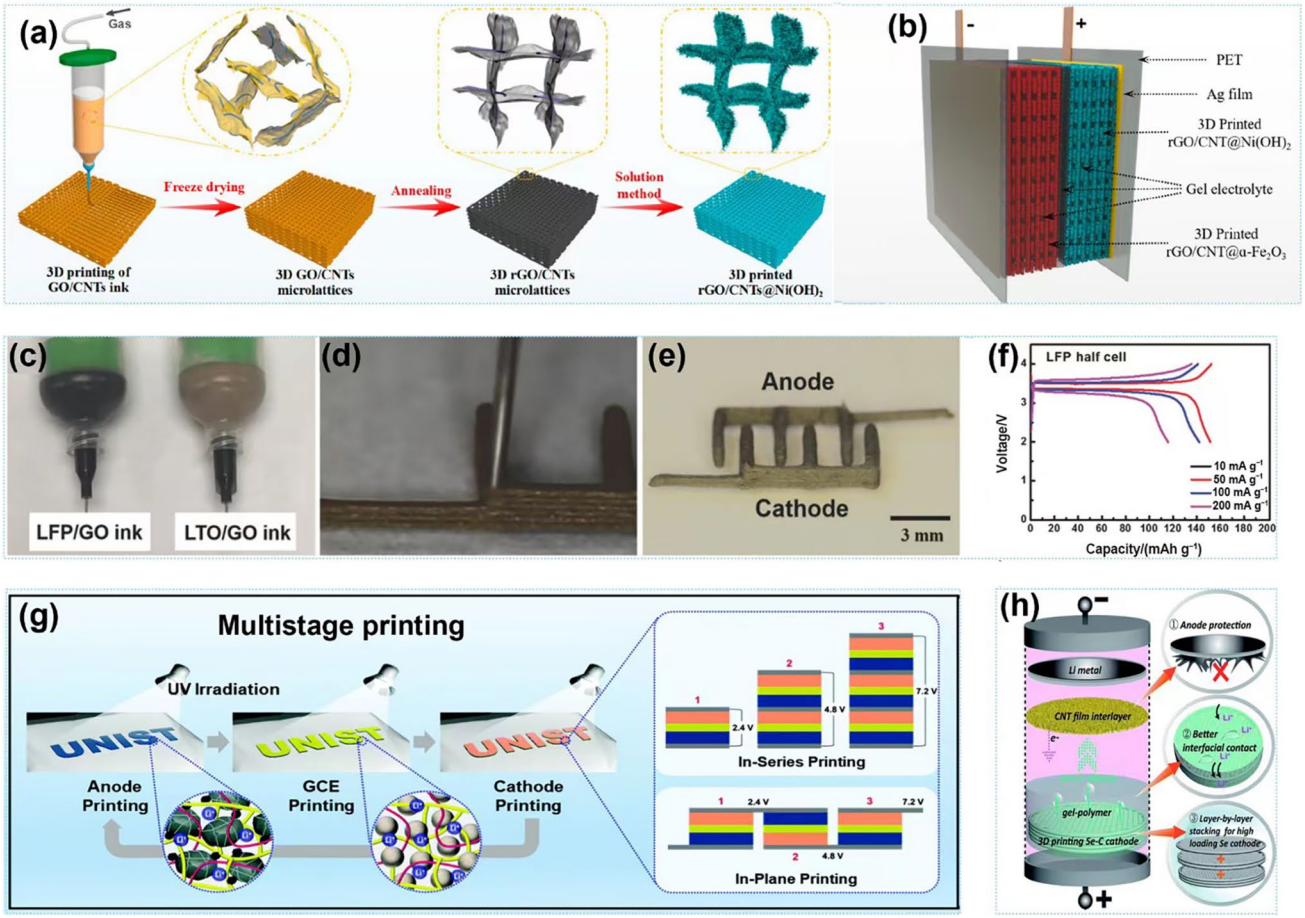

Fig. 5 **a, b** Schematic of fabrication of the cathode and anode of a 3D printed Ni–Fe battery and a schematic of the printed Ni–Fe battery device tested in a gel electrolyte. Reprinted with permission from Ref. [121]. Copyright © 2020, American Chemical Society. **c–f** 3D printed schematic of the electrodes and the charging and discharging curves of the half-cell. Reprinted with permission from Ref. [40]. Copyright © 2016, John Wiley and Sons. **g** Schematic of the flexible/shape-versatile bipolar cells prepared via the UV-assisted multistage printing process. Reprinted with permission from Ref. [49]. Copyright © 2020, Royal Society of Chemistry. **h** Schematic illustration of the 3D-printed Se cathode for promoting Li^+ immigration in a quasi-solid-state lithium-selenium battery model. Reprinted with permission from Ref. [107]. Copyright © 2020, Royal Society of Chemistry

nanosheets and porous α-Fe_2O_3 nanorod arrays into the aforementioned rGO aerogel microlattices to form electrodes ensures the coupling between the inorganic nanocrystals and the carbon framework, resulting in electrons from the active material rapidly transferred to the current collector. The active material loading of the electrodes exceeds 130 mg and the compressibility is as high as 60%. The printed quasi-solid-state Ni–Fe battery device exhibits a volumetric energy density of 28.1 mWh cm^{-3}, a power density of 10.6 mW cm^{-3}, and is stable for more than 1 500 cycles even under severe mechanical stress. Their synthesis strategy not only provides an efficient method for printing the fabrication of compressible batteries, but also facilitates future applications in stress-resistant flexible/wearable electronics.

In order to realize full-component printing of SSBs, expand the fabrication of more energy in multi-dimensional/multi-scale complex structure storage devices. Hu and his workers developed GO-based electrode composite inks and SSE inks to enable full-component 3D printing of SSBs [40]. As shown in Fig. 5c–e, the 3D printed SSBs were successfully fabricated using GO-based aqueous inks consisting of highly concentrated graphene oxide sheets as well as cathode and anode active materials. The highly concentrated graphene oxide flakes provide the necessary viscosity to bond the electrode materials together and enable 3D printing. Due to nozzle-induced shear stress, the GO flakes align in the extrusion direction, which enhances the conductivity of the electrodes. In addition, the inherent porous structure of the GO flakes provides a large surface area to load the electrodes with live nanoparticles and to hold the electrolyte. Based on this research, a class of GO-based printed composite inks can be designed and constructed for the fabrication of advanced structures, architectures, and systems with a variety of functional and energy storage applications. As shown in Fig. 5f,

the rGO-based electrodes were tested at various specific currents, and the charging and discharging capacities tended to decrease as the specific current value increased. At a specific current of 200 mA g^{-1}, the battery shows a higher charging capacity than the discharging capacity. This may be attributed to the fact that the rGO matrix lengthens the Li^+ diffusion path and thus hinders diffusion and reduces capacity, which is reflected in the increased capacity loss at higher specific currents.

Combining 3D printing technology with the preparation of graphene-based composite materials enables rapid manufacturing molding of composite materials to create products with complex structures. The addition of graphene enables 3D printed products with better mechanical properties and functional characteristics, while also allowing easier preparation of gradient functional products. It is worth mentioning that graphene can be compounded with polymer solid electrolytes, while the addition of polymer stabilizes the ink to prevent graphene precipitation and delamination, and also adjusts the ink viscosity to be in a printer-friendly range. Many of the technologies for forming graphene/polymer-based composites using 3D printing are not mature enough yet, making the prospect of application in the field of printing SSBs worthy of anticipation. CNTs have been widely used to fabricate different devices such as transistors [122], sensors [123], supercapacitors [124] and printed batteries [51] due to their large specific surface area, high chemical stability, high mechanical strength, and excellent electrical and thermal properties. In batteries, it is common to use similar methods based on carbon nanotube-mediated surface modification to modify electrodes to improve battery performance. For instance, Kim et al. [49] demonstrated a printed bipolar all-solid-state LiB with extraordinary shape versatility, flexibility, charge–discharge behavior, flammability, and fabrication simplicity (Fig. 5g). Single-walled CNTs are coated to increase their electrical conductivity. Experimental results show that the introduction of a conductive single-walled CNTs layer on the surface of the active material leads to an increase in the electronic conductivity of the resulting electrode. The coin-type half-cells were tested at a constant charge current density of 0.1 C, and the results showed that the discharge rate capability of the single-walled carbon nanotube-coated electrodes was significantly improved.

To meet the flexible and breathable energy storage device requirements for wearable applications. Wang et al. [39] used 3D printing to fabricate flexible all-fiber lithium-ion batteries. In their design, fiber electrodes were printed separately using CNT-containing high-viscosity polymer ink, and all-fiber lithium-ion batteries were assembled by wrapping the printed fiber electrodes using gel polymers as quasi-SSEs. The interconnected CNTs facilitate the transport of electrons and can obtain excellent electrochemical performance. The all-fiber device exhibits a high specific capacity of 110 mAh g^{-1} at a current density of 50 mA g^{-1} and maintains good flexibility of the fiber electrodes, potentially integrating into textiles for future wearable electronic applications. In addition, Gao et al. [107] showed that CNTs can also inhibit the growth of lithium dendrites (Fig. 5h). The prepared CNT ink is first extruded through a 200 mm diameter nozzle. The printed CNT layer was placed in a freeze dryer for 24 h. Finally, a self-contained CNTs that can effectively protect the interlayer of Li anode during lithiation and delithiation cycling is obtained. The assembled symmetrical battery can operate stably for 400 h (3 mA cm^{-2} and 3 mAh cm^{-2}). And the SSB exhibits excellent cycle stability and remarkable rate capability, providing an areal capacity of 12.99 mAh cm^{-2} at 3 mA cm^{-2}.

The effect of CNTs with many excellent mechanical, electrical and chemical properties compounded with electrode active materials on the composite properties depends to a large extent on their mass fraction, dispersion status and the interaction between the carbon nanotubes and the matrix. In addition to this for example, the orientation of carbon nanotubes in the composite, the orientation of fibers in the lamellae, and the inhomogeneity of functional groups on the surface modification of carbon nanotubes have the potential to contribute to the improvement of the final mechanical properties of the composite.

4.1.2 Elemental Electrode Materials

The inactive metal or nonmetal battery is based on the electroplating and stripping of the metal on the negative side of lithium and the conversion reaction of the inactive metal or nonmetal on the positive side. Their reaction mechanism is different from the ion deintercalation mechanism of lithium-ion batteries, but an electrochemical reaction mechanism. The nontopological nature of these reactions endows the high theoretical specific capacity of lithium anodes and inactive metal or non-metal cathodes [125].

Among the numerous energy storage systems explored so far, lithium-sulfur batteries have attracted much attention due to their high theoretical capacity (1 672 mAh g^{-1}), low cost, and naturally abundant sulfur, making them a promising alternative to commercial lithium candidate batteries for ion batteries. Although Li-S batteries have been widely used, they still face several problems that hinder their practical application, such as the low conductivity of sulfur (5×10^{-28} S m^{-1}) and the high solubility of polysulfides caused by the "shuttle effect" [126]. In order to solve the shuttle problem of polysulfides in lithium-sulfur batteries, Kim et al. [48] fabricated for the first time a bipolar all-solid-state Li-S battery that exhibit excellent safety, flexibility, and form factors. As shown in Fig. 6a, it was fabricated by a solvent-free drying, ultraviolet (UV) curing-assisted stepwise printing process at room temperature, without the high-temperature/

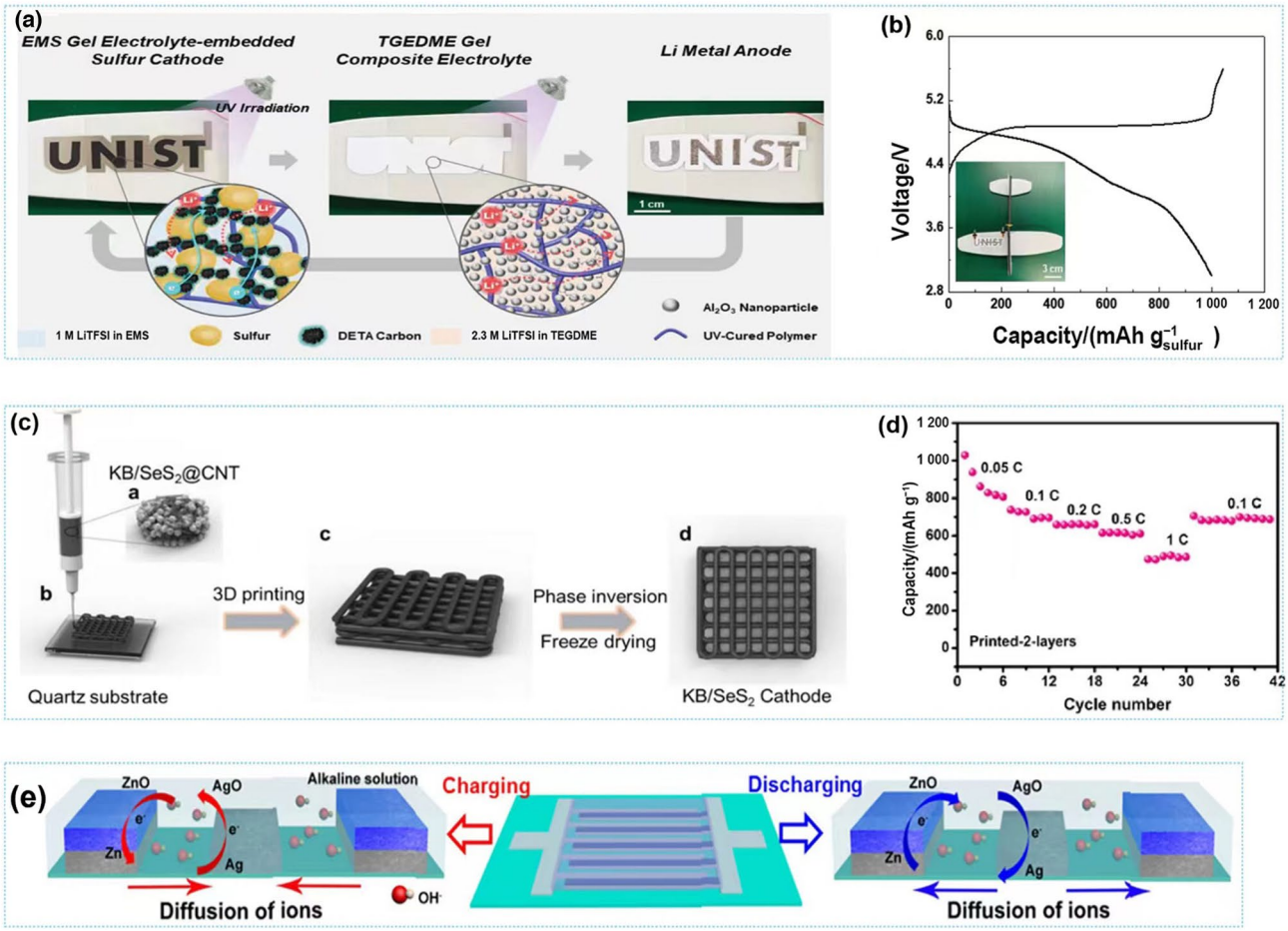

Fig. 6 **a** Schematic of the printed bipolar all-solid-state Li-S batteries through UV curing-assisted stepwise printing process. **b** Charge/discharge curve of all-solid-state lithium-sulfur battery (charge/discharge current density of 0.1 C/0.1 C). (**a, b**) Reprinted with permission from Ref. [48]. Copyright © 2019, John Wiley and Sons. **c, d** Schematic of extrusion-based 3D printing of selenium disulfide/ketjenblack composites cellular structures and the C-rate performance of the cathode. Reprinted with permission from Ref. [128]. Copyright © 2020, Elsevier. **e** Schematic diagram of the microsized Ag/Zn batteries. Reprinted with permission from Ref. [129]. Copyright © 2020, John Wiley and Sons

high-pressure sintering step commonly used in inorganic solid electrolytes. Two thermodynamically incompatible and nonflammable gel electrolytes based on ethyl methyl sulfone and tetraethylene glycol dimethyl ether were used to address the grain boundary resistance of conventional inorganic solid electrolytes and the shuttle effect of polysulfides in lithium-sulfur batteries long-term problems. The ethyl methyl sulfone gel electrolyte embedded in the sulfur cathode facilitates the utilization of sulfur, while the tetraethylene glycol dimethyl ether gel composite electrolyte acts as a polysulfide repelling separator. The resulting bipolar all-solid-state Li-S battery exhibits extraordinary advancements in form factor, mechanical flexibility, and safety. The rational design of the battery components and structure described above, combined with a simple UV-curing assisted step printing process, enables the resulting all-solid-state lithium-sulfur battery to show significant improvements in bipolar configuration, safety, mechanical flexibility, and aesthetic diversity, far beyond what can be achieved with conventional lithium-sulfur battery technology. As shown in Fig. 6b, the letter-shaped bipolar all-SSB shows normal charge/discharge curves at the charge/discharge current density of 0.1 C/0.1 C.

Some researchers have also explored lithium-selenium (Li-Se) batteries, since Se is an element in the periodic table that belongs to the same main group as S. Compared with S, the semiconducting Se shows a higher electronic conductivity of 1×10^{-5} S m^{-1}, which is 10^{22} higher than that of S, enabling Li-Se batteries with high electrochemical kinetics. In addition, Li-Se batteries have comparable volume capacities to Li-S (3253 mAh cm^{-3} vs. 3 467 mAh cm^{-3}) [127]. More importantly, it is widely believed that Li-Se batteries undergo a solid-state lithiation process, a poly Se-free process in carbonate electrolytes. In other words, there is no "shuttle effect" during the charge/discharge process, which contributes

to high utilization of selenium and extended cycle life. Gao et al. [107] proposed a combination of printed CNT interlayers with 3D printed Se cathodes filled with gel polymer electrolytes in high Se loading cathodes to protect lithium anodes for ultra-high energy/power density quasi-solid-state light-emitting diodes. 3D printed Se serves as a host for impregnation of gel polymer electrolytes to prepare interconnected Li transport channels in thick Se cathodes, enabling rapid Li transport. Correspondingly, the SSE with ultra-high Se loading of 20 mg cm^{-2} achieves an areal capacity of 12.99 mAh cm^{-2} at 3 mA cm^{-2}.

Interestingly, according to related reports, heterocyclic Se_xS_y molecules combine the advantages of S and Se, have higher capacity than pure Se, and have better conductivity and cycling stability than pure S. As an important member of the Se_xS_y family, SeS_2 is the most reported material with a theoretical capacity of 1 123 mAh g^{-1} and a specific energy density of 1 743 Wh kg^{-1}. Shen et al. [128] printed three-dimensional self-supporting electrodes for $LiSeS_2$ batteries by DIW on the basis of high solid content ink (Fig. 6c). The characteristic rheological properties of the ink give it good printing performance and can stably extrude 3D printed cell scaffolds. In such a printed structure, a low-cost commercial conductive ketjenblack with abundant pores was chosen as the host material for selenium sulfide. For the well-controlled 3D printed ketjenblack/SeS_2 electrode, the area SeS_2 loading reaches 7.9 mg cm^{-2}. More importantly, due to hierarchical porosity engineering, the 3D-printed honeycomb ketjenblack/SeS_2 cathode achieves a first discharge capacity of up to 9.5 mAh cm^{-2} at 1.8 mA cm^{-2}, and 80 cycles at such a high mass loading. As shown in Fig. 6d, it is the initial discharge capacity of SeS_2 at 0.05 C, 0.1 C, 0.2 C, 0.5 C and 1 C, indicating that the SeS_2 electrode has good rate stability. This 3D-printed Li-SeS_2 battery electrode could guide more ultra-capacity energy storage systems towards practical applications.

The content of active materials (i.e., sulfur, selenium, etc.) in the flexible cathode should be further increased to achieve higher energy density of the whole battery. It is worth noting, however, that in printing fabrication, one of the limitations is that mechanical flexibility suffers if the sulfur content is increased [130]. Therefore, more efficient 3D conductive and mechanical networks are required to accommodate more cathode active materials while maintaining better flexibility.

Because lithium resources are limited, researchers have developed batteries based on other metals. So far, various types of promising quasi-solid or solid-state metal-based rechargeable batteries have been developed, including alkali metal ions (Li^+, Na^+ and K^+), multivalent metal ions Al^{3+}, Zn^{2+} and Mg^{2+}, and nickel base cells [131]. For example, Kong et al. [121] prepared Ni–Fe battery anode and cathode materials using 3D printed hybrid aerogels as scaffolds. Bi et al. [129] used a combination of mask-assisted jet printing and electrochemical deposition to fabricate cross-type Ag and Zn microelectrodes (Fig. 6e). First, silver ink composed of silver nanoparticles, adhesives and organic solvents is sprayed on polyethylene terephthalate film, and the polyethylene terephthalate film is covered with a shadow mask of the desired shape. After evaporating the organic solvent, a cross-type Ag array was obtained. Highly conductive forked-finger silver arrays were used as cathode materials and coated with polyvinyl alcohol-potassium hydroxide gel electrolytes to obtain quasi-solid-state microbatteries. Compared with other aqueous zinc-based micropower sources, the quasi-solid-state microstrips exhibit superior energy and power densities [129]. In addition, microbatteries of different structures can be fabricated in series or in parallel on different substrates to output higher voltages or currents through internal connections. Furthermore, the microbatteries can maintain stable performance in the bent or cut state. These all illustrate the feasibility of combining tiny batteries with flexible and wear-resistant electronics.

4.1.3 Oxide Electrode Materials

There is no essential difference between the cathode materials used in solid-state lithium batteries and the cathode materials in liquid systems. The material systems involved mainly include LFP, $LiMn_2O_4$ and high-capacity $LiCoO_2$, LTO, $LiNi_{1-x-y}Co_xMn_yO_2$ and $LiNi_{1-x-y}Co_xAl_yO_2$. The most often utilized electrode materials in solid-state printed batteries are LTO and LFP, which have low volume expansion, high-rate capability, high stability, and safety. In recent years, there has been an increasing number of studies on LTO/LFP-based electrode printing.

Clogging of DIW nozzles is usually caused by phase separation of fillers such as Al_2O_3 powder, and thermal annealing and processing solvents inevitably cause severe damage to previously printed bottom layers. As shown in Fig. 7a, in order to maintain their electrochemical performance as well as shape consistency and scalability, Bae et al. [132] designed that all components of the SSB need to be printed sequentially to avoid damaging the underlying layer. Specifically, novel material strategies are proposed to simultaneously provide thixotropic fluid behavior and appropriate viscosity of the printable gel electrolyte to address the aforementioned problems caused by phase separation ceramic additives or slow fabrication processes. The gel polymer electrolyte in the battery is composed of ethoxylated trimethylolpropane triacrylate (ETPTA) and polydimethylsiloxane (PDMS). LFP and LTO slurries with high active material loading were rheologically optimized for printing cathodes and anodes, respectively.

The growing demand for wearable electronics has promoted the development of flexible and wearable energy

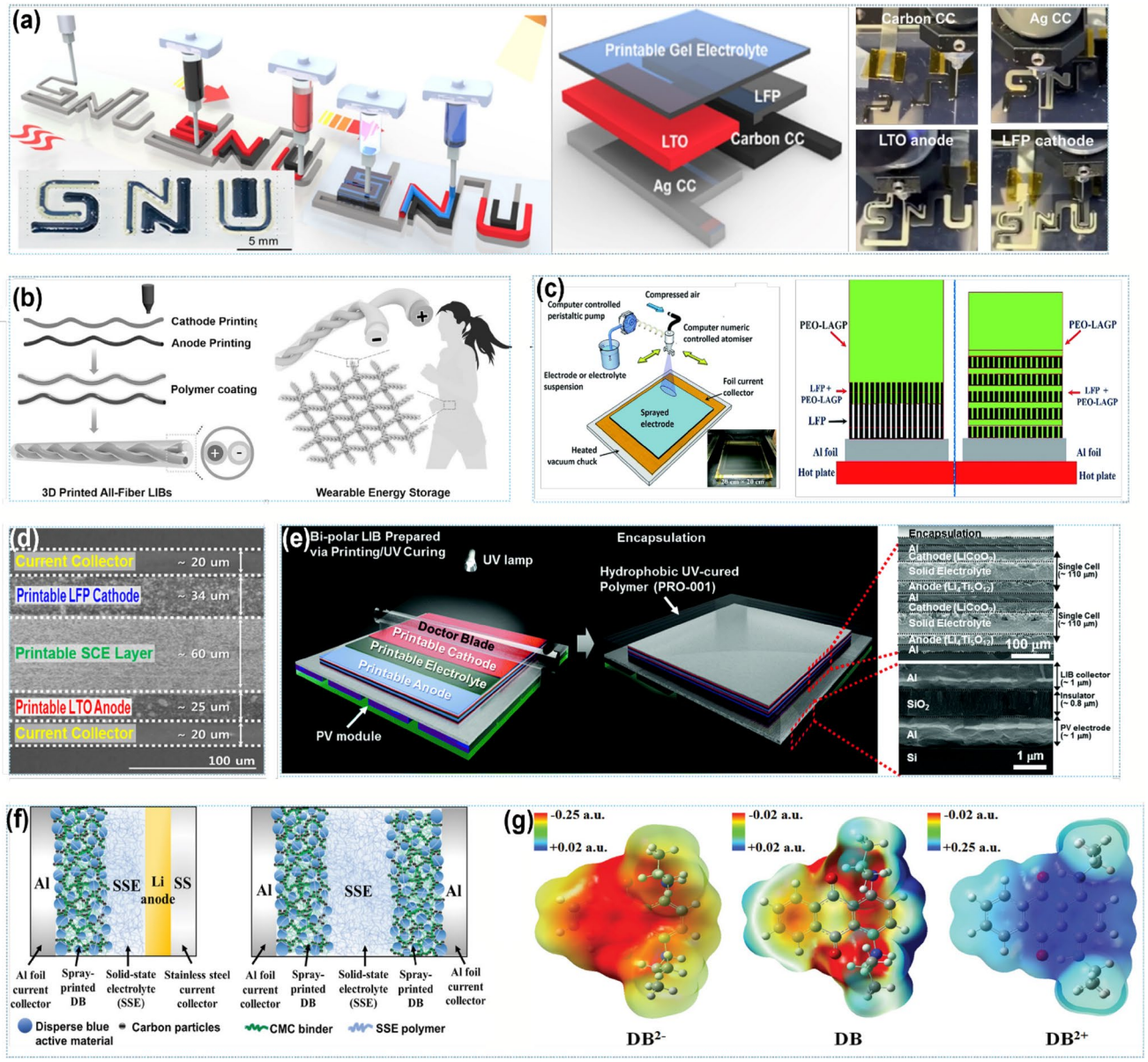

Fig. 7 **a** Scalable and shape-common all-printed SSBs and individual component structures using 3D printing. Reprinted with permission from Ref. [132]. Copyright © 2023, John Wiley and Sons. **b** Schematic diagram of the manufacturing process and wearable applications of 3D printed all-fiber flexible lithium-ion batteries. Reprinted with permission from Ref. [39]. Copyright © 2017, John Wiley and Sons. **c** Spray printed different configurations of LFP layers as well as PEO-LAGP layers. Reprinted with permission from Ref. [108]. Copyright © 2019, Royal Society of Chemistry. **d** SEM image (cross-sectional view) of printable SSBs (LFP cathode, SCE layer, LTO anode). Reprinted with permission from Ref. [134] Copyright © 2015, American Chemical Society. **e** Schematic of the print-based step-by-step fabrication of a solid-state bipolar LIB cell directly on a c-Si PV module, as well as a cross-sectional SEM image of the bipolar LIB cell and a seamless unitized interface between the bipolar LIB cell and the c-Si PV module. Reprinted with permission from Ref. [135]. Copyright © 2017, Royal Society of Chemistry. **f** Schematic diagram of the half- and full-cell (symmetric) configurations of spray-printed electrodes. **g** Mulliken electrostatic potential distributions for the DB molecule in the reduced, neutral and oxidized forms obtained by DFT calculations. (**f, g**) Reprinted with permission from Ref. [101]. Copyright © 2019, John Wiley and Sons

devices. The fabrication of wearable batteries using 3D printing approaches is highly desired because of their capability of printing arbitrary shapes and sizes and configuring multiple materials at different positions as needed. In 2017, Hu and coworkers presented a 3D-printed wearable Li-ion battery with excellent mechanical strength and high flexibility [39]. The active electrode materials of LTO, LFP and PVDF were dissolved in NMP solution to serve as printing inks. PVDF-co-HFP soaked with limited $LiPF_6$ in ethylene carbonate/diethyl carbonate solution was coated on the

surface of printed fibers as quasi-SSEs. Then, the coated anode and cathode fibers were twisted together and packaged with an outer heat shrink tube (Fig. 7b). The surface of the PVDF-co-HFP coated yarn contained lots of pores that could absorb and contain liquid electrolytes locally. In the bending state, the all-fiber battery could power an LED lightening for several minutes, exhibiting excellent flexibility and stability of the structure. Furthermore, due to its superior flexibility, the printed fibers can be woven into fabrics for wearable energy devices. The all-fiber battery displayed a discharge specific capacity of about 110 mAh g^{-1} at 50 mA g^{-1} and a Coulombic efficiency of 93%, respectively. This research demonstrates a cost-effective method of producing all-fiber Li-ion batteries and provides new possibilities for future wearable electronic applications. Rodriguez et al. [133] demonstrated that aerosol jet-printed LFP cathodes have about 10 mAh g^{-1} higher capacity per cycle than standard tape-cast electrodes at the same mass loading and electrode thickness. Rate-capacity testing showed that these gains in achievable capacity occurred mainly at high current densities, suggesting improved lithiation kinetics for the AJP cathode. Studies have shown that AJP cathodes contain large electrolyte conducting channels near the electrode surface that taper into the bulk. Even though the pore volume was reduced by 55% by calendering, remnants of these channels remained. The unique cathode structure of the AJP electrode enables a 30% increase in the electrochemically active surface area compared to the tape-cast electrode.

Bu et al. [108] investigated a co-spray printing method to print a thin layer of honeycomb LFP cathode material inlaid with a mixed electrolyte layer (Fig. 7c). Honeycomb electrodes with staggered solid electrolyte sublayers improve interfacial contact between electrodes. The honeycomb interleaved electrodes also exhibited the best performance in terms of capacity and cycling stability at all tested temperatures when combined with lithium foils in solid-state lithium-ion battery configurations. Kim et al. [134] used a stencil printing technique to print the LTO anode paste on an aluminum current collector, which was then exposed to UV radiation for a short period of less than 30 s. Subsequently, a thin layer of printable solid-state composite electrolyte was introduced on the LTO anode through the same stencil printing and UV-curing process. Then, the LFP cathode paste was directly printed on the solid-state composite electrolyte layer/LTO anode unit and subjected to UV irradiation. After placing the Al current collector on top of the printable LFP cathode/printable solid-state composite electrolyte layer/printable LTO anode assembly, a fully integrated multilayer structure battery was ultimately obtained (Fig. 7d).

The combination of energy production and energy storage systems is the ultimate solution to meet the growing demand for high energy density power sources. Um et al. [135] demonstrated a novel monolithically integrated, light-rechargeable portable power source based on miniature crystalline silicon photovoltaics and printed solid-state lithium-ion batteries (Fig. 7e). A solid-state LIB with a bipolar cell configuration is fabricated directly on the aluminum electrodes of miniature crystalline silicon photovoltaic modules via a tandem printing process, enabling seamless architectural/electrical connection of two different energy systems. To prepare the electrode slurry, the electrolyte precursor mixture consists of UV-curable ethoxylated trimethylolpropane triacrylate monomer and high-boiling electrolytes, mixed with electrode active materials: the cathode material is $LiCoO_2$, and the anode material is LTO. The LTO anode paste was printed on the aluminum electrodes of Si photovoltaic modules using a stencil printing technique, and then exposed to UV light for a short period of time for less than 30 s. Using the same stencil printing and UV curing process, $LiPF_6$ was introduced on the surface of the LTO anode to form a thin solid electrolyte. Then, the LCO cathode paste was directly printed on the solid electrolyte layer/LTO anode unit and exposed to UV light irradiation. After placing an aluminum current collector on the printed LCO cathode/printed SCE layer/printed LTO anode assembly, a solid-state LiB unit cell was obtained.

The surface chemistry of the active material, the concentration and type of conductive additives, polymer loading, and solvent play an important role in forming the electrode microstructure. Shen et al. [102] utilized ink engineering to enhance the performance of composite electrodes in SSBs. By tuning the ternary component interactions within the ink (polymer, solvent, active material), the capacity of the LTO anode is increased by 3–4 times. They demonstrate that the choice of solvent and binder can significantly alter the battery performance of the studied configurations. Less agglomeration in the electrode and better contact between the cathode and electrolyte are achieved, leading to spatially uniform Li^+ flux and uniform distribution of local current density. Ink engineering has been shown to significantly increase the capacity of LTO/Li half-cells. A combination of ink engineering and interfacial modification routes is proposed for scalable production of high-performance SSBs.

4.1.4 Other Electrode Materials

In addition to the above-mentioned common electrode materials, some researchers also use organic compounds as electrodes [101, 136]. In general, the dissolution of organic molecules in contact with the electrolyte can be partially improved by polymerizing the monomer molecules or/and using SSEs. Unpolymerized benzoquinone small molecules exhibit reasonable energy storage properties when using as SSEs, which is beneficial because monomeric organic electrodes tend to have higher electrode potentials and electronic conductivities than polymer electrodes. However, it

is well known that the typical disadvantages of SSEs compared with liquid electrolytes are low ionic conductivity and increased and variable interfacial contact resistance, limiting the penetration of electrode structures. To address these issues, Leung et al. [101] introduced a layer-by-layer spray technique as a route to fabricate porous organic electrodes based on widely available low-cost quinoid dye molecules with controlled thickness (Fig. 7f, g). Half-cell and full-cell solid-state configurations were evaluated at different C rates at ambient temperature using a range of electrochemical techniques. To date, this work is the first to report the performance of a symmetric SSB based entirely on organic electrode and electrolyte materials at voltages in excess of 1 V.

In terms of electrodes for printed SSBs, in addition to the traditional transition metal oxides and graphite electrodes, a series of high-performance cathode and anode materials are also being developed for printing SSB electrodes, including high-voltage oxide cathodes, high-capacity sulfide cathodes, and composite negative electrodes with good stability. Although there is no side reaction of decomposition of solid electrolytes at the interface of solid electrolytes and electrode materials, the compatibility of the electrode/electrolyte interface is poor due to the solid characteristics, and the interface impedance is too high, which seriously affects the ion transfer, and ultimately leads to the low cycle life and poor rate performance of solid batteries. In addition, the energy density of battery component materials cannot meet the requirements of large-scale batteries. Research on printed electrode materials focuses on two aspects: firstly, modification of electrode materials and their interfaces to improve electrode/electrolyte interface compatibility; secondly, development of new electrode material inks to further enhance the electrochemical performance of SSBs; finally, the combination of ink engineering of electrodes and interfacial modification routes for scalable production of high-performance SSBs.

4.2 Electrolytes

The goal of developing printed SSEs technology is to make it successfully applied to printed SSBs, which is essential for achieving high safety, higher energy/power density, and long-cycle performance [17]. Its scientific advancement has a direct impact on the SSB manufacturing process [137]. Solid electrolytes now face several challenges, including low ionic conductivity and high interfacial resistance at ambient temperature, as well as poor interfacial stability between active materials and solid electrolytes during circulation. Recently, increasing attention has been focused on the preparation of high-performance electrolytes with high ionic conductivity, low activation energy, and low electronic conductivity [138]. There are many types of solid electrolytes, mainly solid inorganic electrolytes [26, 81, 100], solid polymer electrolytes [139, 140] and solid composite electrolytes [88, 93]. Inorganic SSEs are characterized by high modulus and often fail to provide good interfacial contact when matched with electrodes, especially for lithium metal electrodes [141]. Poor interfacial contact can significantly increase the interfacial impedance during battery cycling [27]. Furthermore, when an inorganic solid electrolyte is matched with a high-voltage cathode, side reactions are prone to occur at the interface of electrode, resulting in poor interface stability and a negative impact on battery kinetics. Polymer electrolytes, on the other hand, are softer, lighter, and easier to match with electrodes than inorganic solid electrolytes, and their electrode affinity is significantly superior to inorganic ceramics [142]. Furthermore, most polymer electrolytes are flexible and expandable, which is conducive to practical battery manufacturing. However, polymer electrolytes generally have low lithium ion mobility, which results in a much lower electrical conductivity than that of conventional organic liquids, which also limits the wide application of polymer electrolytes [143]. At the same time, the heat resistance and mechanical properties of the polymer electrolyte are low, which makes it impossible for a single polymer electrolyte to completely prevent the growth of lithium dendrites and ensure the safety performance of the battery when used in the field of lithium metal batteries [144]. Therefore, in order to make full use of the respective advantages of inorganic and polymer electrolytes and avoid their respective defects, inorganic and polymer electrolytes are usually compounded by various methods to develop solid-state composite electrolytes [145].

Solid electrolytes that can be used in SSBs need to meet the following performance requirements.

1. High ionic conductivity. The ionic conductivity directly affects the bulk resistance of the battery. For solid electrolytes, the ionic conductivity is generally required to reach 10^{-4}–10^{-3} S cm^{-1}.
2. The higher Li^+ migration number. Ideally, the number of transitions is 1. If the migration number is too low, anions will be enriched on the electrode surface, the concentration polarization of the battery will be aggravated, and the impedance will increase.
3. Excellent chemical, electrochemical and thermal stability. It has stable chemical properties with metal lithium and cathode materials, does not react with water, carbon dioxide, has a high electrochemical decomposition potential (> 4.5 V vs. Li^+/Li), and has a thermal expansion coefficient that matches the electrode and high temperature thermal stability.

4. Certain mechanical strength. The growth of lithium dendrites is inhibited, and at the same time, it can meet the needs of solid-state lithium battery assembly.

With the advancement of printing technology, the battery's electrolyte can also be printed directly, reducing manufacturing procedures, time, and costs. Printed SSEs have received rapidly growing attention due to urgent process upgrades. Up to now, various types of printable SSEs have been investigated (Table 1). Nonetheless, the understanding of printed electrolytes for interfacial reactions and battery structure and performance is still at an early stage. In this section, we summarize and discuss current electrolytes for printed SSBs based on the above SSEs classification.

4.2.1 Inorganic Solid Electrolyte

High ionic conductivity and hardness characterize inorganic electrolytes, yet they are brittle and have a high interfacial impedance with electrodes [145]. Inorganic solid electrolytes can also support battery operation at low and high temperatures (for example, from − 50 to 200 °C or higher), where conventional liquid electrolytes would freeze, boil, or decompose. The low activation energy of fast ionic conductance helps to reduce the variation of ionic conductance with temperature and ensures the reliability of the work. Furthermore, solid materials are not expected to exhibit bulk polarization due to the invariance of the anionic framework, which may lead to higher power capacity [151]. Inorganic solid electrolytes can be mainly divided into oxide electrolytes and sulfide electrolytes. According to the material structure, oxide solid electrolytes can be divided into two types: crystalline and glassy (amorphous). Crystalline electrolytes include garnet-type solid electrolytes [66], perovskite-type $Li_{3x}La_{2/3-x}TiO_3$, NASICON type $Li_{1+x}Al_xTi_{2-x}(PO_4)_3$ and $Li_{1+x}Al_xGe_{2-x}(PO_4)_3$, and glassy electrolytes include anti-perovskite $Li_{3-2x}M_xHalO$ electrolytes and thin-film solid electrolytes lithium phosphorus oxynitride (LiPON).

Oxide solid electrolytes have high chemical stability and can exist stably in the atmospheric environment, which is conducive to the large-scale production of all-SSBs. The current research focus is on improving the room temperature ionic conductivity and its compatibility with electrodes. The current methods to improve ionic conductivity are mainly element replacement and heterovalent element doping. Furthermore, electrode compatibility is a significant concern that limits its utilization. The interface formed by the poor contact between the electrode and the electrolyte and the bulk resistance formed by the thicker electrolyte will lead to a higher resistance of the SSB [152]. Typically, flat particle solid electrolytes with planar interfaces are developed to minimize the interfacial contact area. The distinguishing feature of 3D printing is its ability to quickly explore different structure–property relationships

Table 1 Summary of the basic properties of SSEs. Data are extracted from different sources, and thus are with different significant digits

Classification	Composition	Symmetry	Ionic conductivity/(S cm^{-1})	*T* (measurement temperature)	Activation energy	References
Inorganic electrolyte	$Li_7La_3Zr_2O_{12}$	Cubic	0.5×10^{-4}	25 °C	–	[26]
	$Li_{6.5}La_3Zr_{1.5}Ta_{0.5}O_{12}$	Cubic	1×10^{-3}	RT	0.34	[100]
	$Li_{1.3}Al_{0.3}Ti_{1.7}(PO_4)_3$	Rhombohedral	4.24×10^{-4}	25 °C	–	[81]
	Nb doped $Li_7La_3Zr_2O_{12}$	–	2×10^{-6}	25 °C	60 kJ mol^{-1}	[66]
	$Li_{1+x}Al_xTi_{2-x}(PO_4)_3$	–	1.2×10^{-4}	RT	–	[146]
Organic polymers	PEO-LiTFSI	–	2.18×10^{-3}	90 °C	–	[84]
	PEO-CTA	–	3×10^{-4}	22 °C	–	[147]
	PEO-SCN-LiTFSI	–	3.7×10^{-4}	25 °C	0.037 eV	[89]
	PEO-LiDFOB	–	7×10^{-4}	45 °C		[72]
	ETPTA-DADMA	–	1.2×10^{-3}	RT	–	[139]
	ETPTA-PDMS	–	6.25×10^{-3}	RT	–	[132]
	EMS-TEGDME	–	4.3×10^{-4}	RT	–	[48]
Composite electrolyte	Epoxy-$Li_{1.4}Al_{0.4}Ge_{1.6}(PO_4)_3$	–	1.6×10^{-4}	RT	36.7 kJ mol^{-1}	[88]
	PEO-ZIF67	–	2.94×10^{-4}	60 °C	0.36 eV	[148]
	PEO-LLZO-LiTFSI	–	1.6×10^{-4}	70 °C	0.56 eV	[93]
	PEO-S-hBN/TEGDME	–	0.49×10^{-4}	RT	–	[149]
	PVDF-co-HFP	–	0.78×10^{-3}	RT	–	[82]
	ETPTA-DADMA-Ti-SiO_2@Al_2O_3	–	0.4×10^{-3}	RT	–	[150]

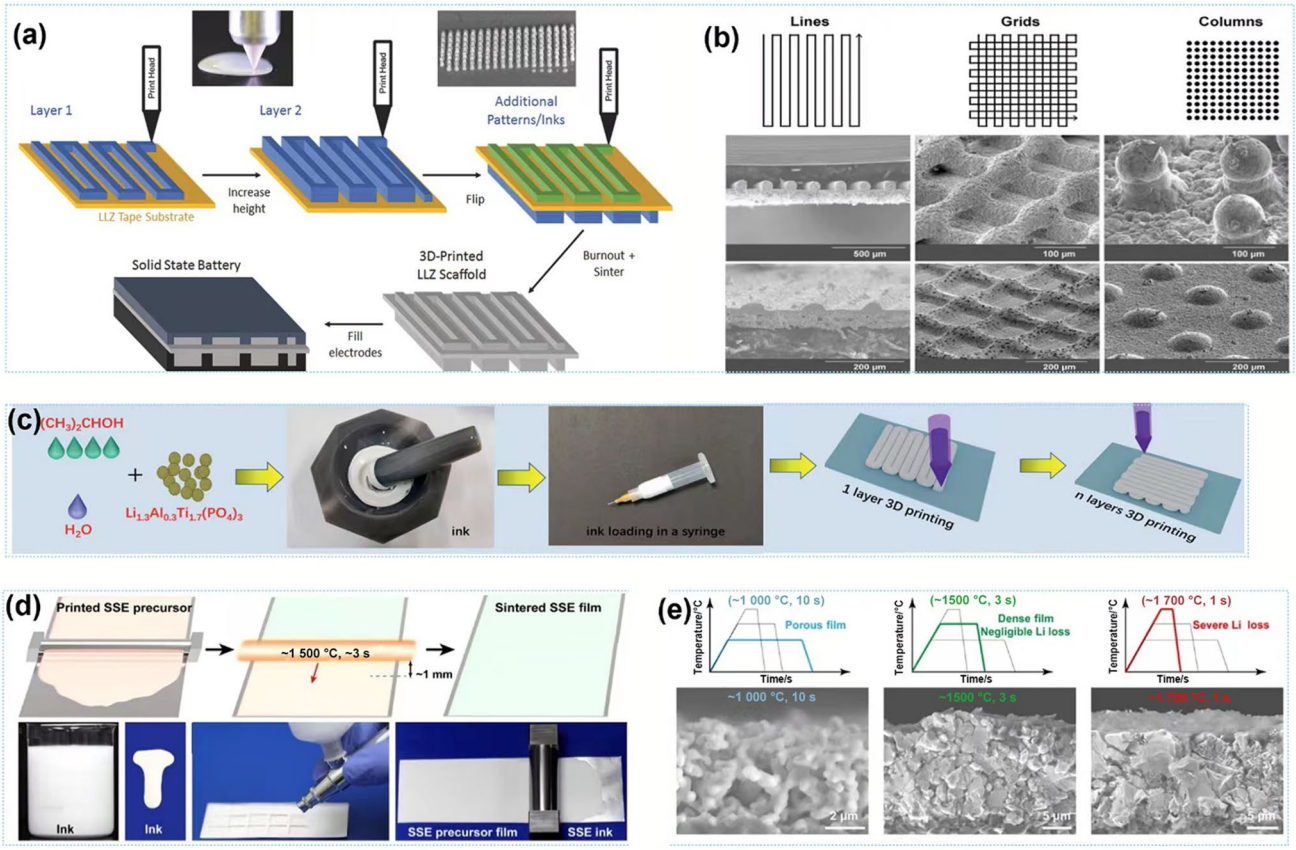

Fig. 8 **a** Schematic of the process to 3D-print solid electrolyte structures. **b** Diagrams and SEM images of 3D-printed LLZ microstructures comparing the 3D-printed conformal and self-supporting inks after sintering, including line, grid, and column patterns. (**a, b**) Reprinted with permission from Ref. [26]. Copyright © 2018, John Wiley and Sons. **c** Schematic of DIW printing procedure of LATP ceramic SSEs. Reprinted with permission from Ref. [81]. Copyright © 2021, John Wiley and Sons. **d** Schematic of the film printing technique, and ink preparation, ink properties, and printing of SSE precursor inks by the squeegee method. **e** Schematic and cross-sectional morphology of printed SSE films with scalability and flexibility as well as LLZTO garnet films sintered at different temperatures and times. (**d, e**) Reprinted with permission from Ref. [100]. Copyright © 2020, Science

over a wide range of lengths. Solid electrolyte microstructures formed by 3D printing can rapidly study the interface structure-performance relationship in solid electrochemical devices. McOwen et al. [26] developed various ink formulations and printed thin, non-planar, and complex-structured $Li_7La_3Zr_2O_{12}$ solid electrolytes with different properties by 3D printing technology (Fig. 8a, b). The area specific resistance of the 3D printed symmetric Li|$Li_7La_3Zr_2O_{12}$|Li battery is very low in the electrochemical cycle test. Through 3D printing technology to further optimize the structure of SSEs, the research shows that the specific resistance per unit area of the SSB can be significantly reduced, and the energy density and power density of the battery can be improved. Liu et al. [81] printed $Li_{1.3}Al_{0.3}Ti_{1.7}(PO_4)_3$-based hybrid solid-state electrolytes on LFP cathodes by DIW, which can easily achieve various shapes without sacrificing high ion transport performance (Fig. 8c). The printed free-standing $Li_{1.3}Al_{0.3}Ti_{1.7}(PO_4)_3$ ceramic solid electrolyte has a high ionic conductivity of 4.24×10^{-4} S cm^{-1} and a discharge capacity of 150 mAh g^{-1} at 0.5 C. The battery exhibits good cycling stability in the cycling test at 60 °C. The DIW strategy of SSEs demonstrates a new avenue for advanced solid-state energy storage with high ion transport and custom fabrication.

Synthesis of ceramic SSE thin films based on traditional processes usually requires sintering at high temperatures (from 600 to 1 100 °C) for several hours to obtain the crystal structure required for high ionic conductivity. However, prolonged sintering also leads to severe Li and Na loss and correspondingly low ionic conductivity due to the volatility of these light elements at high temperatures [17]. In order to solve the above problems, Ping et al. [100] developed a printing and radiant heating method to synthesize ceramic solid electrolyte films directly from precursors, followed by rapid (~3 s) high temperature (~1 500 °C) reaction sintering (Fig. 8d, e). In a typical process, precursor films are printed on substrates of precisely tunable thickness by controlling ink concentration and wet thickness. The air-dried precursor

films were then brought into intimate contact with a radiant heating tape (typically ~ 1 500 °C) for rapid proximity sintering (Fig. 8e). This joule-heated tape is passed through the precursor film with a gap of about 0.5 mm and a total heating duration of a few seconds to complete the sintering process, potentially enabling reel-to-reel processing. This rapid heating enables the formation of dense polycrystalline film structures with negligible loss of volatile elements due to the short sintering time. The sintered $Li_{6.5}La_3Zr_{1.5}Ta_{0.5}O_{12}$ solid electrolyte film has a dense, uniform structure and excellent ionic conductivity (1 mS cm^{-1}). Furthermore, the fabrication time from precursor to final product is typically ~ 5 min, which is 10 to 100 times faster than conventional SSE synthesis. This printing and rapid sintering process also allows multilayer structures to be fabricated layer-by-layer without cross-contamination. The printing and radiant heating technology can be easily extended to other thin-film SSEs, opening unprecedented opportunities in developing safe, high-performance SSBs and other thin-film devices.

In comparison to oxide solid electrolytes, sulfide solid electrolytes (such as Li_6PS_5Cl) offer higher ionic conductivity, lower grain boundary resistance, and a larger oxidation potential [153]. It is due to the huge ionic radius and strong polarization of sulfur, which allows it to form larger lithium ion transport channels [153, 154]. The lower electronegativity of sulfur than oxygen weakens the bonding of lithium ions to adjacent skeletal structures and increases the concentration of free lithium ions. Sulfide electrolytes have superior chemical and electrochemical stability because numerous main group elements can form stronger covalent bonds with sulfur, resulting in a more stable sulfide that does not react with lithium metal. Sulfide solid electrolytes are classified into sulfide crystalline solid electrolytes, sulfide glass and glass–ceramic solid electrolytes according to their crystal types. However, there are still no reports on the use of sulfide solid electrolytes made by the printing process for SSBs. It may be that sulfide solid electrolytes are prone to side reactions with air, water, etc. [155], and many challenges still need to be overcome in the process.

4.2.2 Polymer Solid Electrolyte

Polymer solid electrolyte (SPE), composed of polymer matrix (such as polyester, polase and amine) and lithium salts (such as $LiClO_4$, $LiAsF_4$, $LiPF_6$ and $LiBF_4$), has attracted extensive attention due to its light weight, good viscoelasticity and excellent machining performance [156]. Compared with inorganic SSEs, polymer SSEs are flexible and make good interfacial contact with electrodes. At the same time, they have good electrochemical stability and are easy to process and prepare [142]. Polymer electrolytes generally have low elastic moduli and are therefore very suitable for flexible batteries. Good safety performance, low mass density, and high shear modulus make it an important application prospect in the field of lithium metal batteries. PEO, polyacrylonitrile (PAN), polyvinylidene fluoride (PVDF), polymethyl methacrylate (PMMA), polypropylene oxide (PPO), polyvinylidene chloride (PVDC), and other single-ion polymer electrolytes have been used as SPEs in the past [144]. However, ion transport in solid polymer electrolytes mainly occurs in the amorphous region, and the high crystallinity of unmodified polymer electrolytes at room temperature results in low ionic conductivity, which has a significant impact on the high-current charge–discharge capability. Researchers improved the movement ability of polymer chain segments by reducing the crystallinity, thus improving the conductivity of the system [144]. The simplest and most effective method was to conduct inorganic particle hybrid treatment on the polymer matrix. The addition of these inorganic particles disturbs the order of polymer chain segment in matrix and reduces its crystallinity [157]. The interaction between polymer, lithium salt and inorganic particles increases the lithium ion transport channel and improves the conductivity and ion migration number. Inorganic fillers can also adsorb trace impurities in the composite electrolyte and improve the mechanical properties.

In addition to employing polymers as electrolytes to alleviate the problem of interface impedance in SSBs, the contact area can also be enhanced by using three-dimensional structural components in batteries. He et al. [89] fabricated a solid polymer electrolyte by the SLA printing process (Fig. 9a), combining polyethylene glycol diacrylate with 1 wt% (wt% means the weight percentage) phenylbis (2,4,6-trimethylbenzoyl)phosphine oxide, succinonitrile and LiTFSI were mixed in a mass ratio of 1.5:1.0:1.4 to prepare polyethylene glycol giacrylate precursor. A cross-linked PEO with three-dimensional archimedes spirals was then printed by the SLA process. During the printing process, according to the designed model, a laser with a wavelength of 355 nm passes through the surface of the filament, and after each layer is cured, the stage moves down. The resulting solid polymer electrolyte replicates the designed geometry on a flat substrate with a thickness of 100 μm, with spiral walls of 100 μm in width, 150 μm in height, and 200 μm in pitch. The three-dimensional archimedes helical solid-phase extraction is rationally designed, which shortens the transport path of lithium ions from the electrolyte to the electrode, enhances the interfacial adhesion, and increases the mass loading of active materials. The battery exhibits an ionic conductivity of 3.7×10^{-4} S cm^{-1} at 25 °C, decreased interfacial impedance after 250 cycles and a high specific capacity of 128 mAh g^{-1}. To achieve precise nanostructure control, Lee et al. [147] reported the fabrication of solid polymer electrolytes consisting of nanoscale ion-conducting channels embedded in a rigid crosslinked polymer matrix by light-mediated 3D printing. The robust solid polymer electrolyte has an ionic

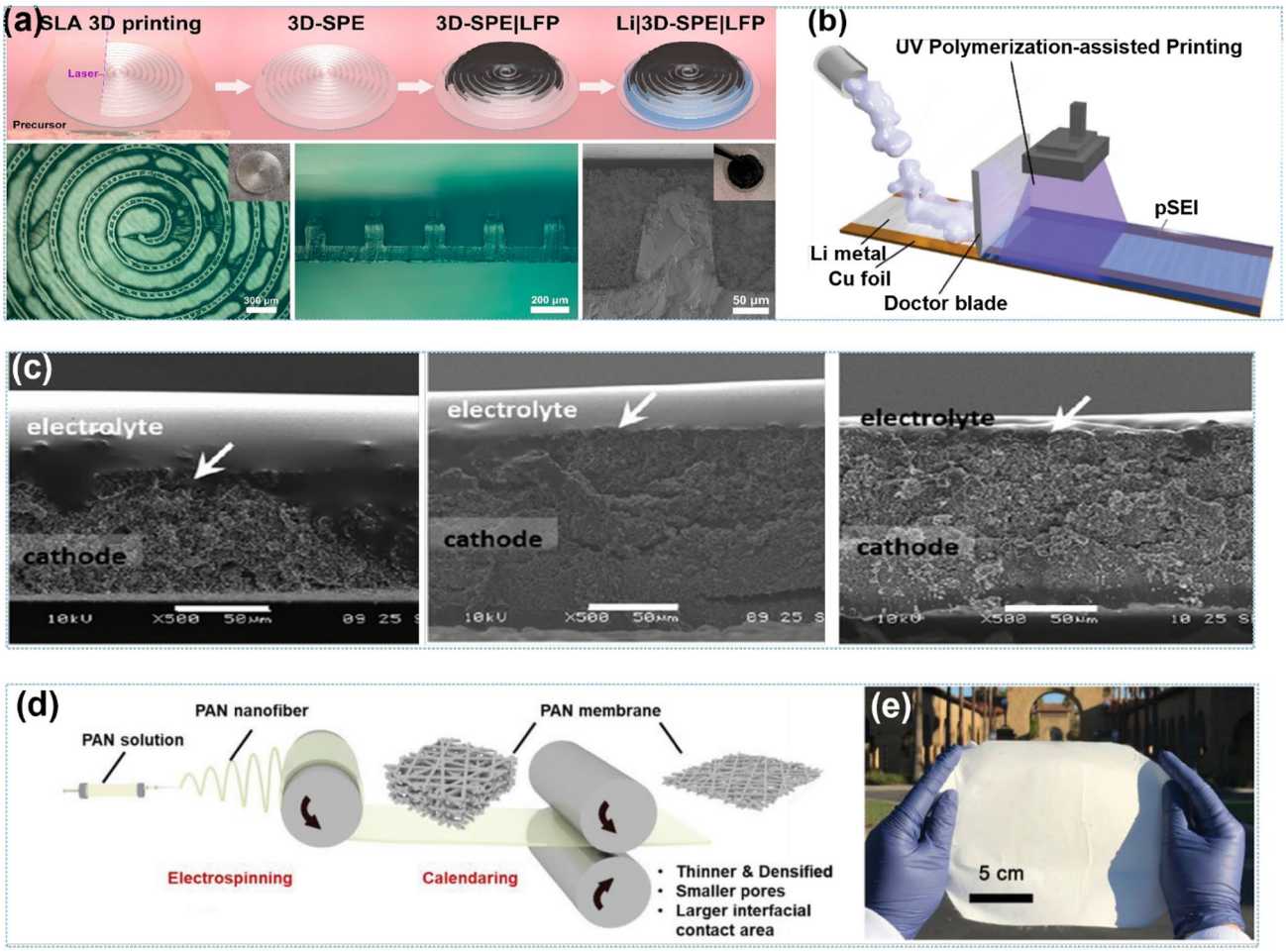

Fig. 9 **a** Schematic illustration of processing and morphology of solid polymer electrolyte. Reprinted with permission from Ref. [89]. Copyright © 2020, American Chemical Society. **b** Schematic illustration depicting the direct printing-driven fabrication procedure of the printable solid electrolyte interphase mimic. Reprinted with permission from Ref. [139]. Copyright © 2020, John Wiley and Sons. **c** Cross-sectional SEM images of aerosol jet printed solid polymer composite electrolytes with different number of prints. Reprinted with permission from Ref. [72]. Copyright © 2019, John Wiley and Sons. **d, e** Schematic diagram of PAN film preparation and photo of PAN film. Reprinted with permission from Ref. [140]. Copyright © 2022, John Wiley and Sons

conductivity as high as 3×10^{-4} S cm^{-1} at room temperature. Li metal electrodes often exhibit poor oxidation stability after exposure to humid environments, which is a must for practical applications.

Despite the growing demand for lithium metals as anode for SSBs, little attention has been paid to their oxidative stability, which must be achieved for practical applications. It is necessary to make thin lithium metal electrodes exhibit excellent oxidation stability and reliable full-cell performance after exposure to humid environments, which is driven by chemical/structural uniqueness. Cho et al. [139] fabricated a polymer SSE for oxidation-resistant lithium metal electrodes by UV polymerization-assisted printing on lithium metal electrodes (Fig. 9b). This solid polymer electrolyte is a UV polymerized ETPTA and diallyldimethylammonium bis(trifluoromethanesulfonyl)imide (DADMA-TFSI) based, where ETPTA (as an organic mimetic) and DADMA-TFSI (as an inorganic mimetic) provide moisture resistance and high Li-ion transport (1.2×10^{-3} S cm^{-1}) and high Li-ion migration numbers (0.69), respectively. The solid polymer electrolyte enables thin lithium metal electrodes to exhibit excellent antioxidative stability and reliable full-cell performance after exposure to humidity.

Various printing technologies have their own advantages and disadvantages. In order to explore the application of aerosol jet printing technology in solid electrolytes, Deiner et al. [72] used the AJP technique for the first time to deposit directly a polymer SSE on an LFP cathode substrate (Fig. 9c). The AJP electrolyte composed of PEO, lithium difluoro(oxalate)borate, and alumina nanoparticles is smooth, conformal, and non-porous. The ionic conductivity

of the printed solid polymer electrolyte PEO/LiDFOB/Al_2O_3 (EO:Li = 10:1) at 45 °C was > 1×10^{-5} S cm^{-1}. In the half-cell structure, the cells with this printed electrolyte were discharged at C/15 with a capacity of > 85 mAh g^{-1} at 45 °C and > 160 mAh g^{-1} at 75 °C. It was found that the geometry and transport properties of the aerosol jet-printed solid polymer composite electrolyte layer were sensitive to the ink formulation, mainly the chemistry of the lithium salt anion, and secondarily the EO:Li ratio. The realization of AJP of solid polymer composite electrolytes opens a path for the large-scale fabrication of solid-state lithium-ion batteries.

Ultrathin and lightweight solid electrolytes are necessary to obtain energy densities comparable to or greater than liquid electrolyte batteries. Cui and co-authors [140] reported a novel scalable, ultra-thin and high temperature resistant solid state polymer electrolyte for SSBs. The preparation process of the ultra-thin solid-state polymer electrolyte is shown in Fig. 9d, e. PAN films can be prepared in a scalable and roll-to-roll manner using electrostatic spinning and subsequent calendering. The roll-to-roll approach enables the PAN films to be thinner and denser, resulting in smaller pores and providing a larger interfacial contact area with the electrodes. The results show that symmetrical cells can provide over 300 h of cycling capability at 0.5 mA cm^{-2}. SSBs fabricated with only 5 µm-thick lithium PAN-PEO/bis(trifluoromethanesulfonyl) imide reach 300 cycles at 60 °C at a rate of 0.3 C. The design extends cell operation to 120 and 150 °C for 500 cycles at a C/2 rate and 100 cycles at a 2 C rate, respectively.

4.2.3 Composite Solid Electrolyte

Inorganic-polymer composite electrolytes combine the advantages of inorganic and polymer solid electrolytes, making them particularly suitable for the mass production of SSBs [145]. Compared with pure polymer solid electrolytes, composite solid electrolytes have lower melting temperature and glass transition temperature [145]. In general, ion transport in organic–inorganic composite solid electrolyte is accomplished through the amorphous region of the polymer. The introduction of filler and the increase of lithium content can increase the proportion of amorphous region of the composite electrolyte to promote ion transport [158]. The presence of fillers can not only improve the ionic conductivity and mechanical properties of the electrolyte, but also achieve stable compatibility between the electrolyte and the lithium anode. For example, Xia and coworkers [148] developed a PEO/MOF hybrid SSE with effective dendrite suppression via a room-temperature 3D printing strategy. As the porous ZIF-67 filler facilitates the uniformity of Li deposition and the formation of mesophase, the as-prepared hybrid SSE shows enhanced dendrite suppression, which further improves Li^+ migration and comprehensive performance in the PEO chains. Li//Li symmetric cells with the obtained electrolyte can withstand lithium metal plating/stripping at 0.1 mA cm^{-2} for more than 950 h without short circuiting. The battery assembled with the LFP cathode maintained a capacity retention of 95% after 100 cycles at 0.2 C. The authors also incorporated other MOF (including MOF-74, UIO-66, ZIF-8) packing materials to demonstrate the generalizability of the method.

Typically, composite electrolytes are formed by mechanically random mixing of ceramic and polymer electrolytes. Some studies have shown that the alignment of ceramic nanowires perpendicular to the electrode shows a greater increase in overall conductivity than randomly embedded particles, mainly due to the enhanced conduction of space charge alignment along the ceramic/polymer interface [159, 160]. Zekoll et al. [88] invoked printing techniques to control ceramic-polymer ratios and 3D structures to form structured hybrid electrolytes that contain 3D ordered bicontinuous interlocking channels: one filled with a ceramic electrolyte to ensure a continuous channel for ion transport through the electrolyte, and the other filled with an electrically insulating polymer to tune mechanical properties. This 3D channel connectivity maximizes the possibility of interrupting alternative paths of surrounding currents. Figure 10a shows the fabrication process of the hybrid electrolyte with 3D bicontinuous microstructure. Briefly, SLA was first used to fabricate cubically designed polymer templates with many empty channels. Then, the inner voids of the polymer template were filled with ceramic lithium-ion conductor $Li_{1.4}Al_{0.4}Ge_{1.6}(PO_4)_3$ powder. Next, the filled template was burned in air to remove the polymer template and sinter the $Li_{1.4}Al_{0.4}Ge_{1.6}(PO_4)_3$ phase, thereby forming a structured $Li_{1.4}Al_{0.4}Ge_{1.6}(PO_4)_3$ scaffold. The original space of the polymer template is eventually occupied by the insulating polymer, forming a hybrid electrolyte with 3D bicontinuous ceramic and polymer microchannels. Using this method, different microarchitectures can be created by SLA. The high porosity of the 3D printed template (up to 85%) allows the ionically conductive ceramic to cover majority of the volume, resulting in good ionic conductivity of the hybrid electrolyte. After optimization, the hybrid $Li_{1.4}Al_{0.4}Ge_{1.6}(PO_4)_3$-epoxy electrolyte exhibits higher electrical conductivity (1.6×10^{-4} S cm^{-1}) and enhanced mechanical properties, addressing the key challenges of all-SSBs. Figure 10b shows the stress–strain curves obtained for the three sample types in the strain rate control measurements, starting from the contact of the support pin with the sample. The bending of the sample is observed as a linear stress–strain dependence. 3D printing of solid electrolytes enables the fabrication of electrodes and electrolytes with unique structures, whereas traditional molding and tape casting methods are limited to random porosity and planar geometries.

To advance the large-scale fabrication of SSBs, Baade et al. [93] propose curtain coating as a method to fabricate composite SSEs at coil speeds exceeding 80 m min^{-1} in a roll-to-roll process (Fig. 10c, d). As shown in Fig. 10e, rheological measurements indicated that the slurry exhibited

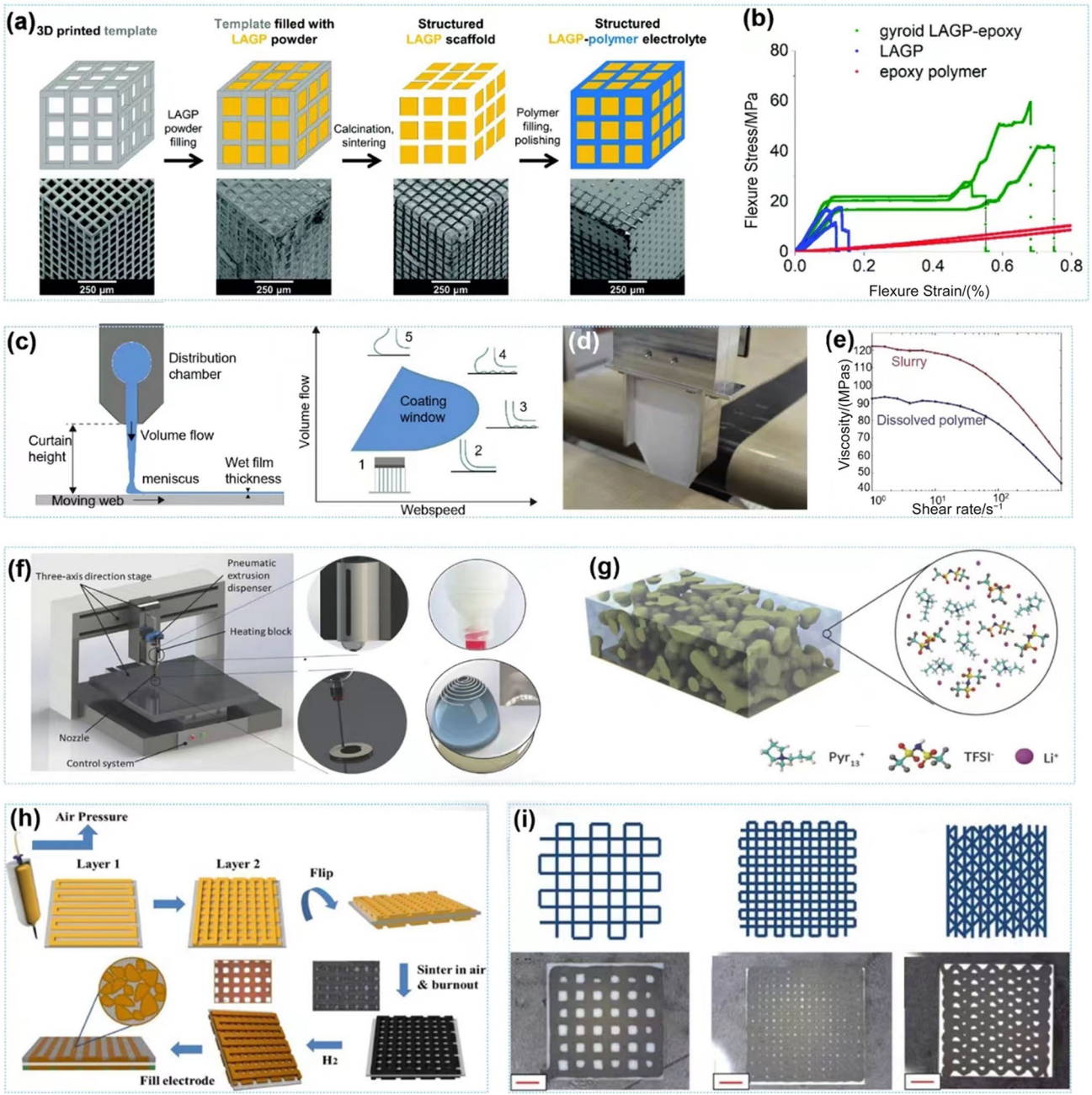

Fig. 10 **a** Schematic diagram of the template procedure used to synthesize the structured hybrid electrolyte, and corresponding SEM images of each synthesis stage of the LAGP-epoxy electrolyte. **b** Stress–strain curves obtained from four-point bending of LAGP, epoxy polymer and gyroid LAGP-epoxy electrolytes. (**a, b**) Reprinted with permission from Ref. [88]. Copyright © 2018, Royal Society of Chemistry. **c** Schematic diagram of curtain and uniform coating and the curtain situation corresponding to different volume flow rates. **d** Photographs of the stabilization curtain of the composite solid electrolyte in acetonitrile and the rheological properties of the slurry and PEO (without LLZO) in acetonitrile. **e** Stress–strain curves obtained from four-point bending of LAGP, epoxy polymer and gyroid LAGP-epoxy electrolytes. (**c–e**) Reprinted with permission from Ref. [93]. Copyright © 2021, Elsevier. **f, g** Schematic diagram of high temperature DIW system and solid electrolyte ink manufacturing process and solid electrolyte structure. Reprinted with permission from Ref. [82]. Copyright © 2018, John Wiley and Sons. **h** Schematic detailing the DIW process for patterning Cu scaffolds directly onto the LATP electrolyte. **i** Diagram of the printed pattern and the scaffolds with different line spacing and pores after heat treatment in air. (**h, i**) Reprinted with permission from Ref. [146]. Copyright © 2021, Elsevier

shear-thinning behavior and a viscosity of 60 mPas at a shear rate of 1 000 s^{-1}. The approach can produce consistent electrolyte membranes with thicknesses of less than 15 μm and is compatible with existing lithium-ion battery electrode production facilities. The solid electrolyte in this experimental system is: aluminum-doped lithium lanthanum zirconate and PEO (a mass ratio of 4.45:1.00) and bis(trifluoromethanesulfonimide) lithium salt (an EO: after mixing with Li molar ratio of 10.4:1.0), LLZO and PEO salts (an EO: Li molar ratio of 10.4:1.0) were prepared. To form the slurry, LLZO, PEO and LiTFSI were mixed in anhydrous acetonitrile (17.5% solids). The study shows that the conductivity increases from 3×10^{-6} S cm^{-1} at 20 °C to 1.6×10^{-4} S cm^{-1} at 70 °C with increasing temperature, and the 13.8 mm and 27.8 mm thick films exhibit the same conductance rate, indicating that the preparation process is uniform at different web speeds. The activation energies of the lithium transition are 0.83 eV (below 40 °C) and 0.56 eV (above 40 °C), respectively. These values indicate that the conduction of lithium ions in the film is dominated by the polymer matrix. Proper distribution of thermally conductive nanomaterials in polymer batteries offers new opportunities to mitigate performance degradation associated with localized hot spots and safety concerns in batteries. Cheng et al. [149] utilized the DIW method to fabricate PEO composite polymer electrolytes embedded with silane-treated hexagonal boron nitride (S-hBN) platelets. The Li-ion half-cell fabricated with the printed composite polymer electrolyte and LFP cathode exhibited a high discharge specific capacity of 146.0 mAh g^{-1} and a stable Coulombic efficiency of 91% at room temperature for 100 cycles at room temperature. This work contributes to the development of printable thermally conductive polymers for safer battery operation.

While printing has received a great deal of attention for printing batteries in advancing the next generation, challenges remain in the printing of electrolytes. Early electrolyte fabrication studies required additional process steps such as solvent evaporation, which hindered the simultaneous production of electrodes and electrolytes in fully printed batteries. Cheng et al. [82] designed a high-temperature DIW 3D printer from a robotic deposition system and developed a solid electrolyte ink to enable 3D printing of hybrid solid electrolyte batteries (Fig. 10f). The mixed electrolyte ink can be printed directly onto electrodes without any surface treatment of the substrate and post-treatment of the electrolyte, which will improve the efficiency of electrolyte preparation and incorporation into batteries. As shown in Fig. 10g, the hybrid SSE consists of a solid polymer matrix and an ionic liquid electrolyte. In addition to providing sufficient mechanical support to separate the electrodes, the solid polymer matrix allows the diffusion of lithium ions. Nano-TiO_2 particles were added to PVDF-co-HFP-based polymer ink to improve its viscosity, adjust the contact angle, and improve its electrochemical performance. Furthermore, the 3D-printed hybrid electrolyte prepared by the high-temperature DIW process showed lower interfacial resistance due to the formation of a unique dense interface between the electrolyte and the electrode. Interestingly, the interfacial resistance of this method is significantly reduced compared to the conventional method of casting electrolytes stacked on the electrodes.

In order to solve the scientific and technological problems existing in SSBs, in addition to the heating modification of the above-mentioned printing machine, an external heating source can also be used [139]. Oh et al. [150] proposed a new material for single-ion conducting quasi-solid-state soft electrolyte, which combined with a UV-curing-assisted multi-stage printing process to fabricate seamlessly integrated solid-state lithium batteries without the need for high-temperature/high-pressure sintering steps. Driven by the solid-state soft electrolyte and the monolithic cell architecture, the semi-solid Li-metal batteries exhibited stable charge/discharge performance (cycling retention, rate capability, and bipolar configurations with tunable voltages and high gravimetric/volumetric energy densities (476 Wh kg^{-1}/1 102 Wh L^{-1} at four-stacked cells with 16.656 V) under ambient operating conditions. Moreover, the low-temperature performance, mechanical flexibility, and safety (nonflammability) were achieved for the semi-solid Li-metal batteries, which far exceeded those of the previously reported solid-state LMBs. The solid-state soft electrolyte described herein can be suggested as a promising single-ion conducting SSE platform that can lead us closer to the practically viable solid-state LMBs.

Energy storage devices employing printed solid electrolytes have many advantages, especially in terms of flexible design and improved electrochemical performance. In order to provide energy-consuming devices with paper-based electronics for flexible and wearable systems, Yang et al. [161] designed hydrogel-reinforced cellulose paper for use as separators and solid electrolytes for paper batteries. Zn-metal batteries printed on hydrogel-reinforced cellulose paper have an apparent volumetric energy density of ≈26 mWh cm^{-3} and also demonstrate cuttability and compatibility with flexible circuits and devices. However, the electrolytes themselves still have many hurdles to overcome before printed solid electrolytes can be used for commercialization. For inorganic SSEs, researchers will continue their efforts to explore new compounds and structural types that support fast ionic conductivity. The use of high-throughput computational techniques and experiments will help to identify new candidate compounds. In addition to the modification of known electrode materials that have been successful in liquid batteries, we should explore novel electrode materials and protective coatings that are more suitable for SSB applications, including electrode materials that exhibit low

isotropic volume expansion upon cycling. Many strategies such as chemical doping, new synthesis/processing routes, and dense film preparation remain to be explored to further optimize traditional electrolyte materials and discover new inorganic electrolytes. The technical challenges to be addressed include developing highly scalable synthetic routes and tailoring mechanical properties to achieve stable operation of printed solid-state devices.

In the case of solid polymer electrolytes, the design should focus on improving the conductivity at room temperature or lower, designing the cathode-electrolyte interface, and tuning the structure to inhibit dendrite formation. Glass transition temperature, crystallinity and ion-pair dissociation remain the most important parameters to be considered when designing high conductivity polymer electrolyte inks. The presence of electron-absorbing groups on the main chain, cross-linking of chains to reduce migration of polymer chains to the interface, and salt additives to form a stable electrode–electrolyte interface are expected to improve the anodic stability of polyethers. Increased energy storage modulus and nanostructured polymer electrolytes have been shown to be essential for stable anodic metal deposition. There are almost always trade-offs when trying to design a single polymeric material with all these properties, so composite or multiphase systems appear to be a more promising way to achieve these requirements.

4.3 Current Collectors

To achieve the goal of all-printed SSBs with design diversity, other printable battery modules, such as current collectors and packaging materials, should also be developed. Unfortunately, there is usually less research in this area and more effort is required. Conductive current collectors and electrodes are important components for conducting electrochemical reactions in batteries. Before printing Li-ion battery electrodes directly on gold electrodes, Lewis et al. [162] fabricated gold current collectors by a combination of photolithographic patterning and electron beam deposition. There are also metal current collectors (e.g., gold, copper, aluminum and nickel) and other non-metal current collectors for printable supercapacitors that can be used as references in the battery field [32]. The growing demand for higher capacity rechargeable Li-ion batteries highlights the need for new battery materials, structures and assembly strategies. Wei et al. [163] report the design, fabrication, and electrochemical performance of fully 3D-printed lithium-ion batteries composed of thick semi-solid electrodes with high areal capacitance. Specifically, semi-solid cathodes and anode inks were created, as well as UV-curable packaging and inks for direct writing to LIBs of arbitrary geometries. These fully 3D printed and packaged Li-ion batteries were encapsulated between two glassy carbon current collectors, delivering an areal capacity of 4.45 mAh cm^{-2} at a current density of 0.14 mA cm^{-2}, equivalent to 17.3 Ah L^{-1}. The ability to produce high-performance LIBs in custom form factors opens new avenues for direct integration of batteries into 3D printed objects. As shown in Fig. 7a, the authors achieved full-component printing of an SSB in which highly conductive silver and carbon pastes are used to print the anode and cathode collectors, respectively, providing design freedom and chemical stability for cell operation with good compatibility with the electrodes [132].

The drastic volume change of Li metal during the plating/stripping process can lead to internal interfacial stress fluctuations, which can crack the surface of the artificial interfacial layer [164]. Structurally engineered Li metal anodes with microstructured surfaces, which suppress the formation of Li dendrites by reducing charge distribution and lowering the local current density, thereby enhancing the stability of Li anodes [109]. A 3D porous current collector or scaffold is utilized to transform the planar Li metal anode into a 3D structure, while the porous nature of the 3D current collector provides high surface area and volume so that even if Li dendrites form, they are confined within the scaffold [165]. Therefore, it is particularly important to construct excellent 3D structural components through printing engineering. Cipollone et al. [146] developed a 3D printing method to fabricate 3D anode structures with controllable size, geometry, and chemical composition (Fig. 10h). And sequential learning based on hybrid design is used to guide the design and optimization of ink formulations, rheological parameters, and operating parameters during 3D printing. As shown in Fig. 10i, the ink is printed directly on the solid electrolyte, resulting in scaffolds with different pore size ranges. The results show that the 3D printed structure is beneficial to both the stabilization of the interface and the inhibition of the growth of lithium dendrites. The Li|Cu@LATP@Cu|Li symmetric cell with 3D printed copper scaffolds exhibits a polarization voltage of 60 mV at a current density of 0.05 mA cm^{-2}.

5 Printing Processes and Optimization

The printing process involves the application of specific inks to selected substrates to form predefined pattern layers with specific thicknesses. These printing processes vary considerably in terms of ink formulation, minimum feature size and application. In conventional processes, after ink deposition, the deposited ink needs to be dried, which means that the solvent required for the printing process itself needs to evaporate. Second, device functionality is usually substrate-independent, expanding the range of substrates on which these devices can be fabricated. In addition, printing enables large-scale directional deposition with surface features that

would otherwise be impossible to achieve. However, when printing SSBs, both accuracy and resolution are compromised. Furthermore, printing may not always replicate the properties and microstructure of the deposited material. For example, printing may not preserve the surface chemistry of functional materials if polymer binders cannot be avoided in ink formulations. Inkjet printing may not produce flat deposits like langmuir blodgett coatings. However, for many applications, the resolution of various printing technologies is sufficient and is increasing. As long as the desired functional materials can be incorporated into the ink system, printing is suitable for the fabrication of SSBs for a wide range of applications. In this section, we discuss the basics of optimizing the printing process, from ink formulations to methods that help to achieve optimized print morphology and structure. Comparison of different representative research studies can be found in Table 2.

5.1 Ink Formulations

Polymer binders, solvents, additives, and active chemicals are common components of printed battery inks. Suitable additives and active substances are micro/nanoparticles, nanoplates, nanowires, carbonaceous or ionic liquids. Common active materials include carbon-based materials, metal oxide materials, conducting polymers, and nanomaterials

Table 2 Development of printed SSBs and their main properties and components. Datas are extracted from different sources, and thus are with different significant digits

Printing technique	Post-treatments	Electrolyte	Cathode; anode	Battery type	Electrochemical performance	References
IJP	Drying	PYR13-LiTFSI	LFP; LTO	Li ion	85 mAh g^{-1} at 0.03 C	[64]
Screen-printing	Annealing	Nb doped $Li_7La_3Zr_2O_{12}$ and Li_3BO_3	$LiCoO_2$; Li	Li ion	100 mAh g^{-1} at10 μAh cm^{-2}	[66]
Screen-printing	UV curing	EMS-TEGDME	S/C; Li	Li-S	1 100 mAh g^{-1} at 0.1 C	[48]
Screen-printing	UV curing	ETPTA-$LiPF_6$-EC-PC-Al_2O_3	LFP; LTO	Li ion	160 mAh g^{-1} at 0.05 C	[134]
Screen-printing	UV curing	ETPTA-$LiPF_6$-EC-PC-Al_2O_3	LFP; LTO	Li ion	0.5 mAh cm^{-2} at 1.0 C	[135]
Screen-printing	UV curing	ETPTA-Al_2O_3	V_2O_5; Zn	Zn ion	160 mAh g^{-1} at 20 mA g^{-1}	[166]
3D printing	UV curing	ETPTA-PDMS	LFP; LTO	Li ion	135 mAh g^{-1} at 0.2 C	[132]
3D printing	Drying	$Li_{1+x}Al_xTi_{2-x}(PO_4)_3$	Li	Li-Li	Polarization voltage of 60 mV at 0.05 mA cm^{-2}	[146]
3D printing	Drying	PEO-ZIF67	LFP; Li	Li ion	160 mAh g^{-1} at 0.2 C	[148]
3D printing	Annealing	PVDF-co-HFP and Al_2O_3	LFP; LTO	Li-ion	117 mAh g^{-1} at 50 mA g^{-1}	[40]
3D printing	Freeze-drying	PVDF-co-HFP and SiO_2	Se/C; Li	Li-Se	12.99 mAh cm^{-2} at 3 mA cm^{-2}	[107]
3D printing	Drying	PVDF-co-HFP and $LiPF_6$-EC/DEC	LFP/LTO	Li-Se	110 mAh g^{-1} at 50 mA g^{-1}	[39]
3D printing	Annealing	PVA/KOH gel electrolyte	$Ni(OH)_2$; α-Fe_2O_3	Ni-Fe	28.1 mWh cm^{-3} at 10.6 mW cm^{-3}	[121]
Spray printing	Drying	PVA/KOH gel electrolyte	Ag; Zn	Ag-Zn	0.30 mWh cm^{-2} at 0.67 mW cm^{-2}	[129]
Spray printing	Drying	PEO-LITFSI-$Li_{1.5}Al_{0.5}Ge_{1.5}(PO_4)_3$	LFP; Li	Li ion	150 mAh g^{-1} at 0.1 C	[108]
Spray printing	Sintering	$Li_{6.5}La_3Zr_{1.5}Ta_{0.5}O_{12}$	$LiBO_2$-$LiCoO_2$; Li	Li ion	~87 mAh g^{-1} at 30 mA g^{-1}	[100]
AJP	Drying	PEO-LiDFOB-Al_2O_3	LFP; Li	Li ion	85 mAh g^{-1} at C/15	[72]
SLA	Drying	PEO-SCN-LiTFSI	LFP; Li	Li ion	166 mAh g^{-1} at 0.1 C	[89]
SLA	Calcining	$Li_{1.4}Al_{0.4}Ge_{1.6}(PO_4)_3$	–	–	1.6×10^{-4} S cm^{-1}	[88]
DIW	Freeze-drying	$Li_{1.3}Al_{0.3}Ti_{1.7}(PO_4)_3$	LFP; Li	Li ion	150 mAh g^{-1} at 0.5 C	[81]
DIW	UV curing	PEO-S-hBN	LFP; Li	Li ion	146.0 mAh g^{-1} at 17 mA g^{-1}	[149]
DIW	Elevated-temperature printing	PVDF-co-HFP and TiO_2	MnO_2; LFP/LTO	Li ion	~115 mAh g^{-1} at 32 mA g^{-1}	[82]
DIW	Drying	DADMA-TFSI	$LiCoO_2$; Li	Li ion	115 Ah L^{-1} at 0.5 C	[139]
FDM	Drying	PEO/LiTFSI	–	–	2.18×10^{-3} S cm^{-1}	[84]
R2R	Drying	PAN-PEO/LiTFSI	LFP; Li	Li ion	168.9 mAh g^{-1} at 0.1 C	[140]

such as graphene. Additives are used to modify or customize the physical properties of the ink to meet the requirements of the printing process. Binders are used to keep the active components together as well as the substrate. Post-treatments like annealing are often required to facilitate solvent evaporation, thereby solidifying the deposited material. Solvents are occasionally critical to the stability of the ink and to meet the requirements of various printing processes. The basic function of the printing process is to transfer ink from the printing plate to the substrate. When performing multi-layer printing, it is very vital to use the right solvent. A range of solvents, including aqueous and organic solvents, are frequently utilized depending on the printing technique, substrate, and device structure. Ink formulation is the first consideration in the fabrication of printed SSBs and is critical to both successful printing and the quality of the printed devices. For example, dispersions of most nanomaterials can be used directly for spraying, whereas preparing inks for inkjet, flexographic and gravure processes require complex processes. Therefore, one of the biggest challenges is to develop inks for printing solid electrolytes with a high ionic conductivity ($> 10^{-4}$ S cm^{-1}) and mechanical and thermal stability. Current research efforts in this topic are focused on the difficulties involved in designing and optimizing specialized inks for distinct battery components to match the efficiency, stability, and processability criteria of diverse printing processes.

McOwen et al. [26] reported $Li_7La_3Zr_2O_{12}$-based inks with two binder systems that can be built into thin, non-planar, complex structures after sintering. Further research and optimization of electrolyte structures using these 3D printing ink formulations could lead to significantly lower full-cell resistance and higher energy and power densities for SSBs. In addition, the reported ink composition can be used as model formulations for other solid electrolyte or ceramic inks, perhaps for 3D printing in related fields. Zekoll et al. [88] used SLA to fabricate 3D structured templates and filled the templates with $Li_{1.4}Al_{0.4}Ge_{1.6}(PO_4)_3$. After the polymer template was removed, $Li_{1.4}Al_{0.4}Ge_{1.6}(PO_4)_3$ scaffolds were created. A complicated 3D-structured hybrid electrolytes were created after filling the channels of the LAGP scaffold with polymers (polypropylene or epoxy). In above contributions, post-processing procedures such as heat treatment and freeze-drying are required to remove solvents and templates after printing. Even with only a small amount of solvent, these post-processing procedures distort the 3D structure. Therefore, large-scale development of such printing inks for the SSB industry can be extremely challenging. Some researchers have modified the ink by adding nanoscale ceramic fillers to achieve the desired rheological properties. For example, Cheng et al. [82] designed a high-temperature DIW 3D printer to implement a hybrid solid electrolyte battery. The hybrid electrolyte ink can be printed directly to the electrode without any surface treatment of the substrate and post-treatment of the electrolyte. This will improve the efficiency of electrolyte preparation and addition to the battery. Hybrid SSEs consist of a solid polymer matrix and an ionic-liquid electrolyte. In addition to providing sufficient mechanical support to separate the electrodes, the solid polymer matrix allows the diffusion of lithium ions. Nano-TiO_2 particles were added to PVDF-co-HFP-based polymer ink to improve its viscosity, adjust the contact angle, and improve its electrochemical performance. Furthermore, the 3D-printed hybrid electrolyte prepared by the high-temperature DIW process showed lower interfacial resistance due to the formation of a unique dense interface between the electrolyte and the electrode. Interestingly, the interfacial resistance of this method is significantly reduced compared to the conventional method of casting electrolytes stacked on the electrodes.

5.2 Tuning of Printing Parameters

Small changes in printing parameters can greatly affect the quality of printed patterns, which can result in pattern irregularities, reduced resolution, and non-uniform film morphology [167]. For example, printing speed, nip distance, repeatability accuracy, substrate material selection and surface properties (pretreatment) need to be considered for printing machinery. For ink, parameters such as viscosity, uniformity, composition, absorption characteristics, solvent evaporation characteristics, and drying characteristics need to be considered. In screen printing, it is necessary to pay attention to the mesh width of the printing screen, the thickness of the stencil material, the jump height, and the hardness, alignment angle and pressure of the squeegee roller. Screen printing offers the possibility to adapt the printing technique to the specific requirements of the product to be printed. By understanding the interaction between basic printing parameters, it is possible to process substrates and functional printing pastes of various viscosity ranges, as well as multi-layer printing of different layer thicknesses, in one printing cycle. By modifying printing parameters such as the mesh number and wire diameter, blade geometry of the squeegee and printing speed, it is possible to control the printing resolution and thickness of the printing ink layer, as well as the roughness of the particles dissolved in the printing paste. A detailed view of mesh parameters provides greater insight into the flexibility of screen printing in terms of print jobs and materials that can be processed. The mesh geometry is determined by the thread diameter, mesh number, and mesh opening. These parameters allow calculation of open mesh area, which represents the percentage of ink penetration area that affects ink release characteristics and print layer thickness. Another important factor is the theoretical ink volume, which approximates the ink consumption of each individual

screen-printed grid and the maximum achievable thickness of the printed wet layer on a non-absorbent substrate. The main factors to consider when implementing printed electronics are the printing resolution relative to line edge sharpness and the layer thickness of the printing paste deposited on the substrate. Predetermining the average particle size of the paste is necessary to select an appropriate screen printing mesh capable of handling a particular paste. Sufficient ink penetration can be ensured by selecting a mesh with three times the average particle size of the printing paste.

However, printing settings do not influence all materials, and different printing methods and processes have diverse impacts. For example, the ionic conductivity of room temperature gels (0.37 mS cm^{-1}) is an order of magnitude lower than that of pure ionic liquid-based electrolytes (2.4 mS cm^{-1}). However, the gels are considered to have comparable conductivity compared to glassy LiPON in dry solid polymer PEO-based electrolytes (0.01 mS cm^{-1}) [168] and room temperature electrolytes (< 10 μS cm^{-1}) [169]. To make thin samples, PVDF-HFP-based gels were printed on glass substrates with a 30-gauge (150 μm inner diameter) needle and dried on a hot plate at 60 °C for 45 min. It was found that the microstructure of the gel was hardly affected by printing parameters (such as needle size, film size, printing speed, and substrate material), and more dependent on gel composition and post-processing conditions, such as drying temperature [170].

5.3 Interface Engineering

SSBs using solid electrolytes show the potential for improved safety and higher energy and power densities compared to conventional lithium-ion batteries. However, a key bottleneck still remains: the high impedance of various solid/solid interfaces remains a challenge [27, 138, 152]. SSEs, whereas liquid batteries, are unable to flow or penetrate into gaps and spaces, resulting in inadequate physical contact between particles. Because the cathode, electrolyte, and anode are all solid, manufacturing an SSB necessitates stacking the cathode, electrolyte, and anode in a specific order, resulting in a plethora of interfaces, including cathode-electrolyte, anode-electrolyte, electrolyte-electrolyte, current collector-electrolyte [27]. Generally, high-energy applications require high Li^+ ion mobility and wide voltage window, efficient charge–discharge, minimal power loss for resistive heating, good structural stability and electrode–electrolyte interface compatibility for battery safety. In order to improve the particle interface contact, Tan et al. [171] demonstrated that all these cells were aged at 35 °C for 24 h before electrochemical testing by injection printing method for electrode/electrolyte preparation. This aging can promote electrolyte penetration into the electrode body to achieve a well-wetted electrode–electrolyte contact to avoid high polarization. In addition, injection printing enables uniform mixing of electrodes and electrolytes, which improves interfacial compatibility, reduces interfacial resistance, and facilitates charge transfer. Hu et al. and colleagues [100] reported a solution-based printing process followed by rapid high temperature (~ 1 500 °C) reaction sintering of $LiBO_2$-LLZTO composite solid electrolyte films. This printing and rapid sintering process also allows multilayer structures to be fabricated layer by layer without cross-contamination. A printed SSB with a conformal interface and excellent cycling stability is demonstrated. The resulting material is characterized by uniform distribution of $LiBO_2$ among LLZTO grains with conformal interfaces. The interface resistance of this sintered cell is as low as ~ 100 Ω cm^2 at 60 °C due to the conformal interface.

To ensure adequate cycle life, solid-state technologies require additional interfacial engineering directly at the electrode fabrication step for adhesion and mechanical compliance. Curtain coatings offer a clear path to address the current bottlenecks associated with SSB manufacturing: it enables high-throughput manufacturing compatible with existing infrastructure, lowers barriers to market adoption, and offers new solutions for interface engineering plan [93, 172]. For solid-state technology, this enables simultaneous deposition of cathode and SSE layers for subsequent assembly with lithium metal anodes and current collectors through multilayer curtain coating [173]. In addition, the use of polymers is a well-established approach to address adhesion and mechanical stability issues in SSB technology [143, 174]. By applying heat during the calendering process, a dense film can be obtained, and as a current collector, the ceramic and the polymer have good adhesion. The possibility of adding low molecular weight polymers or even polymers thermally activated by the hot pressing process can be used to further improve interfacial stability, contact with solid particles, and electrochemical performance. The possibility of multi-layer coatings means that the layers can be formed in parallel, allowing for a gapless interface.

5.4 Post-Treatments

Printed SSB modules are constructed by direct printing or requiring post-processing processes such as sintering [26], freeze-drying [81], annealing [40], and UV curing [49]. These post-processing procedures are commonly used because the printed active material should have a combination of high electrical conductivity, electrochemical activity, and mechanical stability. It should be noted that some of these post-processing processes may result in shrinkage and/or distortion of the printing system as well as manufacturing complexity, thereby reducing print repeatability and reproducibility. Therefore, the compatibility between post-processing methods and printed materials is an important consideration in practical manufacturing.

Sintering is commonly used in functional material-based conductive inks, which often contain organic additives to prevent nanoparticle aggregation and precipitation. Nanoparticles lose their organic shells and form physical contact with each other after sintering. But sintering electrolyte films presents a huge challenge, during which an SSE needs to be sintered at high temperatures (from 600 to 1 100 °C) for several hours to achieve the crystal structure required for high ionic conductivity. However, prolonged sintering also leads to severe losses of Li and Na and correspondingly low ionic conductivity due to the volatility of these light elements at high temperatures. Therefore, ceramic SSE films usually exhibit poor crystallinity or significant lithium loss [175]. Lowering the processing temperature to prevent severe lithium loss or adding excess lithium to compensate has been a common strategy in traditional ceramic thin film deposition techniques [176]. However, this leads to poor composition control and a potentially porous structure. Furthermore, these low-temperature sintered SSEs have an amorphous structure, resulting in a limited increase in electrical conductivity up to 2.9×10^{-5} S cm^{-1} [176], which is far from the bulk value (~ 10^{-3} S cm^{-1}). Hu and colleagues [100] reported a solution-based printing process followed by rapid (~ 3 s) high temperature (~ 1 500 °C) reaction sintering for the fabrication of high-performance ceramic SSE thin films. The SSE exhibits dense, uniform structure and excellent ionic conductivity up to 1 mS cm^{-1}. Furthermore, the fabrication time from precursor to final product is typically around 5 min, which is 10–100 times faster than conventional SSE synthesis. This printing and rapid sintering process also allows multilayer structures to be fabricated layer by layer without cross-contamination. This technique can be easily extended to other thin-film SSEs, which opens up previously unexplored opportunities for developing safe, high-performance SSBs and other thin-film devices.

Freeze drying is also called sublimation drying. A drying method in which water-containing materials are frozen below freezing, the water is converted to ice, and then the ice is removed by converting the ice to vapor under a relatively high vacuum. After printing the electrodes, Fu et al. [40] used freeze-drying and thermal annealing post-treatment procedures to remove the electrode's aqueous solvent and thermally reduce the GO material. Due to the strong hydrogen bonding between water molecules and GO functional groups, fresh electrodes can be left for more than 10 h without any sign of structural failure. After the water was removed from the printed electrodes by freeze-drying, the dried samples retained their structural dimensions and were stable in the surrounding environment for several weeks. Heat treatment (2 h at 600 °C in Ar/H_2) for thermal reduction of graphene oxide for printed electrodes. After thermal annealing, the electrical conductivities of LFP/rGO and LTO/rGO electrodes are 31.6 and 6.1 S cm^{-1}, respectively, which are relatively higher than the unheated samples (10^{-6}–10^{-7} S cm^{-1}).

Ultraviolet curing (commonly known as UV curing) is a fast photochemical process in which high-intensity ultraviolet light is used to instantly cure or "dry" inks, coatings or adhesives [177]. UV formulations are liquid monomers and oligomers mixed with a small percent of photoinitiators, and then exposed to UV energy [139]. In a few seconds, the formulation inks, coatings or adhesives instantly "harden" or cure, ready for the next processing step. Kim et al. [49] developed a novel flexible/shaped multifunctional bipolar all-solid-state LIB by UV curing-assisted multistage printing, which does not require the high-pressure/-temperature sintering process employed by typical inorganic electrolytes-based all-solid-state LIBs. The printed LTO anodes were obtained by printing the LTO anode paste on an aluminum fluid using a stencil printing technique without any processing solvents, and then exposing it to UV light. UV irradiation was performed using a Hg UV lamp with a peak intensity of about 2 000 mW cm^{-2}. Subsequently, on top of the LTO anode, a gel composite electrolytes paste was introduced by the same stencil printing and UV curing process, resulting in a printed solid-state gel composite electrolytes layer on the LTO anode. The printed LCO cathode was then fabricated by directly printing the LCO cathode paste onto the gel composite electrolytes layer/LTO anode unit followed by UV irradiation. After placing the aluminum current collector on top of the printed LCO cathode/printed gel composite electrolytes layer/printed LTO anode assembly, a seamlessly integrated all-solid-state single full cell was obtained. On top of the prepared single full cell, the printing/UV curing process is repeated, enabling the fabrication of printed bipolar cells.

To maintain the structural integrity of printed SSBs, the printable electrolyte needs to meet two requirements. First, the ink is required to have the proper viscosity to be continuously extruded from the nozzle and stacked layer by layer. Second, tissue shrinkage is to be avoided during the coagulation process. Typically, solvent volatilization and solidification are achieved by post-processing heat treatments, which alter the shape of the electrolytic layer, causing it to shrink and eventually deform. Therefore, more printing processes should be further analyzed, explored, and optimized to achieve high-efficiency solid-state energy storage. DIW and SLA are the two most popular 3D printing technologies for solid-state energy storage today, while other technologies still have unique characteristics. For example, selective laser melting and electron beam melting have shown excellent capabilities for producing large metal-based materials that are attractive as large conducting hosts. At the same time, 3D printing parameters (such as printing resolution) also need to be further optimized to facilitate electric/ion transport and improve electrochemical performance [135].

6 Conclusions and Perspectives

SSBs fabricated using various printing techniques have been demonstrated. Although these printing fabrication techniques show great potential for fabricating SSBs, they suffer from several limitations and challenges, the most important of which include resolution, surface quality, and material availability. Among these printing techniques, screen printing has a rigid stencil and relatively low resolution. Inkjet printing offers higher resolution, but clogged nozzles are a common problem, resulting in higher demands on the printing ink. Inkjet printing parameters affect liquid footprint size. For example, when the dot spacing increases, the line width decreases. The minimum linewidth is determined by the maximum droplet spacing for stable coalescence, and the maximum linewidth is determined by the minimum droplet spacing below which expansion instability occurs. Intuitively, reducing the nozzle diameter minimizes the point or line footprint size. However, it is difficult to generate droplets and eject them from nozzles with sub-micron diameters due to the large resistive capillary pressure at the ejection ports, which places higher demands on the inks used when printing SSBs. The resolution of R2R printing is relatively wide, but requires high equipment cost. Although SLA is capable of printing extremely complex structures at fast printing speeds, one of the limitations of SLA-printed electrolytes is the addition of photopolymers, which somehow degrades the performance of SSBs. The DIW process needs to overcome the rheological limitations of the ink and issues associated with drying processes such as solvent evaporation.

Although the different methods vary widely, the material availability of the printing process for SSBs is generally low, except for some coating methods. Most complex printing techniques require the ink to exhibit certain rheological properties, which means strict requirements on the size, solvent, concentration, etc. of the active material. It is sometimes difficult to efficiently transfer active materials into desired solvents with tailored concentrations while preventing aggregation. For example, sulfide-based solid electrolytes (such as Li_6PS_5Cl and $Li_{10}GeP_2S_{12}$), because they are prone to side reactions with air and water, it is currently difficult to combine them with printing processes. For another example, in the Li–S battery system, it is necessary to further increase the content of the active material in the flexible positive electrode to achieve a higher overall energy density of the battery. However, it is worth noting that in printing fabrication, one of the limitations is that the mechanical flexibility is affected if the sulfur content is increased. Therefore, more efficient conductive and mechanical networks are required to accommodate more cathode active materials. In particular, printing SSBs would benefit greatly if printing inks with fast curing, long-term stability, and satisfactory mechanical properties could be developed based on more materials. So far, the mature printing inks available for SSBs are mainly based on the addition of GO or CNTs-based materials. It is often difficult to impart the required fast-drying ability and mechanical strength to printing inks without compromising the conductivity of the active material. Therefore, it is necessary to choose the printing technology wisely according to the requirements in practical applications, and future research will require significant efforts to fabricate printed SSBs with better structural and electrochemical properties, mainly focusing on the development of printable active electrode materials and SSEs with higher electrochemical properties.

The development of a new generation of printed SSBs is still in its early stages. A lot of effort is required before real technical implementations can emerge. In summary, some current challenges and future directions for the practical realization of printed SSBs are as follows.

1. In the past, researchers worked hard to develop SSEs for energy storage devices and made them into thin-film structures using conventional techniques. However, among these materials, only a few have been applied in the printing research of SSEs. Compared with traditional SSE materials, printable electrolyte materials not only focus on electrochemical and mechanical properties, but also focus on printability. Therefore, developing high ionic conductivity electrolytes with more printability is a future research direction.
2. Regardless of the printing technology used, ink functionality and processability are key issues, and ink characteristics must be customized for each printing process. For material printing and structural shaping, the various rheological behaviors required, including sufficient viscosity and viscoelasticity, are prerequisites for diverse printing processes. Although the addition of filler materials is the most important way to modify printable inks, the increased viscosity may affect the transport of ions through the electrolyte and reduce the ionic conductivity of the printed electrolyte. Therefore, the selection of additives is a development direction in the future research of printable electrolytes, and it is also a direction to optimize the filler concentration.
3. After the ink is printed and deposited, post-processing is very important, usually requiring drying, curing or sintering steps to obtain functional layers or functional devices. During post-processing, solid electrolytes usually need to be sintered at high temperatures (from 600 to 1 100 °C) for several hours to obtain the crystal structure required for high ionic conductivity. However, due to the volatility of light elements at high temperatures, prolonged sintering also leads to severe loss of Li and Na and correspondingly low ionic conductivity. Under high temperature for a long time, ceramic electrolytes

either have poor crystallinity, or serious loss of lithium and sodium, and low ionic conductivity. Adding excess Li to compensate or reducing the process temperature to prevent severe Li loss is a common strategy in conventional fabrication techniques. However, this leads to a potentially porous structure and poor compositional control, further distorting the shape and complex structure of the electrolyte layer, leading to its shrinkage and eventual deformation. Therefore, the temperature and time of sintering become very critical, and it is particularly important to develop various low-temperature sintering inks and advanced sintering technologies. And we still don't really understand the underlying physical phenomena that occur during the sintering process and the corresponding sintering mechanisms. Further understanding of the different sintering mechanisms that contribute to the enhanced performance of SSB devices is crucial.

4. Post-processing changes the shape of the electrolyte layer, causing it to shrink and eventually deform. This shrinkage can be minimized by printing the electrolyte layer directly onto the electrodes. Meanwhile, the development of solvent-free printable materials can be considered as a solution to overcome this challenge.
5. Although the solid electrolyte is directly printed on the surface of the Li metal electrode, a certain interfacial stability can be achieved. However, the severe chemical instability of lithium metal narrows the range of fabrication conditions (such as ambient air conditions) and printable electrolyte ink materials (such as solvents, additives, lithium salts, and processing solvents) for printing SSEs. Therefore, antioxidation treatment of Li metal surfaces or the use of anode-free electrodes to achieve reliable Li plating/stripping cycling capability is a future research direction.
6. Although oxide solid electrolytes are kinetically stable when coupled with oxide cathodes, the wettability of the interface is poor due to the high Young's modulus of ceramic oxides. The mechanical incompatibility of the interface between electrodes and solid electrolytes is another critical issue. Before considering the conductivity and final experimental synthesis, it is important to prioritize component screening based on the interface properties of the solid electrolyte and specific electrodes, and to incorporate certain interface design and other interface treatment techniques to improve the interface stability during the printing process.
7. Printing optimization is the key to producing high-quality SSB devices. Therefore, tuning the printing process, such as ink formulation, droplet delivery, wet film formation, and curing, is an important task for researchers in the field of printed SSBs. These processes are often not well understood and far from well controlled. Therefore, printer software should be more user-friendly and intelligent. If the printing optimization process could be simplified, researchers would be much more productive. For example, the integration of post-processing and printing processes, and the combination of dry preparation and printing of electrodes and electrolytes are also research directions worthy of attention. By combining chemical, geometric, mechanical, electrochemical and interfacial transport properties and printing fabrication processes, more advanced solid-state energy storage or energy conversion systems can be expected in the future.

Acknowledgements This work was financially supported by the Shenzhen Science and Technology Program (Grant Nos. KQTD20200820113045083, ZDSYS20190902093220279 and JCYJ20220818102403007), and Shenzhen Research Fund for Returned Scholars (DD11409017 and DD11409018).

Ethics statement There are no financial conflicts of interest to disclose.

References

1. Hannan, M.A., Lipu, M.S.H., Hussain, A., et al.: A review of lithium-ion battery state of charge estimation and management system in electric vehicle applications: challenges and recommendations. Renew. Sustain. Energy Rev. **78**, 834–854 (2017). https://doi.org/10.1016/j.rser.2017.05.001
2. Dunn, B., Kamath, H., Tarascon, J.M.: Electrical energy storage for the grid: a battery of choices. Science **334**, 928–935 (2011). https://doi.org/10.1126/science.1212741
3. Armand, M., Tarascon, J.M.: Building better batteries. Nature **451**, 652–657 (2008). https://doi.org/10.1038/451652a
4. Nishi, Y.: Lithium ion secondary batteries; past 10 years and the future. J. Power Sources **100**, 101–106 (2001). https://doi.org/10.1016/S0378-7753(01)00887-4
5. Tarascon, J.M., Armand, M.: Issues and challenges facing rechargeable lithium batteries. Nature **414**, 359–367 (2001). https://doi.org/10.1038/35104644
6. Lin, D.C., Liu, Y.Y., Cui, Y.: Reviving the lithium metal anode for high-energy batteries. Nat. Nanotechnol. **12**, 194–206 (2017). https://doi.org/10.1038/nnano.2017.16
7. Xu, W., Wang, J.L., Ding, F., et al.: Lithium metal anodes for rechargeable batteries. Energy Environ. Sci. **7**, 513–537 (2014). https://doi.org/10.1039/C3EE40795K
8. Zhai, P.B., Liu, L.X., Gu, X.K., et al.: Interface engineering for lithium metal anodes in liquid electrolyte. Adv. Energy Mater. **10**, 2001257 (2020). https://doi.org/10.1002/aenm.202001257

9. Krauskopf, T., Richter, F.H., Zeier, W.G., et al.: Physicochemical concepts of the lithium metal anode in solid-state batteries. Chem. Rev. **120**, 7745–7794 (2020). https://doi.org/10.1021/acs.chemrev.0c00431
10. Cheng, X.B., Zhang, R., Zhao, C.Z., et al.: Toward safe lithium metal anode in rechargeable batteries: a review. Chem. Rev. **117**, 10403–10473 (2017). https://doi.org/10.1021/acs.chemrev.7b00115
11. Guo, Y.P., Li, H.Q., Zhai, T.Y.: Reviving lithium-metal anodes for next-generation high-energy batteries. Adv. Mater. **29**, 1700007 (2017). https://doi.org/10.1002/adma.201700007
12. Yang, C.P., Fu, K., Zhang, Y., et al.: Protected lithium-metal anodes in batteries: from liquid to solid. Adv. Mater. **29**, 1701169 (2017). https://doi.org/10.1002/adma.201701169
13. Janek, J., Zeier, W.G.: A solid future for battery development. Nat. Energy **1**, 1–4 (2016). https://doi.org/10.1038/nenergy.2016.141
14. Hu, Y.S.: Batteries: getting solid. Nat. Energy **1**, 1–2 (2016). https://doi.org/10.1038/nenergy.2016.42
15. Liu, K., Liu, Y.Y., Lin, D.C., et al.: Materials for lithium-ion battery safety. Sci. Adv. **4**, eaas9820 (2018). https://doi.org/10.1126/sciadv.aas9820
16. Zhao, Q., Stalin, S., Zhao, C.Z., et al.: Designing solid-state electrolytes for safe, energy-dense batteries. Nat. Rev. Mater. **5**, 229–252 (2020). https://doi.org/10.1038/s41578-019-0165-5
17. Manthiram, A., Yu, X.W., Wang, S.F.: Lithium battery chemistries enabled by solid-state electrolytes. Nat. Rev. Mater. **2**, 16103 (2017). https://doi.org/10.1038/natrevmats.2016.103
18. Kato, Y., Hori, S., Saito, T., et al.: High-power all-solid-state batteries using sulfide superionic conductors. Nat. Energy **1**, 1–7 (2016). https://doi.org/10.1038/nenergy.2016.30
19. Tu, Z.Y., Choudhury, S., Zachman, M.J., et al.: Fast ion transport at solid-solid interfaces in hybrid battery anodes. Nat. Energy **3**, 310–316 (2018). https://doi.org/10.1038/s41560-018-0096-1
20. Xia, S.X., Wu, X.S., Zhang, Z.C., et al.: Practical challenges and future perspectives of all-solid-state lithium-metal batteries. Chem **5**, 753–785 (2019). https://doi.org/10.1016/j.chempr.2018.11.013
21. Zheng, Y., Yao, Y.Z., Ou, J.H., et al.: A review of composite solid-state electrolytes for lithium batteries: fundamentals, key materials and advanced structures. Chem. Soc. Rev. **49**, 8790–8839 (2020). https://doi.org/10.1039/d0cs00305k
22. Thompson, T., Yu, S., Williams, L., et al.: Electrochemical window of the Li-ion solid electrolyte $Li_7La_3Zr_2O_{12}$. ACS Energy Lett. **2**, 462–468 (2017). https://doi.org/10.1021/acsenergylett.6b00593
23. Li, Y.X., Wu, Y.J., Wang, Z.X., et al.: Progress in solvent-free dry-film technology for batteries and supercapacitors. Mater. Today **55**, 92–109 (2022). https://doi.org/10.1016/j.mattod.2022.04.008
24. Schnell, J., Tietz, F., Singer, C., et al.: Prospects of production technologies and manufacturing costs of oxide-based all-solid-state lithium batteries. Energy Environ. Sci. **12**, 1818–1833 (2019). https://doi.org/10.1039/C8EE02692K
25. Deiner, L.J., Bezerra, C.A.G., Howell, T.G., et al.: Digital printing of solid-state lithium-ion batteries. Adv. Eng. Mater. **21**, 1900737 (2019). https://doi.org/10.1002/adem.201900737
26. McOwen, D.W., Xu, S.M., Gong, Y.H., et al.: 3D-printing electrolytes for solid-state batteries. Adv. Mater. **30**, e1707132 (2018). https://doi.org/10.1002/adma.201707132
27. Banerjee, A., Wang, X.F., Fang, C.C., et al.: Interfaces and interphases in all-solid-state batteries with inorganic solid electrolytes. Chem. Rev. **120**, 6878–6933 (2020). https://doi.org/10.1021/acs.chemrev.0c00101
28. Gaikwad, A.M., Arias, A.C., Steingart, D.A.: Recent progress on printed flexible batteries: mechanical challenges, printing technologies, and future prospects. Energy Technol. **3**, 305–328 (2015). https://doi.org/10.1002/ente.201402182
29. Costa, C.M., Gonçalves, R., Lanceros-Méndez, S.: Recent advances and future challenges in printed batteries. Energy Storage Mater. **28**, 216–234 (2020). https://doi.org/10.1016/j.ensm.2020.03.012
30. Dai, J., Ogbeide, O., MacAdam, N., et al.: Printed gas sensors. Chem. Soc. Rev. **49**, 1756–1789 (2020). https://doi.org/10.1039/C9CS00459A
31. Espera, A.H., Jr., Dizon, J.R.C., Chen, Q.Y., et al.: 3D-printing and advanced manufacturing for electronics. Prog. Addit. Manuf. **4**, 245–267 (2019). https://doi.org/10.1007/s40964-019-00077-7
32. Zhang, Y.Z., Wang, Y., Cheng, T., et al.: Printed supercapacitors: materials, printing and applications. Chem. Soc. Rev. **48**, 3229–3264 (2019). https://doi.org/10.1039/C7CS00819H
33. Li, M.R., Zhou, S.Q., Cheng, L.K., et al.: 3D printed supercapacitor: techniques, materials, designs, and applications. Adv. Funct. Mater. **33**, 2208034 (2023). https://doi.org/10.1002/adfm.202208034
34. Sousa, R.E., Costa, C.M., Lanceros-Méndez, S.: Advances and future challenges in printed batteries. Chemsuschem **8**, 3539–3555 (2015). https://doi.org/10.1002/cssc.201500657
35. Lyu, Z.Y., Lim, G.J.H., Koh, J.J., et al.: Design and manufacture of 3D-printed batteries. Joule **5**, 89–114 (2021). https://doi.org/10.1016/j.joule.2020.11.010
36. Tian, X.C., Xu, B.G.: 3D printing for solid-state energy storage. Small Methods **5**, 2100877 (2021). https://doi.org/10.1002/smtd.202100877
37. Zhang, F., Wei, M., Viswanathan, V.V., et al.: 3D printing technologies for electrochemical energy storage. Nano Energy **40**, 418–431 (2017). https://doi.org/10.1016/j.nanoen.2017.08.037
38. Wang, C.W., Fu, K., Kammampata, S.P., et al.: Garnet-type solid-state electrolytes: materials, interfaces, and batteries. Chem. Rev. **120**, 4257–4300 (2020). https://doi.org/10.1021/acs.chemrev.9b00427
39. Wang, Y.B., Chen, C.J., Xie, H., et al.: 3D-printed all-fiber Li-ion battery toward wearable energy storage. Adv. Funct. Mater. **27**, 1703140 (2017). https://doi.org/10.1002/adfm.201703140
40. Fu, K., Wang, Y.B., Yan, C.Y., et al.: Graphene oxide-based electrode inks for 3D-printed lithium-ion batteries. Adv. Mater. **28**, 2587–2594 (2016). https://doi.org/10.1002/adma.201505391
41. Ragones, H., Vinegrad, A., Ardel, G., et al.: On the road to a multi-coaxial-cable battery: development of a novel 3D-printed composite solid electrolyte. J. Electrochem. Soc. **167**, 070503 (2019). https://doi.org/10.1149/2.0032007jes
42. Gao, Y., Guo, Q.Y., Zhang, Q., et al.: Fibrous materials for flexible Li-S battery. Adv. Energy Mater. **11**, 2002580 (2020). https://doi.org/10.1002/aenm.202002580
43. Mo, F.N., Liang, G.J., Huang, Z.D., et al.: An overview of fiber-shaped batteries with a focus on multifunctionality, scalability, and technical difficulties. Adv. Mater. **32**, 1902151 (2020). https://doi.org/10.1002/adma.201902151
44. Yu, X.W., Liu, Y.T., Pham, H., et al.: Customizable nonplanar printing of lithium-ion batteries. Adv. Mater. Technol. **4**, 1900645 (2019). https://doi.org/10.1002/admt.201900645
45. Cohen, E., Menkin, S., Lifshits, M., et al.: Novel rechargeable 3D-microbatteries on 3D-printed-polymer substrates: feasibility study. Electrochim. Acta **265**, 690–701 (2018). https://doi.org/10.1016/j.electacta.2018.01.197
46. Egorov, V., Gulzar, U., Zhang, Y., et al.: Evolution of 3D printing methods and materials for electrochemical energy storage. Adv. Mater. **32**, 2000556 (2020). https://doi.org/10.1002/adma.202000556

47. Zhang, M.C., Zhao, M.Y., Jian, M.Q., et al.: Printable smart pattern for multifunctional energy-management E-textile. Matter **1**, 168–179 (2019). https://doi.org/10.1016/j.matt.2019.02.003
48. Kim, S.H., Kim, J.H., Cho, S.J., et al.: All-solid-state printed bipolar Li-S batteries. Adv. Energy Mater. **9**, 1901841 (2019). https://doi.org/10.1002/aenm.201901841
49. Kim, S.H., Choi, K.H., Cho, S.J., et al.: Flexible/shape-versatile, bipolar all-solid-state lithium-ion batteries prepared by multistage printing. Energy Environ. Sci. **11**, 321–330 (2018). https://doi.org/10.1039/C7EE01630A
50. Lin, Z.J., Mao, M.L., Yue, J.M., et al.: Wearable bipolar rechargeable aluminum battery. ACS Mater. Lett. **2**, 808–813 (2020). https://doi.org/10.1021/acsmaterialslett.0c00145
51. Reyes, C., Somogyi, R., Niu, S.B., et al.: Three-dimensional printing of a complete lithium ion battery with fused filament fabrication. ACS Appl. Energy Mater. (2018). https://doi.org/10.1021/acsaem.8b00885
52. Maurel, A., Grugeon, S., Fleutot, B., et al.: Three-dimensional printing of a $LiFePO_4$/graphite battery cell via fused deposition modeling. Sci. Rep. **9**, 1–14 (2019). https://doi.org/10.1038/s41598-019-54518-y
53. Sun, K., Wei, T.S., Ahn, B.Y., et al.: 3D printing of interdigitated Li-ion microbattery architectures. Adv. Mater. Deerfield Beach Fla **25**, 4539–4543 (2013). https://doi.org/10.1002/adma.201301036
54. Xia, X.X., Afshar, A., Yang, H., et al.: Electrochemically reconfigurable architected materials. Nature **573**, 205–213 (2019). https://doi.org/10.1038/s41586-019-1538-z
55. Lanceros-Méndez, S., Costa, C.M. (eds.): Printed Batteries: Materials, Technologies and Applications. John Wiley & Sons, New York (2018)
56. Van Osch, T., Perelaer, J., De Laat, A., et al.: Inkjet printing of narrow conductive tracks on untreated polymeric substrates. Adv. Mater. **20**, 343–345 (2008). https://doi.org/10.1002/adma.200701876
57. Jang, D., Kim, D., Moon, J.: Influence of fluid physical properties on ink-jet printability. Langmuir **25**, 2629–2635 (2009). https://doi.org/10.1021/la900059m
58. Derby, B.: Inkjet printing of functional and structural materials: fluid property requirements, feature stability, and resolution. Annu. Rev. Mater. Res. **40**, 395–414 (2010). https://doi.org/10.1146/annurev-matsci-070909-104502
59. Reynolds, O.: XXIX. An experimental investigation of the circumstances which determine whether the motion of water shall be direct or sinuous, and of the law of resistance in parallel channels. Phil. Trans. R. Soc. **174**, 935–982 (1883). https://doi.org/10.1098/rstl.1883.0029
60. Bergeron, V., Bonn, D., Martin, J.Y., et al.: Controlling droplet deposition with polymer additives. Nature **405**, 772–775 (2000). https://doi.org/10.1038/35015525
61. McKinley, G.H., Renardy, M.: Wolfgang von ohnesorge. Phys. Fluids **23**, 127101 (2011). https://doi.org/10.1063/1.3663616
62. Kolchanov, D.S., Mitrofanov, I., Kim, A., et al.: Inkjet printing of Li-rich cathode material for thin-film lithium-ion microbatteries. Energy Technol. **8**, 1901086 (2020). https://doi.org/10.1002/ente.201901086
63. Gao, M., Li, L.H., Song, Y.L.: Inkjet printing wearable electronic devices. J. Mater. Chem. C **5**, 2971–2993 (2017). https://doi.org/10.1039/C7TC00038C
64. Delannoy, P.E., Riou, B., Lestriez, B., et al.: Toward fast and cost-effective ink-jet printing of solid electrolyte for lithium microbatteries. J. Power Sources **274**, 1085–1090 (2015). https://doi.org/10.1016/j.jpowsour.2014.10.164
65. Park, M.S., Hyun, S.H., Nam, S.C.: Mechanical and electrical properties of a $LiCoO_2$ cathode prepared by screen-printing for a lithium-ion micro-battery. Electrochim. Acta **52**, 7895–7902 (2007). https://doi.org/10.1016/j.electacta.2007.06.041
66. Ohta, S., Komagata, S., Seki, J., et al.: All-solid-state lithium ion battery using garnet-type oxide and Li_3BO_3 solid electrolytes fabricated by screen-printing. J. Power Sources **238**, 53–56 (2013). https://doi.org/10.1016/j.jpowsour.2013.02.073
67. Cheng, M., Jiang, Y.Z.: 3D-printed solid-state electrolytes for electrochemical energy storage devices. J. Mater. Res. **36**, 4547–4564 (2021)
68. Huang, Y., Leu, M.C., Mazumder, J., et al.: Additive manufacturing: current state, future potential, gaps and needs, and recommendations. J. Manuf. Sci. Eng. **137**, 014001 (2015). https://doi.org/10.1115/1.4028725
69. Wilkinson, N.J., Smith, M.A.A., Kay, R.W., et al.: A review of aerosol jet printing: a non-traditional hybrid process for micromanufacturing. Int. J. Adv. Manuf. Technol. **105**, 4599–4619 (2019)
70. Secor, E.B.: Principles of aerosol jet printing. Flex. Print. Electron. **3**, 035002 (2018). https://doi.org/10.1088/2058-8585/aace28
71. Secor, E.B.: Guided ink and process design for aerosol jet printing based on annular drying effects. Flex. Print. Electron. **3**, 035007 (2018). https://doi.org/10.1088/2058-8585/aadffd
72. Deiner, L.J., Jenkins, T., Howell, T., et al.: Aerosol jet printed polymer composite electrolytes for solid-state Li-ion batteries. Adv. Eng. Mater. **21**, 1900952 (2019). https://doi.org/10.1002/adem.201900952
73. Lewis, J.A., Smay, J.E., Stuecker, J., et al.: Direct ink writing of three-dimensional ceramic structures. J. Am. Ceram. Soc. **89**, 3599–3609 (2006). https://doi.org/10.1111/j.1551-2916.2006.01382.x
74. Jiang, P., Ji, Z.Y., Zhang, X.Q., et al.: Recent advances in direct ink writing of electronic components and functional devices. Prog. Addit. Manuf. **3**, 65–86 (2018). https://doi.org/10.1007/s40964-017-0035-x
75. Jiang, Y.Z., Plog, J., Yarin, A.L., et al.: Direct ink writing of surface-modified flax elastomer composites. Compos. B Eng. **194**, 108061 (2020). https://doi.org/10.1016/j.compositesb.2020.108061
76. Zhang, Q.H., Zhou, J.Q., Chen, Z.H., et al.: Direct ink writing of moldable electrochemical energy storage devices: ongoing progress, challenges, and prospects. Adv. Eng. Mater. **23**, 2100068 (2021). https://doi.org/10.1002/adem.202100068
77. Li, H.P., Liang, J.J.: Recent development of printed micro-supercapacitors: printable materials, printing technologies, and perspectives. Adv. Mater. **32**, 1805864 (2020). https://doi.org/10.1002/adma.201805864
78. Ambrosi, A., Pumera, M.: 3D-printing technologies for electrochemical applications. Chem. Soc. Rev. **45**, 2740–2755 (2016). https://doi.org/10.1039/C5CS00714C
79. Sun, Y.H., Peng, C.Q., Wang, X.F., et al.: Rheological behavior of Al_2O_3 suspensions containing polyelectrolyte complexes for direct ink writing. Powder Technol. **320**, 223–229 (2017). https://doi.org/10.1016/j.powtec.2017.07.049
80. Li, Y.Y., Li, L.T., Li, B.: Direct ink writing of special-shaped structures based on TiO_2 inks. Mod. Phys. Lett. B **30**, 1650212 (2016). https://doi.org/10.1142/s0217984916502122
81. Liu, Z.X., Tian, X.C., Liu, M., et al.: Direct ink writing of $Li_{1.3}Al_{0.3}Ti_{1.7}(PO_4)_3$-based solid-state electrolytes with customized shapes and remarkable electrochemical behaviors. Small **17**, 2002866 (2021). https://doi.org/10.1002/smll.202002866
82. Cheng, M., Jiang, Y.Z., Yao, W.T., et al.: Elevated-temperature 3D printing of hybrid solid-state electrolyte for Li-ion batteries. Adv. Mater. **30**, e1800615 (2018). https://doi.org/10.1002/adma.201800615

83. Guo, R., Ren, Z.C., Bi, H.J., et al.: Electrical and thermal conductivity of polylactic acid (PLA)-based biocomposites by incorporation of nano-graphite fabricated with fused deposition modeling. Polymers **11**, 549 (2019). https://doi.org/10.3390/polym11030549
84. Maurel, A., Armand, M., Grugeon, S., et al.: Poly(ethylene oxide)-LiTFSI solid polymer electrolyte filaments for fused deposition modeling three-dimensional printing. J. Electrochem. Soc. **167**, 070536 (2020). https://doi.org/10.1149/1945-7111/ab7c38
85. Crivello, J.V., Reichmanis, E.: Photopolymer materials and processes for advanced technologies. Chem. Mater. **26**, 533–548 (2014). https://doi.org/10.1021/cm402262g
86. Ge, G., Wang, Q., Zhang, Y.Z., et al.: 3D printing of hydrogels for stretchable ionotronic devices. Adv. Funct. Mater. **31**, 2107437 (2021). https://doi.org/10.1002/adfm.202107437
87. Geng, Q., Wang, D.E., Chen, P.F., et al.: Ultrafast multi-focus 3-D nano-fabrication based on two-photon polymerization. Nat. Commun. **10**, 1–7 (2019). https://doi.org/10.1038/s41467-019-10249-2
88. Zekoll, S., Marriner-Edwards, C., Ola Hekselman, A.K., et al.: Hybrid electrolytes with 3D bicontinuous ordered ceramic and polymer microchannels for all-solid-state batteries. Energy Environ. Sci. **11**, 185–201 (2018). https://doi.org/10.1039/c7ee02723k
89. He, Y.J., Chen, S.J., Nie, L., et al.: Stereolithography three-dimensional printing solid polymer electrolytes for all-solid-state lithium metal batteries. Nano Lett. **20**, 7136–7143 (2020). https://doi.org/10.1021/acs.nanolett.0c02457
90. Goswami, D., Munera, J.C., Pal, A., et al.: Roll-to-roll nanoforming of metals using laser-induced superplasticity. Nano Lett. **18**, 3616–3622 (2018). https://doi.org/10.1021/acs.nanolett.8b00714
91. Tamagaki, H., Ikari, Y., Ohba, N.: Roll-to-roll sputter deposition on flexible glass substrates. Surf. Coat. Technol. **241**, 138–141 (2014). https://doi.org/10.1016/j.surfcoat.2013.10.056
92. Gusain, A., Thankappan, A., Thomas, S.: Roll-to-roll printing of polymer and perovskite solar cells: compatible materials and processes. J. Mater. Sci. **55**, 13490–13542 (2020)
93. Baade, P., Wood, V.: Ultra-high throughput manufacturing method for composite solid-state electrolytes. iScience **24**, 102055 (2021). https://doi.org/10.1016/j.isci.2021.102055
94. Ovhal, M.M., Kumar, N., Lee, H.B., et al.: Roll-to-roll 3D printing of flexible and transparent all-solid-state supercapacitors. Cell Rep. Phys. Sci. **2**, 100562 (2021). https://doi.org/10.1016/j.xcrp.2021.100562
95. Ollinger, M., Kim, H., Sutto, T., et al.: Laser printing of nanocomposite solid-state electrolyte membranes for Li micro-batteries. Appl. Surf. Sci. **252**, 8212–8216 (2006). https://doi.org/10.1016/j.apsusc.2005.10.041
96. Kim, H., Auyeung, R.C.Y., Piqué, A.: Laser-printed thick-film electrodes for solid-state rechargeable Li-ion microbatteries. J. Power Sources **165**, 413–419 (2007). https://doi.org/10.1016/j.jpowsour.2006.11.053
97. Kim, D.S., Kim, J.S., Lee, M.C.: Thin film forming technique based on hybrid spray coating using electrostatic force and air pressure. Jpn. J. Appl. Phys. **53**, 05HC08 (2014). https://doi.org/10.7567/jjap.53.05hc08
98. Huang, C., Grant, P.S.: One-step spray processing of high power all-solid-state supercapacitors. Sci. Rep. **3**, 2393 (2013). https://doi.org/10.1038/srep02393
99. Lee, S.H., Huang, C., Johnston, C., et al.: Spray printing and optimization of anodes and cathodes for high performance Li-Ion batteries. Electrochim. Acta **292**, 546–557 (2018). https://doi.org/10.1016/j.electacta.2018.09.132
100. Ping, W.W., Wang, C.W., Wang, R.L., et al.: Printable, high-performance solid-state electrolyte films. Sci. Adv. **6**, eabc8641 (2020). https://doi.org/10.1126/sciadv.abc8641
101. Leung, P., Bu, J.F., Quijano Velasco, P., et al.: Single-step spray printing of symmetric all-organic solid-state batteries based on porous textile dye electrodes. Adv. Energy Mater. **9**, 1901418 (2019). https://doi.org/10.1002/aenm.201901418
102. Shen, F.Y., Dixit, M.B., Zaman, W., et al.: Composite electrode ink formulation for all solid-state batteries. J. Electrochem. Soc. **166**, A3182–A3188 (2019). https://doi.org/10.1149/2.0141914jes
103. Choi, K.H., Ahn, D.B., Lee, S.Y.: Current status and challenges in printed batteries: toward form factor-free, monolithic integrated power sources. ACS Energy Lett. **3**, 220–236 (2018). https://doi.org/10.1021/acsenergylett.7b01086
104. He, Y.F., Wildman, R.D., Tuck, C.J., et al.: An Investigation of the behavior of solvent based polycaprolactone ink for material jetting. Sci. Rep. **6**, 20852 (2016). https://doi.org/10.1038/srep20852
105. Cao, D.X., Xing, Y.J., Tantratian, K., et al.: 3D printed high-performance lithium metal microbatteries enabled by nanocellulose. Adv. Mater. **31**, 1807313 (2019). https://doi.org/10.1002/adma.201807313
106. Sun, H.T., Zhu, J., Baumann, D., et al.: Hierarchical 3D electrodes for electrochemical energy storage. Nat. Rev. Mater. **4**, 45–60 (2018). https://doi.org/10.1038/s41578-018-0069-9
107. Gao, X.J., Yang, X.F., Wang, S.Z., et al.: A 3D-printed ultra-high Se loading cathode for high energy density quasi-solid-state Li-Se batteries. J. Mater. Chem. A **8**, 278–286 (2020). https://doi.org/10.1039/c9ta10623e
108. Bu, J.F., Leung, P., Huang, C., et al.: Co-spray printing of $LiFePO_4$ and PEO-$Li_{1.5}Al_{0.5}Ge_{1.5}(PO_4)_3$ hybrid electrodes for all-solid-state Li-ion battery applications. J. Mater. Chem. A **7**, 19094–19103 (2019). https://doi.org/10.1039/c9ta03824h
109. Park, S., Jin, H.J., Yun, Y.S.: Advances in the design of 3D-structured electrode materials for lithium-metal anodes. Adv. Mater. **32**, 2002193 (2020). https://doi.org/10.1002/adma.202002193
110. Li, J.F., Liu, X., Crook, J.M., et al.: A 3D printed graphene electrode device for enhanced and scalable stem cell culture, osteoinduction and tissue building. Mater. Des. **201**, 109473 (2021). https://doi.org/10.1016/j.matdes.2021.109473
111. Foster, C.W., Down, M.P., Zhang, Y., et al.: 3D printed graphene based energy storage devices. Sci. Rep. **7**, 42233 (2017). https://doi.org/10.1038/srep42233
112. Lacey, S.D., Kirsch, D.J., Li, Y.J., et al.: Extrusion-based 3D printing of hierarchically porous advanced battery electrodes. Adv. Mater. **30**, 1705651 (2018). https://doi.org/10.1002/adma.201705651
113. Zhu, C., Han, T.Y.J., Duoss, E.B., et al.: Highly compressible 3D periodic graphene aerogel microlattices. Nat. Commun. **6**, 6962 (2015). https://doi.org/10.1038/ncomms7962
114. Jiang, Y.Q., Xu, Z., Huang, T.Q., et al.: Direct 3D printing of ultralight graphene oxide aerogel microlattices. Adv. Funct. Mater. **28**, 1707024 (2018). https://doi.org/10.1002/adfm.201707024
115. Li, Y.J., Gao, T.T., Yang, Z., et al.: 3D-printed, all-in-one evaporator for high-efficiency solar steam generation under 1 sun illumination. Adv. Mater. **29**, 1700981 (2017). https://doi.org/10.1002/adma.201700981
116. Li, Y.Y., Zhu, H.L., Wang, Y.B., et al.: Cellulose-nanofiber-enabled 3D printing of a carbon-nanotube microfiber network. Small Methods **1**, 1700222 (2017). https://doi.org/10.1002/smtd.201700222
117. García-Tuñon, E., Barg, S., Franco, J., et al.: Printing in three dimensions with graphene. Adv. Mater. **27**, 1688–1693 (2015). https://doi.org/10.1002/adma.201405046
118. Zhang, Q.Q., Zhang, F., Medarametla, S.P., et al.: 3D printing of graphene aerogels. Small **12**, 1702–1708 (2016). https://doi.org/10.1002/smll.201503524

119. Barg, S., Perez, F.M., Ni, N., et al.: Mesoscale assembly of chemically modified graphene into complex cellular networks. Nat. Commun. **5**, 1–10 (2014). https://doi.org/10.1038/ncomms5328
120. Kim, J.H., Chang, W.S., Kim, D., et al.: 3D printing of reduced graphene oxide nanowires. Adv. Mater. **27**, 157–161 (2015). https://doi.org/10.1002/adma.201404380
121. Kong, D.Z., Wang, Y., Huang, S.Z., et al.: 3D printed compressible quasi-solid-state nickel-iron battery. ACS Nano **14**, 9675–9686 (2020). https://doi.org/10.1021/acsnano.0c01157
122. Cao, Q., Tersoff, J., Farmer, D.B., et al.: Carbon nanotube transistors scaled to a 40-nanometer footprint. Science **356**, 1369–1372 (2017). https://doi.org/10.1126/science.aan2476
123. Schroeder, V., Savagatrup, S., He, M., et al.: Carbon nanotube chemical sensors. Chem. Rev. **119**, 599–663 (2019). https://doi.org/10.1021/acs.chemrev.8b00340
124. Lu, X.H., Yu, M.H., Wang, G.M., et al.: Flexible solid-state supercapacitors: design, fabrication and applications. Energy Environ. Sci. **7**, 2160 (2014). https://doi.org/10.1039/c4ee00960f
125. Seh, Z.W., Sun, Y.M., Zhang, Q.F., et al.: Designing high-energy lithium-sulfur batteries. Chem. Soc. Rev. **45**, 5605–5634 (2016). https://doi.org/10.1039/c5cs00410a
126. Manthiram, A., Fu, Y.Z., Chung, S.H., et al.: Rechargeable lithium-sulfur batteries. Chem. Rev. **114**, 11751–11787 (2014). https://doi.org/10.1021/cr500062v
127. Zhao, X.S., Yin, L.C., Zhang, T., et al.: Heteroatoms dual-doped hierarchical porous carbon-selenium composite for durable Li-Se and Na-Se batteries. Nano Energy **49**, 137–146 (2018). https://doi.org/10.1016/j.nanoen.2018.04.045
128. Shen, C.L., Wang, T., Xu, X., et al.: 3D printed cellular cathodes with hierarchical pores and high mass loading for Li-SeS_2 battery. Electrochim. Acta **349**, 136331 (2020). https://doi.org/10.1016/j.electacta.2020.136331
129. Bi, S.S., Wan, F., Wang, S., et al.: Flexible and tailorable quasi-solid-state rechargeable Ag/Zn microbatteries with high performance. Carbon Energy **3**, 167–175 (2021). https://doi.org/10.1002/cey2.64
130. Peng, H.J., Huang, J.Q., Zhang, Q.: A review of flexible lithium-sulfur and analogous alkali metal-chalcogen rechargeable batteries. Chem. Soc. Rev. **46**, 5237–5288 (2017). https://doi.org/10.1039/C7CS00139H
131. Yin, L., Scharf, J., Ma, J., et al.: High performance printed AgO-Zn rechargeable battery for flexible electronics. Joule **5**, 228–248 (2021). https://doi.org/10.1016/j.joule.2020.11.008
132. Bae, J., Oh, S., Lee, B., et al.: High-performance, printable quasi-solid-state electrolytes toward all 3D direct ink writing of shape-versatile Li-ion batteries. Energy Storage Mater. **57**, 277–288 (2023). https://doi.org/10.1016/j.ensm.2023.02.016
133. Rodriguez, R., Deiner, L.J., Tsao, B.H., et al.: Aerosol jet-printed LFP cathodes with bimodal pore distribution improve the rate capability of LIB cells. ACS Appl. Energy Mater. **4**, 9507–9512 (2021). https://doi.org/10.1021/acsaem.1c01678
134. Kim, S.H., Choi, K.H., Cho, S.J., et al.: Printable solid-state lithium-ion batteries: a new route toward shape-conformable power sources with aesthetic versatility for flexible electronics. Nano Lett. **15**, 5168–5177 (2015). https://doi.org/10.1021/acs.nanolett.5b01394
135. Um, H.D., Choi, K.H., Hwang, I., et al.: Monolithically integrated, photo-rechargeable portable power sources based on miniaturized Si solar cells and printed solid-state lithium-ion batteries. Energy Environ. Sci. **10**, 931–940 (2017). https://doi.org/10.1039/c6ee03266d
136. Syrový, T., Kazda, T., Akrman, J., et al.: Towards roll-to-roll printed batteries based on organic electrodes for printed electronics applications. J. Energy Storage **40**, 102680 (2021). https://doi.org/10.1016/j.est.2021.102680
137. Liu, J., Bao, Z.N., Cui, Y., et al.: Pathways for practical high-energy long-cycling lithium metal batteries. Nat. Energy **4**, 180–186 (2019). https://doi.org/10.1038/s41560-019-0338-x
138. Xiao, Y.H., Wang, Y., Bo, S.H., et al.: Understanding interface stability in solid-state batteries. Nat. Rev. Mater. **5**, 105–126 (2019). https://doi.org/10.1038/s41578-019-0157-5
139. Cho, S.K., Kim, H.I., An, J.W., et al.: Printable solid electrolyte interphase mimic for antioxidative lithium metal electrodes. Adv. Funct. Mater. **30**, 2000792 (2020). https://doi.org/10.1002/adfm.202000792
140. Ma, Y.X., Wan, J.Y., Yang, Y.F., et al.: Scalable, ultrathin, and high-temperature-resistant solid polymer electrolytes for energy-dense lithium metal batteries. Adv. Energy Mater. **12**, 2103720 (2022). https://doi.org/10.1002/aenm.202103720
141. Zhang, Z.Z., Shao, Y.J., Lotsch, B., et al.: New horizons for inorganic solid state ion conductors. Energy Environ. Sci. **11**, 1945–1976 (2018). https://doi.org/10.1039/C8EE01053F
142. Zhao, Y., Wang, L., Zhou, Y.N., et al.: Solid polymer electrolytes with high conductivity and transference number of Li ions for Li-based rechargeable batteries. Adv. Sci. **8**, 2003675 (2021). https://doi.org/10.1002/advs.202003675
143. Yao, P.H., Yu, H.B., Ding, Z.Y., et al.: Review on polymer-based composite electrolytes for lithium batteries. Front. Chem. **7**, 522 (2019). https://doi.org/10.3389/fchem.2019.00522
144. Ding, P.P., Lin, Z.Y., Guo, X.W., et al.: Polymer electrolytes and interfaces in solid-state lithium metal batteries. Mater. Today **51**, 449–474 (2021). https://doi.org/10.1016/j.mattod.2021.08.005
145. Fan, L.Z., He, H.C., Nan, C.W.: Tailoring inorganic-polymer composites for the mass production of solid-state batteries. Nat. Rev. Mater. **6**, 1003–1019 (2021). https://doi.org/10.1038/s41578-021-00320-0
146. Cipollone, D., Yang, H., Yang, F., et al.: 3D printing of an anode scaffold for lithium batteries guided by mixture design-based sequential learning. J. Mater. Process. Technol. **295**, 117159 (2021). https://doi.org/10.1016/j.jmatprotec.2021.117159
147. Lee, K., Shang, Y., Bobrin, V.A., et al.: 3D printing nanostructured solid polymer electrolytes with high modulus and conductivity. Adv. Mater. **34**, 2204816 (2022). https://doi.org/10.1002/adma.202204816
148. Li, C.G., Deng, S.L., Feng, W.H., et al.: A universal room-temperature 3D printing approach towards porous MOF based dendrites inhibition hybrid solid-state electrolytes. Small **19**, 2300066 (2023). https://doi.org/10.1002/smll.202300066
149. Cheng, M., Ramasubramanian, A., Rasul, M.G., et al.: Direct ink writing of polymer composite electrolytes with enhanced thermal conductivities. Adv. Funct. Mater. **31**, 2006683 (2021). https://doi.org/10.1002/adfm.202006683
150. Oh, K.S., Kim, J.H., Kim, S.H., et al.: Single-ion conducting soft electrolytes for semi-solid lithium metal batteries enabling cell fabrication and operation under ambient conditions. Adv. Energy Mater. **11**, 2101813 (2021). https://doi.org/10.1002/aenm.202101813
151. Famprikis, T., Canepa, P., Dawson, J.A., et al.: Fundamentals of inorganic solid-state electrolytes for batteries. Nat. Mater. **18**, 1278–1291 (2019). https://doi.org/10.1038/s41563-019-0431-3
152. Tan, D.H.S., Banerjee, A., Chen, Z., et al.: From nanoscale interface characterization to sustainable energy storage using all-solid-state batteries. Nat. Nanotechnol. **15**, 170–180 (2020). https://doi.org/10.1038/s41565-020-0657-x
153. Lee, J., Lee, T., Char, K., et al.: Issues and advances in scaling up sulfide-based all-solid-state batteries. Acc. Chem. Res. **54**, 3390–3402 (2021). https://doi.org/10.1021/acs.accounts.1c00333
154. Zhang, Q., Cao, D.X., Ma, Y., et al.: Sulfide-based solid-state electrolytes: synthesis, stability, and potential for all-solid-state batteries. Adv. Mater. **31**, e1901131 (2019). https://doi.org/10.1002/adma.201901131

155. Lau, J., DeBlock, R.H., Butts, D.M., et al.: Sulfide solid electrolytes for lithium battery applications. Adv. Energy Mater. **8**, 1800933 (2018). https://doi.org/10.1002/aenm.201800933
156. Zhou, Q., Ma, J., Dong, S.M., et al.: Intermolecular chemistry in solid polymer electrolytes for high-energy-density lithium batteries. Adv. Mater. **31**, e1902029 (2019). https://doi.org/10.1002/adma.201902029
157. Lee, M.J., Han, J., Lee, K., et al.: Elastomeric electrolytes for high-energy solid-state lithium batteries. Nature **601**, 217–222 (2022). https://doi.org/10.1038/s41586-021-04209-4
158. Liu, W.Y., Yi, C.J., Li, L.P., et al.: Designing polymer-in-salt electrolyte and fully infiltrated 3D electrode for integrated solid-state lithium batteries. Angew. Chem. Int. Ed. **60**, 12931–12940 (2021). https://doi.org/10.1002/anie.202101537
159. Liu, W., Lee, S.W., Lin, D.C., et al.: Enhancing ionic conductivity in composite polymer electrolytes with well-aligned ceramic nanowires. Nat. Energy **2**, 1–7 (2017). https://doi.org/10.1038/nenergy.2017.35
160. Fu, K.K., Gong, Y.H., Dai, J.Q., et al.: Flexible, solid-state, ion-conducting membrane with 3D garnet nanofiber networks for lithium batteries. Proc. Natl. Acad. Sci. USA **113**, 7094–7099 (2016). https://doi.org/10.1073/pnas.1600422113
161. Yang, P.H., Li, J., Lee, S.W., et al.: Printed zinc paper batteries. Adv. Sci. **9**, 2103894 (2022). https://doi.org/10.1002/advs.202103894
162. Sun, K., Wei, T.S., Ahn, B.Y., et al.: 3D printing of interdigitated Li-ion microbattery architectures. Adv. Mater. **25**, 4539–4543 (2013). https://doi.org/10.1002/adma.201301036
163. Wei, T.S., Ahn, B.Y., Grotto, J., et al.: 3D printing of customized Li-ion batteries with thick electrodes. Adv. Mater. **30**, 1703027 (2018). https://doi.org/10.1002/adma.201703027
164. Lu, L.L., Ge, J., Yang, J.N., et al.: Free-standing copper nanowire network current collector for improving lithium anode performance. Nano Lett. **16**, 4431–4437 (2016). https://doi.org/10.1021/acs.nanolett.6b01581
165. Yun, Q.B., He, Y.B., Lv, W., et al.: Chemical dealloying derived 3D porous current collector for Li metal anodes. Adv. Mater. **28**, 6932–6939 (2016). https://doi.org/10.1002/adma.201601409
166. Bu, F., Li, C., Wang, Q.Z., et al.: Ultraviolet-assisted printing of flexible all-solid-state zinc batteries with enhanced interfacial bond. Chem. Eng. J. **449**, 137710 (2022). https://doi.org/10.1016/j.cej.2022.137710
167. Pudas, M., Hagberg, J., Leppävuori, S.: Printing parameters and ink components affecting ultra-fine-line gravure-offset printing for electronics applications. J. Eur. Ceram. Soc. **24**, 2943–2950 (2004). https://doi.org/10.1016/j.jeurceramsoc.2003.11.011
168. Meyer, W.H.: Polymer electrolytes for lithium-ion batteries. Adv. Mater. **10**, 439–448 (1998). https://doi.org/10.1002/(SICI)1521-4095(199804)10:6<439::AID-ADMA439>3.0.CO;2-I
169. Dudney, N.J.: Solid-state thin-film rechargeable batteries. Mater. Sci. Eng. B **116**, 245–249 (2005). https://doi.org/10.1016/j.mseb.2004.05.045
170. Wright, P.K., Dornfeld, D.A., Chen, A., et al.: Dispenser printing for prototyping microscale devices. Trans. NAMRI/SME **38**, 555–561 (2010)
171. Tan, G.Q., Wu, F., Zhan, C., et al.: Solid-state Li-ion batteries using fast, stable, glassy nanocomposite electrolytes for good safety and long cycle-life. Nano Lett. **16**, 1960–1968 (2016). https://doi.org/10.1021/acs.nanolett.5b05234
172. Wang, L.G., Li, J., Lu, G.L., et al.: Fundamentals of electrolytes for solid-state batteries: challenges and perspectives. Front. Mater. **7**, 111 (2020). https://doi.org/10.3389/fmats.2020.00111
173. Döll, H.: Curtain coating: when the curtain falls. Wochenbl. Papierfabr. **138**, 483–488 (2010)
174. Li, S., Zhang, S.Q., Shen, L., et al.: Progress and perspective of ceramic/polymer composite solid electrolytes for lithium batteries. Adv. Sci. **7**, 1903088 (2020). https://doi.org/10.1002/advs.201903088
175. Yan, X.F., Han, W.Q.: Preparation and application of garnet electrolyte thin films: promise and challenges. Org. Chem. Plus (2020). https://doi.org/10.37256/ocp.11202081
176. Pfenninger, R., Struzik, M., Garbayo, I., et al.: A low ride on processing temperature for fast lithium conduction in garnet solid-state battery films. Nat. Energy **4**, 475–483 (2019). https://doi.org/10.1038/s41560-019-0384-4
177. Gambe, Y., Kobayashi, H., Iwase, K., et al.: A photo-curable gel electrolyte ink for 3D-printable quasi-solid-state lithium-ion batteries. Dalton Trans. **50**, 16504–16508 (2021). https://doi.org/10.1039/d1dt02918e

Shiqiang Zhou received his Master degree from National Center for International Research on Photoelectric and Energy Materials, Yunnan University. He is now a Ph.D. candidate under Prof. Jun Wei's supervision in the Shenzhen Key Laboratory of Flexible Printed Electronics Technology Center, Harbin Institute of Technology. His current research mainly focuses on using different printing methods to fabricate solid-state lithium-ion batteries.

Mengrui Li received her Master degree from College of Bioresources Chemical & Materials Engineering, Shaanxi University of Science and Technology. Since 2021, she has been pursuing her Ph.D. degree at the School of Materials Science and Engineering, Harbin Institute of Technology (Shenzhen) under the supervisor of Prof. Jun Wei. Her research interest mainly focuses on the design and fabrication of 3D printed energy storage devices, and the related mechanisms.

Peike Wang received her Bachelor degree from Center for International Research on Photoelectric and Energy Materials, Yunnan University. Since 2022, she has been pursing Master degree in the Key Laboratory of Flexible Printed Electronics Technology Center, Harbin Institute of Technology (Shenzhen). Her research mingly focuses on flexible printed electronic devices.

Lukuan Cheng is currently a Ph.D. candidate under the supervision of Prof. Jun Wei at Harbin Institute of Technology (Shenzhen). He received his Bachelor degree in the School of Materials Science and Engineering from Harbin Institute of Technology, 2020. He obtained his Master degree in the School of Materials Science and Engineering from Harbin Institute of Technology, 2023. His research interests focus on novel electrode and separator materials for high-performance Li/Zn-ion batteries.

Lina Chen is currently an assistant research fellow in the School of Materials Science and Engineering at Harbin Institute of Technology (Shenzhen). She received her B.Sc. degree from Harbin Institute of Technology in 2015 and then obtained her Ph.D. degree from Shandong University in 2019. Her research interest has focused on energy storage devices, key electrode materials and 3D printing technology.

Yan Huang received her Ph.D. degree in the University of Rochester (USA) in 2013. Then she moved to City University of Hong Kong (China) as a postdoctoral fellow, followed by a Research Fellow. She has been a professor in the School of Materials Science and Engineering at Harbin Institute of Technology (Shenzhen), China since 2017. Her research interests include aqueous energy and application in flexible/wearable electronics.

Suzhu Yu is a professor at the School of Materials Science and Engineering, Harbin Institute of Technology (Shenzhen). She received her Ph.D. degree from Nanyang Technological University of Singapore and was appointed as a Scientist at Singapore Institute of Manufacturing Technology prior to the current position. Her research focuses on additive manufacturing, flexible printed electronics and functional material development. She has led a number of research and industry projects, and published more than 100 papers.

Funian Mo received his Ph.D. degree from the City University of Hong Kong, China, under the supervision of Prof. Chunyi Zhi. He is currently an assistant research fellow in Prof. Jun Wei's group at the Flexible Printed Electronics Technology Center at Harbin Institute of Technology (Shenzhen), China. In the past five years, he has published over 10 papers in *Nature Reviews Materials, Energy & Environmental Science, Advanced Materials, Advanced Energy Materials, Advanced Functional Materials, Advanced Science, Science Bulletin*, etc., with an *H*-index of 34. His research interests cover the areas of polymer chemistry, nanotechnology, and flexible energy storage devices with a focus on Zn-ion batteries.

Jun Wei is the professor in Harbin Institute of Technology (Shenzhen). Concurrently, he is the University President Assistant, the Director of Shenzhen Key Laboratory of Flexible Printed Electronics Technology, and the Director of Flexible Printed Electronics Center. Before this appointment, he was the Principal Scientist and Director of Research Liaison Office in Singapore Institute of Manufacturing Technology (SIMTech), the Additive Manufacturing Programme Manager for the Agency for Science, Technology and Research (A*STAR). Dr. Wei's research includes additive manufacturing, flexible printed electronics. He has authored and coauthored over 800 publications with citations over 2 700 times and an *H*-index of 82.